3D Printing of Ceramics: Advantages, Challenges, Applications, and Perspectives

Susmita Bose^{1,*}, E. Koray Akdogan², Vamsi K. Balla³, Sushant Ciliveri¹, Paolo Colombo^{4,5}, G. Franchin⁴, Nicholas Ku⁶, Priya Kushram¹, Fangyong Niu⁷, Joshua Pelz⁶, Andrew Rosenberger⁶, Ahmad Safari², Zachary Seeley⁸, Rodney W. Trice⁹, Lionel Vargas-Gonzalez⁶, Jeffrey P. Youngblood⁹, Amit Bandyopadhyay^{1,*}

- ¹ W. M. Keck Biomedical Materials Research Lab, School of Mechanical and Materials Engineering, Washington State University, Pullman, WA 99164, USA.
- ² Department of Materials Science and Engineering, School of Engineering, Rutgers, The State University of New Jersey, Piscataway, NJ 08854, USA.
 - ³ Bioceramics and Coating Division, CSIR-Central Glass and Ceramic Research Institute, Kolkata 700032, India.
 - ⁴ Department of Industrial Engineering, University of Padova, Padova, Italy.
- ⁵ Department of Materials Science and Engineering, Pennsylvania State University, University Park, PA 16802, USA.
- ⁶ Ceramics and Transparent Materials Branch, DEVCOM Army Research Laboratory, Aberdeen Proving Ground, MD 21005, USA.
 - ⁷ State Key Laboratory of High-performance Precision Manufacturing, Dalian University of Technology, Dalian City, 116024, China.
 - ⁸ Lawrence Livermore National Laboratory, Livermore, CA 94550, USA.
 - ⁹ School of Materials Engineering, Purdue University, West Lafayette, IN 47907, USA.
 - *Corresponding author's emails: sbose@wsu.edu (S. Bose) and amitband@wsu.edu (A. Bandyopadhyay)

Table of contents

Abst	ract	3
1.0 I	ntroduction	4
	1.1 A brief history of ceramic 3D Printing (3DP)	5
	1.2 Commercial 3D Printing processes for advanced ceramics	9
	1.3 Ceramic AM for different industrial sectors	16
2.0	3D Printing processes	17
	2.1 Binder jetting	17
	2.2 Stereolithography of ceramics	29
	2.3 3DP of Ceramics from Liquid Precursors	35
	2.4 Direct Ink Writing (DIW)	40
	2.5 Extrusion-based 3DP of Ceramics	46
	2.6 3D Printing of melt growth ceramics by Laser Directed Energy	52
	Deposition (LDED)	
	2.7 Powder bed fusion (PBF) processing of ceramics	56
3.0 A	applications of 3D Printing of Ceramics	62
	3.1 Structural ceramics	62
	3.2 3D Printed transparent ceramics for future laser gain media	65
	3.3 Biological applications of 3D Printing of ceramics	68
4.0 (Challenges and future directions	76
5.0 A	acknowledgments	81
6.0 E	Declaration of Competing Interest	81
7.0 E	Oata availability statement	81
8.0 F	References	82

Abstract

3D Printing (3DP) technologies have transformed the processing of advanced ceramics for

small-scale and custom designs during the past three decades. Simple and complex parts are

designed and manufactured using 3DP technologies for structural, piezoelectric, and biomedical

applications. Manufacturing simple or complex geometries or one-of-a-kind components without

part-specific tooling saves significant time and creates new applications for advanced ceramic

materials. Although development and innovations in 3DP of ceramics are far behind compared to

metals or polymers, with the availability of different commercial machines in recent years for

3DP of ceramics, exponential growth is expected in this field in the coming decade. This article

details various 3DP technologies for advanced ceramic materials, their advantages and

challenges for manufacturing parts for various applications, and perspectives on future

directions. We envision this work will be helpful to advanced ceramic researchers in industry and

academia who are using different 3DP processes in the coming days.

Keywords: 3D Printing; Additive manufacturing; Ceramics; Piezoelectrics; Bioceramics;

Sensors.

3

1.0 Introduction

Ceramics, particularly non-hydrating advanced ceramic materials, are known for their high melting temperatures and inherent brittleness, posing extreme challenges in manufacturing defect-free components with near-net shapes. Their poor thermal shock resistance and extremely high hardness make them difficult to process through liquid state and machining. Current manufacturing routes for ceramic components can be broadly categorized into dry and wet powder processing. While the latter provides more flexibility in feedstock handling and the ability to make complex geometries, removing liquid from the formed parts is highly prone to defect generation, time-consuming, and energy-intensive. As a result, dry powder-based processing is the most popular method for manufacturing ceramic parts. In both approaches, primary machining is often avoided due to expensive tools that can contribute a significant part of the overall manufacturing cost. The advent of additive manufacturing (AM) or 3D printing (3DP) provides lucrative alternatives to manufacturing near-net shape, complex, and multimaterial ceramic components, without part-specific tooling, for various applications. 3DP constitutes a group of advanced manufacturing technologies that can manufacture components directly from a computer-aided design (CAD) model via layer-by-layer additive depositions.

The first and most important benefit of using 3DP to manufacture ceramic components is the elimination of expensive tooling. 3DP is highly cost-effective in new product design and manufacturing using ceramics since no part-specific tooling is needed. 3DP of ceramics can also decrease the gestation period for the product, prototype development, and component production. 3DP offers design freedom, which allows highly complex parts to be easily fabricated compared to conventional manufacturing routes. Integrating geometrical complexity with high functional performance through 3DP of ceramic parts also reduces or eliminates post-fabrication steps such

as cutting, grinding, and assembling, leading to an overall reduction in the part cost and production lead time. 3DP of ceramic components can be more economical than powder injection molding for complex ceramic parts that often run in low volume production and offer 'accessible ceramic parts production.' Recent developments in 3DP technologies [1,2]enable the fabrication of ceramic components using new materials [3–6], periodic and hierarchical porous structures [7], multi-material components [8], functionally graded materials [9], and ceramic matrix composites [10]. Other generic benefits of ceramic 3DP [1] include customization, ondemand manufacturing, strong and lightweight components, waste minimization, and a broad application range. Despite these potentials and demonstrated benefits, the adoption and growth of 3DP technologies to manufacture ceramic components is relatively slow compared to metals and polymers. This is primarily due to various challenges involved in ceramic 3DP [11], such as (i) feedstock preparation, (ii) effective printing process for ceramics, (iii) critical post-printing issues, such as binder removal and sintering, (iv) inconsistency in the process and resultant mechanical properties, and (v) industrial scalability. Notwithstanding these challenges, increased interest in ceramic 3DP in recent years is evident from start-ups offering 3D Printers and product development opportunities tailored explicitly for ceramics.

1.1. A brief history of ceramic 3D Printing (3DP)

Recent literature [1–3,7,10,12,13] demonstrates a significant increase in the interest in developing dense and porous ceramic parts using 3DP. Due to the inherent processing difficulties of ceramic component manufacturing using traditional manufacturing routes, researchers realized three decades ago that producing near-net shape, complex, and high-performance ceramic components is challenging without using innovative 3DP technologies. The first report on

processing ceramics using 3DP technologies was published in 1990 by Marcus et al. [14,15] and Sachs et al. [16]. The first group used the powder bed fusion process (PBF), i.e., selective laser sintering (SLS), to fabricate Al₂O₃ components, and the latter used the binder jetting (BJ) process to make Al₂O₃/SiO₂ casting cores (Figure 1). In 1991, Al₂O₃ composites (Al₂O₃-P₂O₅ and Al₂O₃-B₂O₅) were successfully fabricated using the SLS process [17]. The influence of feedstock powder size and SLS process parameters on microstructure, dimensional stability, and mechanical properties were investigated. The binder jetting process was applied to fabricate Al₂O₃ and SiC parts using colloidal silica as a binder [18]. Following this binder jetting work, Blazdell et al. [19] demonstrated the potential of the material jetting 3DP process, i.e., ink-jet printing, to make small ceramic parts using ceramic inks based on ZrO₂ and TiO₂. These early investigations prompted new interest in 3DP of ceramics. In 1994, the vat photopolymerization process (Stereolithography, SLA) was demonstrated, for the first time, to have the potential to fabricate ceramic components [20,21], wherein UV-curable aqueous solution with up to 55 vol.% SiO₂ and Al₂O₃ was used to produce investment casting cores and structural parts, respectively. Another AM process, namely, sheet lamination (Laminated Object Manufacturing, LOM), which relies on sequential layer-wise adhesion of thin sheets of materials, was also attempted by Griffin et al. [22,23] to make Al₂O₃ and ZrO₂ ceramic parts.

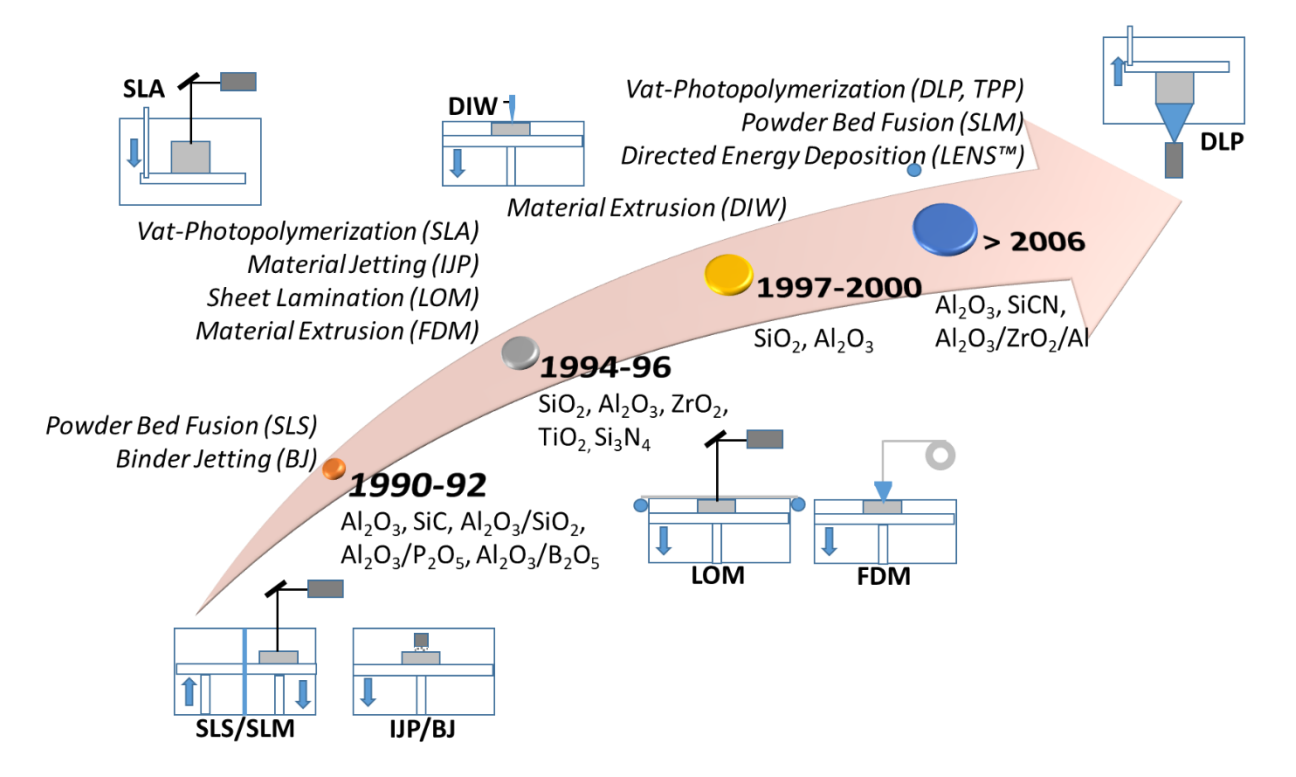


Figure 1. A brief overview of early attempts made for ceramic AM.

Among the different AM processes that attempt to make ceramic parts, fused deposition modeling (FDM) extrusion-based processes are still popular for various reasons. The first use of this technology was reported in 1995 by Agarwala et al. [24]. In this investigation, filaments made using Si₃N₄ with a thermoplastic binder system were extruded to print green ceramic parts, followed by binder removal and sintering, which resulted in up to 90% theoretical density.

Another popular extrusion-based AM process is Direct Ink Writing (DIW, also known as Robocasting), developed in 1997 at Sandia National Laboratories to process highly loaded ceramic slurries and was first reported by Cesarano et al. [25]. Other variants of the vat-photopolymerization-based AM process, namely Digital Light Processing (DLP) and Two-photon polymerization (TPP), have also been attempted to fabricate ceramic components [26][27], respectively. The primary advantage of DLP compared to the standard SLA process is a

significant reduction in the printing time due to complete layer curing in one exposure against point-line-layer curing in the SLA process. The TPP process enables the curing of submicron volume, leading to micro/nanofabrication of ceramic components. Zhou et al.[26] fabricated high-density (99.3%) Al₂O₃ cutting tools with hardness up to 17.5 GPa, comparable to similar tools made using conventional manufacturing routes. Pham et al. [27] successfully fabricated highly complex nano/micro-ceramic structures of SiCN with submicron resolution using the TPP process.

Selective laser melting (SLM) is another powder bed fusion-based AM process similar to SLS, but it can fabricate parts in one step by completely melting ceramic powder layers, providing fully dense parts without any post-sintering step. However, it is more challenging to fabricate ceramic parts using SLM than SLS due to high thermal gradients leading to high thermal stress and consequent cracking/distortion due to poor thermal shock resistance of ceramics. In 2007, Shishkovsky et al. [28] successfully fabricated parts, although with macro defects such as cracks and pores, through the SLM process using feedstock powder containing ZrO₂, Al₂O₃, and Al. Later, high powder bed preheating temperatures reduced the defects in Al₂O₃ parts made using SLM [29]. Directed energy deposition (DED) of ceramics was first reported in 2008 by Balla et al. [30], wherein dense Al₂O₃ parts were successfully fabricated, and property anisotropy was observed in these parts. It is evident from these first-generation studies and recent developments in ceramic 3DP [1,2,7,10] that the critical challenges related to the processing of ceramics are generally similar to those associated with conventional ceramic processing routes. For example, achieving fully dense, uniform, and refined microstructures through high-temperature sintering is essential in both processing routes. The use of preceramic polymers (PCPs) as feedstock to make polymer-derived ceramics (PDCs), although it provides

high flexibility in shaping the parts for both 3DP and conventional processing, still poses challenges related to complete pyrolysis of preceramic polymers to ceramics, high shrinkage and high amount of gas evolution during pyrolysis. The future of successful ceramic 3DP undoubtedly depends on the fundamental and technological understanding of ceramic 3DP-specific process parameters and their influence on part quality.

1.2. Commercial 3D Printing processes for advanced ceramics

Several 3DP technologies have been used to process metals and polymers, but only a few have successfully manufactured defect-free dense ceramic components. These processes are categorized as (i) Vat-Photopolymerization (VPP), (ii) Binder Jetting (BJ), (iii) Material Extrusion (ME), (iv) Powder Bed Fusion (PBF), (v) Material Jetting (MJ), (vi) Sheet Lamination (SL) and (vii) Directed Energy Deposition (DED). Except for some versions of PBF and DED, all other processes involve two steps. In the first step, green ceramic bodies are printed using 3DP technology, followed by debinding and sintering in the second step to obtain densified ceramic components. A summary of different 3DP processes used to manufacture ceramic components is presented in **Table 1** and is briefly described.

Vat-photopolymerization (VPP) processes use photosensitive monomer resins loaded with ceramic powder or recently preceramic polymers selectively cured in a vat, according to the digital layer information, using UV light. The cured parts are thermally processed to remove the cured resin and then sintered to obtain high-strength ceramic parts. VPP is well suited for ceramics with low light absorbance and provides high resolution with a good surface finish. The leading technologies that use VPP are Stereolithography (SLA), Digital Light Processing (DLP),

and Two-photon Photopolymerisation (2PP). Various oxide/ non-oxide ceramics and ceramic composites have been processed using these technologies [1–3,7,10]. However, light scattering by ceramic particles, the requirement of high solids loading to minimize the shrinkage during post-printing thermal processing, and the stability of ceramic-loaded photosensitive monomer resins are significant challenges in these processes.

In the Binder Jetting (BJ) process, an organic liquid binder or binding agent is selectively deposited/sprayed as droplets, using a print head, to join the loose powder spread on a build platform. The next step follows binder removal and sintering of the green parts. High build rates and high-resolution parts characterize the BJ, although it requires free-flowing coarse powder and low-density parts and poses challenges during powder removal of the green parts. The inherent presence of residual porosity in sintered ceramics using BJ has been exploited effectively to make scaffolds for bone tissue engineering applications [31,32]. Alternatively, PCPs can be used as non-sacrificial binders for structural and other engineering applications, enabling good powder compaction and interconnection and enabling high-density parts to be added for low sintering temperatures [33].

Material extrusion (ME) based AM methods use inks, slurries, or pastes, consisting of solvents, gels, thermoplastics/ thermosets loaded with high concentrations of desired ceramic powder or PCPs, that are extruded/ dispersed through an orifice/ nozzle and printed on a build platform, either at room temperature or at high temperature depending on the feedstock. Critical AM technologies in this category are Fused Filament Fabrication (FFF) or Fused Deposition Modeling (FDM), and Direct Ink Writing (DIW). One unique advantage of ME technologies is their utility in processing a wide range of materials [34], multi-material, continuous fiber-reinforced composites [35,36], and functionally graded ceramic parts [37] production. However,

ME processes suffer from limited resolution, printing speed, and bonding between layers and adjacent beads. Controlling the feedstock viscosity is critical to ensure consistent flow through the print head.

Powder Bed Fusion (PBF) methods involve sintering or melting dry powder bedspread on the build platform to create solid layers using high-power lasers. These processes are called selective laser sintering (SLS) and selective laser melting (SLM), depending on the state fusion (solid state or liquid state). These are the only AM technologies that can produce relatively strong solid ceramic parts in a single step. However, poor thermal shock resistance of ceramics often results in cracks in the parts because of the high thermal gradients involved in these processes.

Nevertheless, various ceramics and composites have been attempted using these PBF technologies [1–3,7,10].

The ceramic sheet lamination (SL) process can manufacture ceramic parts of simple shapes by sequential stacking, cutting, and bonding thin ceramic tapes in the green state, followed by standard high-temperature sintering. This technology has also been used to manufacture monolithic ceramics [1,3] and ceramic composites [3,10]. However, the major drawbacks of this process include layer delamination, property anisotropy, and limited part complexity and size.

Material Jetting (MJ) process, Inkjet Printing (IJP), fabricates parts by selectively depositing droplets of ceramic inks (build materials) into 3D objects directly on a substrate using a print head. The printed objects are dried and sintered to obtain solid ceramic parts. The ceramic inks are made using submicron ceramic particles $(10 - 60 \mu m)$ suspended in appropriate solvent or wax. IJP's success depends on ceramic inks' characteristics, such as solids loading, rheology, and

particle size. Although it is a highly versatile process for fabricating miniature ceramic structures, segregating ceramic powder in the dry parts is a significant challenge.

 Table 1. Popular AM technologies for ceramic component manufacturing.

Basic principle	Process category* (Process Steps)	Printing technology	Feedstock	Bonding type	Materials	Potential applications
Light reactive photopolymer curing	Vat-Photopolymerization [1–3,7,10] (Two-step process)	Stereolithography [5,20,21,38,39] Digital Light Processing [5,26,27,40–50] Direct Ink Writing [44,51–59]	Photocurable liquid with powder suspension	Chemical reaction	Al ₂ O ₃ [20,38,40,60]; SiO ₂ [21, 129] [21,61]; ZrO ₂ [26,39,50,62]; SiC [5,27]; HA/TCP; TCP [63]; Bioactive glass [44,45]; TiC [41]; SiOC [5,51,64]; SiC [5,13]; SiCN [27]; YAG [46]; BaTiO3 [47] Al ₂ O ₃ -SiC _w ; SiC-C _{sf} [34,65,66]; SiCN-SiC _{sf} [27];	Functional ceramics, dentistry, precision components, Very high precision components, scaffolds,
Solvent reactive curing	Binder Jetting [31–33,67] (Two-step process)	Binder Jet Printing [16,18,68–72]	Powder		Al ₂ O ₃ [16,18,71]; ZrO ₂ ; HA [69,73–76]; TCP [68,77–79]; MgO/ZnO-TCP; CaSiO ₃ ; SiC [18]; SiC-SiC _w ;	Casting molds, infusion preforms, microporous scaffolds

	Material Extrusion [34–37,41,54] (Two-step process)	Fused Filament Fabrication [24,80] Direct Ink Writing [25,40,41,66,80– 94]	Powder-filled filament, paste	Thermal reaction	[24,66,80,5] SiOC [40,4] SiC-C _f [80] SiC-SiC _w ; [97]; SiO ₂ -	Al ₂ O ₃ [24]; ZrO ₂ ; Si ₃ N ₄ [24,66,80,86]; Mullite-Al ₂ O ₃ ; SiOC [40,41]; SiC-C _{sf} [95]; SiC-C _f [80]; B4C/SiC [96]; SiC-SiC _w ; ZrB ₂ -SiC-SiC _{sf} [97]; SiO ₂ -SiO _{2f} ;	Structural parts, functional ceramics, precision components, scaffolds
Selective fusion of material in a powder bed	Powder Bed Fusion [1–3,7,10,28,98–100] (Single/Two-step process)	Selective Laser Sintering [14,15,17,100– 102] Selective Laser Melting [28,29,98– 100,103,104]	Powder		Al ₂ O ₃ [14,15,17,28]; ZrO ₂ [28,29,99]; ZrO2-Al ₂ O3 [98,100,105,106]; Al ₂ O3-ZrO2-SiO ₂ [233] [102]; SiOC/SiC-SiC; Si ₃ N ₄ -SiC-Mullite; SiC-C _{sf} ;	Casting molds, infusion preforms, microporous scaffolds	
Multi-jet material printing	Material Jetting [19] (Two-step process)	Ink Jet Printing [8,19]	Powder filled liquid	Thermal/ Chemical reaction	Al ₂ O ₃ ; ZrO ₂ [19]; SiC; Si ₃ N ₄ ; MOSi ₂ ; 3Y-TZP [8]; PZT; TiO ₂ [19]; LSM-YSZ; LSCF- CGO;	Functional ceramics, precision components, scaffolds	
Fusion of stacked sheets	Sheet lamination [1,3,10,22,23]	Laminated Object Manufacturing	Sheet material	Thermal reaction	Al ₂ O ₃ [22]; ZrO ₂ [23]; SiO ₂ ; Si ₃ N ₄ ; SiC; RBSiC; LZSA; Si/SiC; ZrO ₂ /Al ₂ O ₃ ; TiC/Ni;	Structural parts,	

(Two-step process)		LZSA; Ti ₃ SiC ₂ ; SiOC-Si-SiC;	large parts

 $^{1. \}quad *ISO/ASTM\ 52900: 2015 (E): Standard\ Terminology\ for\ Additive\ Manufacturing\ -General\ Principles\ -Terminology.$

1.3. Ceramic AM for different industrial sectors

Despite significant progress in ceramic 3D Printing, eliminating defects and residual porosity in the final parts to achieve the desired mechanical and functional performance is challenging. Therefore, most ceramic parts made using 3DP technologies are first utilized in different industrial sectors where porosity benefits specific applications such as lightweight structures, filters, and scaffolds for tissue engineering applications. At the same time, the rapid increase in the current research efforts to fabricate bulk ceramics using a variety of 3DP technologies is expected to expand the applications in other industrial sectors as well. The key industrial sectors that can benefit from ceramic 3DP include biomedical, aerospace/space, defense, automotive, energy, and chemical processing.

For biomedical applications, ceramic implants with appropriate porosity characteristics provide excellent tissue ingrowth, followed by faster osteogenesis, integration, and healing. Therefore, the application of ceramic 3DP with the ability to create such ceramic implants with designed and controlled/ hierarchically graded porosity characteristics (mimicking natural bone) fueled its early growth and adaption in the biomedical sector [32,107]. Similarly, manufacturing of patient-specific customized ceramic implants from patients' CT/MRI scan data for rapid and early-stage stabilization, integration, and healing is only possible through 3DP [108]. Core and molds for turbine and aerofoil components [109] with complex internal cooling channels can be easily made using ceramic 3DP to reduce overall design cycle time and development cost in the aerospace sector. Enhanced turbine efficiencies can be expected from ceramic turbine components (SiC, SiC_f/SiC composites, β-SiALON) made using 3DP [110,111]. The processing flexibility offered by PCPs feedstock to fabricate advanced ceramics and ceramic composites through 3DP (Table 1) greatly enhanced its application potential for high-temperature resistance

component manufacturing, with macro/micro/nanometer lever resolution/features [5,112], for aerospace applications [3]. The energy sector includes various applications such as turbines, heat exchangers, batteries, supercapacitors, fuel cells, powder plants, etc., where ceramic 3DP can potentially and economically create complex parts/devices tailored to enhance efficiency and performance [12]. Ceramic 3DP enabled the fabrication of advanced electrode architectures for batteries to enhance their electrochemical performance in high power/energy density, cycling lifetime, and mechanical performance [113]. Another unique application is stimuli-responsive smart glass devices for energy generation, transmission, and conversion from windows to wearable electronic devices. Catalytic converters and heat exchanges for different energy applications are unique areas where highly complex honeycomb structures with twisted channels [114] and triply periodic minimal surface structures [115] can be easily manufactured using ceramic 3DP for high efficiency. Nuclear energy generation also finds numerous areas to utilize 3DP capabilities to create ceramic components, such as flow channel inserts [116], ceramic breeder parts, and fuel assemblies [117]. Irrespective of industrial sectors, ceramic 3DP offers functional gradation (in materials and geometry), customization, and geometrical complexity at relatively lower cost and production lead times than traditional ceramic manufacturing.

2.0 3D Printing processes

2.1. Binder Jetting

2.1.1. A Historical Overview and Methodology: Binder jetting, a prominent 3D printing process, traces its origins to the late 1980s, pioneered at the Massachusetts Institute of Technology (MIT). In 1993, Emanuel Sachs secured a patent for this groundbreaking technology, utilizing gypsum powder in conjunction with a binder comprised of glycerin and water [118].

Subsequently, industry leaders, including ExOne (PA, USA) and Z Corporation (SC, USA), undertook commercialization efforts. Today, binder jetting is significant among the seven major additive manufacturing processes delineated within ASTM F2792. The fundamental setup of binder jetting involves a powder source, spreading the powder layer onto a build stage. A roller compacts the powder to a precise, uniform slice thickness, with excess material redirected into a powder collection bin. Heat treatment of powders above 100°C before printing is preferred to remove humidity and eliminate agglomerates for uniform powder spreading [71]. Simultaneously, a print head equipped with multiple nozzles dispenses binder droplets onto the build stage, typically employing a thermosetting resin as the binder material, with droplets sized at approximately 10-30 pl, conforming to the CAD design [119]. A heat source is then utilized to facilitate the drying of each layer, and this layer-wise process is iterated until the final layer is complete. It is important to note that while the binder jetting process is notably faster than powder bed laser systems, the subsequent post-processing steps incur both time and energy expenses, consequently augmenting the overall manufacturing costs of the final components. After the printing phase, the parts are carefully removed from the powder bed and subjected to binder curing via heat treatment, vacuum treatment, or exposure to visible light, contingent upon the binder type employed [120]. After curing, the trapped powder is removed from the printed part using an air blower called "depowdering." The part obtained after curing and depowdering is called a green part, which does not have enough strength and undergoes sintering or infiltration to achieve densification and proper mechanical strength [121,122]. Before sintering, these parts must undergo binder burnout, accomplished through thermal de-binding, catalytic de-binding, or solvent extraction [123]. Figure 2 shows an overview of the binder jet process and binder jet fabricated sintered parts of various ceramic compositions. One of the significant advantages of

binder jetting over other 3DP techniques involves its high production rate and high production volume. It also does not involve a support structure during printing for any geometry and reduces the chances of oxidation, residual stresses, and phase change since the process occurs at room temperature and in the atmosphere [124]. It is worth noting that challenges often arise during the post-sintering phase due to ceramic shrinkage, necessitating meticulous optimization in both design and printing operations to attain the precise dimensions requisite for a functional component.

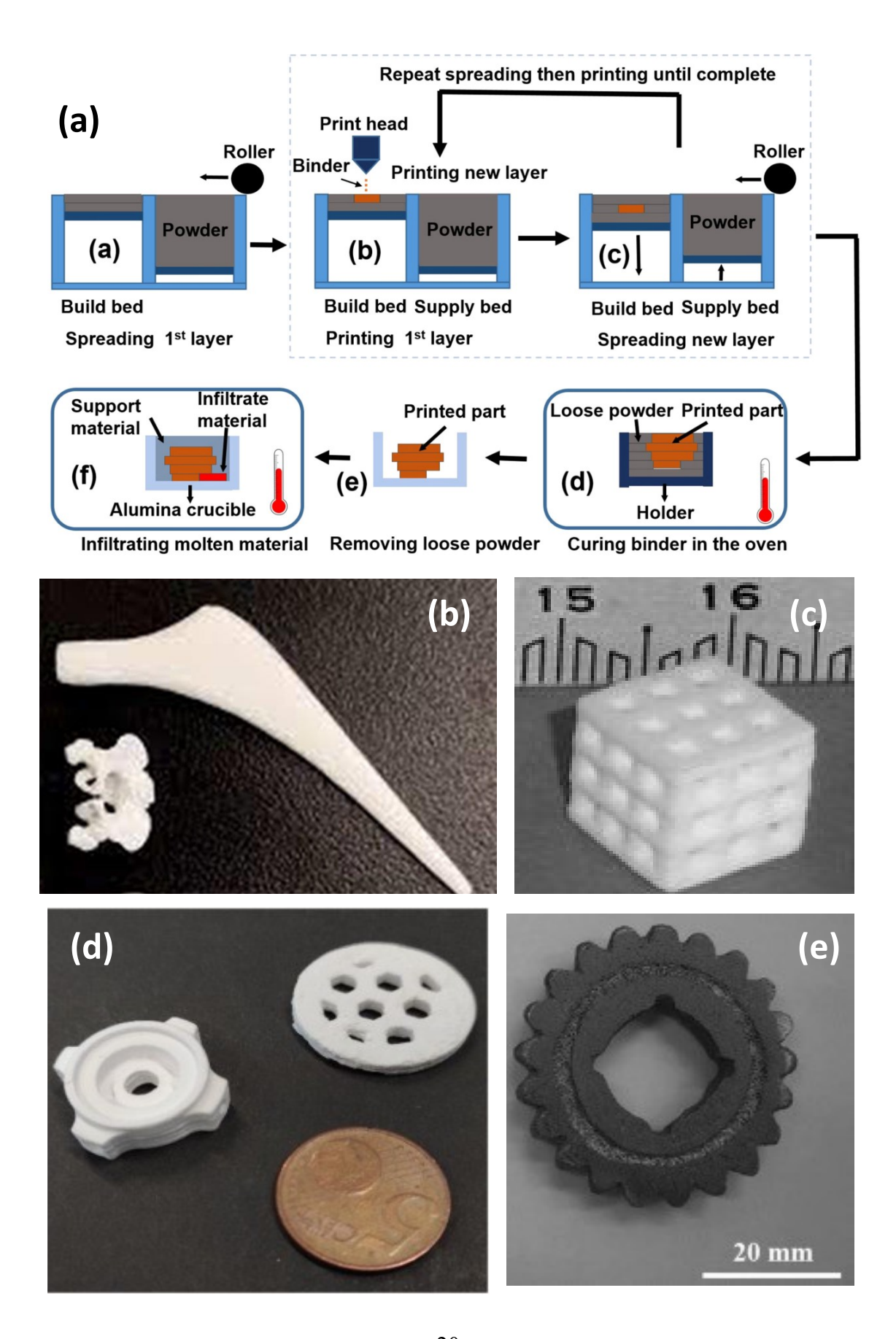


Figure 2. An overview of the binder jet process and parts fabricated via binder jet demonstrating its potential to process complex shapes across different ceramic materials. (a) Process flow schematic of a typical binder jet process [125]; (b) Hip stem and human pelvis fabricated via binder jetting of tricalcium phosphate (TCP) [68]; (c) lithium alumino-silicate porous bone-substitute implant [70]; (d) binder jet printed alumina parts [71]; (e) near-net shape printed part composed of Ti-Al-O-C composite [72].

2.1.2. Factors influencing print quality: Despite its apparent simplicity, the ultimate quality of binder jetted parts is contingent upon many variables. These include the characteristics of the feedstock powder, factors such as flowability, shape, particle size, and particle size distribution, as well as properties intrinsic to the binder itself, including viscosity, chemical stability, interactions with the powder material, binder saturation, and binder composition. Successful parts fabrication through binder jetting necessitates a rigorous optimization process encompassing binder composition, powder attributes, and printing parameters. It is essential to recognize that these characteristics exhibit variability contingent upon the specific composition of the ceramic powder being used, rendering binder jetting a process that lacks versatility when applied across diverse ceramic compositions. Nevertheless, it remains a highly sought-after 3DP technique for ceramics due to its inherent advantages, including the printing process and minimal capital investment requirements compared to laser-based alternatives [73]. This versatility empowers the creation of intricate and diverse designs and structures, cementing binder jetting's significance within ceramics 3D Printing.

2.1.2.1. Powder characteristics: The printability of ceramic components via binder jetting hinges on critical powder characteristics such as flowability, tap density, powder particle shape, size, and distribution. The resolution of the green part depends on the uniformity of powder spread in each layer, a factor heavily influenced by the flowability of the ceramic powder. Poor flowability can lead to in-built defects and undesired internal porosities in the final parts. The shape of ceramic particles is pivotal in determining flowability and packing density. Spherical powders typically exhibit superior flowability compared to irregularly shaped particles. However, while demonstrating good flowability, spherical powders engage in point contact postroller compaction, resulting in higher pore volumes. In contrast, irregularly shaped particles with increased contact overlap exhibit higher packing density, yielding a final part with enhanced bulk density. This phenomenon was demonstrated by Suwanprateeb et al., who observed a 32% higher sintered density and a 20% reduction in porosity in irregularly shaped hydroxyapatite powders compared to their spherical counterparts [76]. A trade-off between flowability and sintered density is inherent in the binder jetting process. Spherical powders facilitate optimal flowability and layer spreading during binder jet operations, whereas irregularly shaped powders contribute to a final sintered part with higher density.

The resolution of binder jetted parts is intricately linked to the layer thickness employed during printing. A lower layer thickness corresponds to a higher resolution of the final part. However, the lowest feasible layer thickness depends on the highest powder particle size. Binder jet operations typically employ particle sizes of 0.2-200 µm. Smaller particle sizes increase Vander Waal forces, causing particle agglomeration and affecting powder flowability. The wettability of the binder is another critical parameter; the binder droplets penetrate the powder layer via capillary action into interparticle pores. It is important to note that the selected binder

should wet the powder particles. Irregularly shaped powders, with greater contact between flat surfaces, exhibit superior wettability compared to spherically shaped powders, which form point contacts at the necks of the pores. Particle size distribution plays a significant role in powder-based 3D printing as it determines the packing density, binder saturation level, and final surface finish [124]. Utilizing multimodal powder emerges as a strategy to enhance part quality and resolution where coarse powder particles ensure good flowability while finer powder particles occupy the pores formed by coarser powders, reducing pore volume and improving overall packing density. Sun et al. demonstrated this concept by achieving increased density (1.6 g/cc) and flexural strength (13.8 MPa) in glass-ceramic materials through a blend of 60% 45-100 µm powders and 40% 1-25 µm, as opposed to 100% monomodal powders of 45-100 µm, which exhibited lower density (1.45 g/cc) and flexural strength (3.5 MPa) [126]. No consensus exists on the optimal particle size, shape, and distribution for binder jetting. Achieving a high-resolution sintered part with increased density necessitates meticulous optimization of available powder particle characteristics alongside printing parameters.

2.1.2.2. Binders: The judicious use of binders is a pivotal factor influencing the quality of parts in the binder jetting process. As previously mentioned, a binder is precisely deposited onto the powder layer through the print head, filling up the pores in each layer via capillary action and eventually creating the desired shape. An ideal binder must exhibit low viscosity and stability against the shear forces induced during printing, be printable, have favorable interaction with powder material, and have an extended shelf life [127–129]. The low viscosity will ensure a smooth flow of individual binder droplets onto the layer and then break off from the print head nozzle easily [127]. It is also important to note that the binder solution should have a boiling

point higher than room temperature to avoid being solidified during printing, and the binder resin should not cross-link during storage and transport. Given the typically monomeric nature of binders and their inherent toxicity, using environmentally low-risk binders is a noteworthy advantage. Optimization of the binder saturation level is a critical parameter that affects the final part resolution. Higher binder saturation may lead to unwanted penetration into the current and previous powder layers, potentially distorting the part resolution [130]. The inherent challenge lies in the limited versatility of binder composition, with specific binders tailored for distinct ceramic compositions to ensure optimal binder-powder interactions and produce high-quality final parts. The particle binding mechanism is categorized into two primary methods: In-liquid and In-bed binding. In-liquid binding relies on the binding action of the jetting liquid, while Inbed binding involves jetting a rheologically simple liquid onto the powder layer along with dry glue particles, facilitating binding upon hydration. In-bed binders often result in voids, as the additives dissolve in water during printing. Conversely, In-liquid binders leave minimal to no residue upon thermal degradation; however, they can cause failure of the printhead due to drying the binder in the nozzle [118]. The binder is often infused with nano-ceramic particles to improve the sintered density and reduce shrinkage. The goal is to fill the voids or interstitial space left by coarse particles during printing [131].

2.1.2.3. Printing parameters: Following the optimization of powder particle and binder characteristics, achieving the desired part density and resolution in the binder jetting process is contingent on carefully selected printing parameters. Starting with the layer thickness, this dimension must exceed the particle size of the largest ceramic powder used. This is usually governed by the resolution and powder particle size. Sachs et al. recommended a layer thickness

at least three times the highest particle size to ensure optimal powder flowability [132]. Higher layer thicknesses may compromise green strength due to reduced powder bed density and inadequate binder penetration. Zhang et al. also showed increased power density and mechanical strength of alumina/glass composite using a binder jet with lower layer thickness [133]. Empirical evidence indicates that the most favorable combination of layer thickness and green body strength lies within 80-130 µm [74,134–139]. Layer thickness could also be affected by powder size distribution as it affects the flowability and spread of the powder to form a desired layer thickness.

After layer thickness, printing speed is another critical parameter that governs the printing step. The printing speed here includes recoat speed (mm/s), roller transverse speed (mm/s), and roller rotation speed (rpm). Recoat speed is the speed of the recoater during powder deposition. The roller transverse speed is the speed at which the roller moves through the powder bed, and the roller rotation speed is the speed at which it rotates while moving across the powder bed [140]. These different speeds and their coordination are necessary factors that need optimization depending on powder type and flowability to obtain desirable parts. Within binder jetting, different types of recoater type have been used to print parts. While the rolling type recoater type results in an inhomogeneous powder layer, the box-type recoater causes non-uniform powder flow from powder aggregation. A recent recoater type, which includes a V-shaped recoating unit with piezo activation, avoids powder aggregation and leads to the formation of a homogenous layer [141,142].

Like layer thickness and printing speed, optimizing binder saturation is a critical step, defined as the ratio of binder droplets jetted from the print head to the volume of interparticle pores in the powder layer. While a high binder saturation is desirable for achieving adequate

green strength and high density, it inevitably results in prolonged printing operation durations. Pereria et al. conducted a notable study illustrating increased binder saturation's impact on enhancing calcium phosphate's bulk density and compressive strength [143]. The orientation of the sample during the build process emerges as a crucial determinant of both strength and surface roughness. A generally preferred approach is to position the high aspect ratio of a single layer in the x-y plane, with the layer height along the z-direction. This orientation in the x-y plane promotes stronger bonding within a single layer compared to the inter-layer bonding along the z-direction. Castilho et al. demonstrated a tangible difference in compressive strength for tricalcium phosphate, showcasing 19 MPa when printed along the y-direction versus 14.4 MPa when the part was oriented along the z-axis [136]. This insight highlights the substantial impact that build orientation can exert on the mechanical properties of the final printed part.

Consequently, thoughtful consideration of build orientation is vital for achieving the desired strength and surface finish combination in binder jetting applications.

2.1.2.4. Post-processing: Following the binder jetting process, a green body is obtained, characterized by a lack of strength, necessitating subsequent sintering to obtain the high-density body. Ideally, the packing density of the green part should be around 60% of the ultimate density of the ceramic [144]. The following step, crucial for achieving desired properties, involves depowdering to remove residual powders from the pores of the printed structure. De-powdering impacts the surface roughness of the final part, as an inadequate process may leave residual powder particles on open surfaces, leading to elevated roughness post-sintering. De-powdering methods include force application throughout the vibration during printing [75], needle-assisted compressed air treatment [145], or the use of boiling fluid within the pores [146]. The selection of the de-powdering technique is contingent on the printed part geometry and design complexity.

After de-powdering, the printed parts undergo the binder removal step. This is typically done through thermal debonding, solvent extraction, or catalytic debinding, followed by sintering [123]. The sintering process involves inter-ceramic particle bonding through atomic diffusion at elevated temperatures to produce dense parts. The sintering temperature is an inherent property of the ceramic composition, and external factors such as powder particle shape and size influence sintering kinetics. Due to a larger contact angle between particles, irregularly shaped particles favor sintering behavior compared to spherically shaped particles that tend to undergo necking during diffusion, resulting in higher residual porosities [76,147]. Reduction in the surface energy is the driving force in sintering; finer particles, possessing higher specific surface energy, promote the sintering process compared to coarser particles [148]. Different sintering methods have been utilized to achieve denser parts with improved mechanical properties. The conventional sintering technique involves the heat energy from an outside heating element. The heat travels from outside to inside through radiation, conduction, and convection. This generates

the temperature gradient and the internal stresses, which cause undesirable defects in the sintered part [149]. Microwave sintering is an advanced technique involving volumetric heating of the part. A microwave is a form of electromagnetic energy with a frequency of 0.3-300 MHz. Here, the material absorbs the microwave energy through electromagnetic radiation and transforms this radiation into heat energy throughout the material [150]. This causes uniform heating and shorter sintering time with controlled grain growth and higher densification when compared with conventional sintering [78].

As highlighted earlier, shrinkage is a critical consideration in the solid-state sintering of ceramics. Meticulous optimization of the designed part's dimensions is imperative to achieve the final sintered part with the required dimensions. Rigorous attention to these factors ensures the successful transformation of green bodies into fully sintered parts with the desired structural integrity and dimensional accuracy.

2.2. Stereolithography of ceramics

2.2.1 Brief history and methodology

Stereolithography (SLA), also known as 'vat photo-polymerization' (VPP), represents the pioneering 3D printing technique developed in the 1980s by Chuck Hull. Initially designed to fabricate photopolymers, SLA's application extended to ceramic fabrication in the 1990s [20]. The SLA process entails a liquid monomer-ceramic particle suspension within a vat, with the build stage moving along the z-direction, **Figure 3a.** A point laser or light source emitting UV-range wavelengths cures the liquid precursor—a photopolymerizable monomer with homogeneously dispersed ceramic particles of nano or micrometer size—onto the build plate as

per the design specified in the CAD file. The build stage progressively descends throughout each layer, covering the preceding layer with the liquid precursor, followed by laser curing. This iterative process continues until the completion of part fabrication, yielding the green part—a cured photopolymer network with ceramic particle inclusions. After fabrication, the green body undergoes post-processing, which encompasses pyrolysis to remove the organics, leaving behind the ceramic structure. This is followed by sintering the ceramic at high temperatures to achieve a purely ceramic structure devoid of polymer traces. Stereolithography's versatility and precision in ceramic fabrication have propelled its adoption across various industries, including aerospace, automotive, and biomedical [2]. As research advances and technology evolves, SLA remains a leading 3D printing technique for ceramic production, offering intricate geometries and precise components that meet the demands of modern manufacturing processes.

In 1996, Yamaguchi introduced a groundbreaking advancement in the field of Stereolithography (SLA) known as 'digital light processing' (DLP), which was further refined by Bertsch et al. in 1997 [151,152]. DLP, similar to SLA, operates by progressively lowering a build stage with each layer. However, it distinguishes itself by employing a mask-based UV light source, typically utilizing a liquid crystal display (LCD) as the dynamic mask generator. This innovation enabled rapid curing of entire layers of photopolymerizable liquid in moments, in contrast to the point curing method employed in traditional SLA. The utilization of ultra-fast light switching and integral projection in DLP significantly reduces printing time compared to SLA. DLP achieves higher resolutions for printed parts than conventional SLA methods [153]. Similar to SLA, the maximum part height achievable in DLP was initially constrained by the height of the build chamber. A significant advancement in DLP technology was made to overcome this limitation, replacing the top-bottom approach with a bottom-up approach, Figure

3b [154]. The key distinction lies in the positioning of the digital light projector: in the top-bottom approach, the projector is located above the curable monomer layer, whereas in a bottom-up approach, it is situated at the bottom of the system, separated from the chamber by a glass window. The build stage is inverted, and ensuring proper curing of the initial layer and its adhesion to the build plate is crucial to prevent part failure. As each layer cures, the build stage ascends within the monomer chamber, while liquid resin flows between the gap beneath the light projector window and the preceding layer, followed by curing of the subsequent layer.

Many factors, such as resin matrix and printing parameters, influence the quality of the final part produced via SLA or DLP. Achieving accurate dimensionality, structural integrity, and surface quality necessitates meticulous optimizations [155,156]. Printing parameters such as layer thickness, exposure time of UV source, and scanning speed further need optimizations along with resin matrix characteristics for a successful printed green body part with accurate dimensionality, structural integrity, and surface quality. The layer thickness determines the final resolution of the printed part. The exposure time of the UV source governs the degree of polymerization and curing of the resin matrix. Precise exposure time control is essential to achieve uniform curing and prevent under- or over-curing. The UV source's scanning speed affects the polymerization and curing rate. Alumina (Al₂O₃) and zirconia (ZrO₂) are among the most commonly used ceramic materials in SLA [38,39]. These materials offer a combination of desirable mechanical, thermal, and chemical properties, making them well-suited for a wide range of applications across various industries. Figure 3 (c-f) shows complex structures printed using stereolithography and digital light processing.

2.2.2 Process and printing parameters

The resin for the ceramic stereolithography contains ceramic powder, a dispersant, and a monomer solution [62]. The process starts with adding the fine ceramic powder to the photocurable resin. Many parameters need optimization for the successful printing of ceramic parts, with ceramic suspension characteristics playing a pivotal role in achieving proper dispersion and homogeneity of particles throughout the resin matrix. Adding organic additives and surfactants can enhance dispersion, reduce viscosity, and improve wetting characteristics, facilitating the uniform distribution of ceramic particles.

For a high-precision and defect-free part, the ceramic suspension should exhibit good rheological behavior, including long-term stability and workable viscosity. The particles in the slurry should be uniformly suspended and remain stable until the printing is complete. The viscosity of the ceramic slurry depends on the extent of the solids loading. With an increase in the loading of ceramic particles, the viscosity of the slurry increases. However, while a low-volume fraction of ceramics particles causes high shrinkage and low density in the final part during sintering, a high-volume fraction of ceramics particles makes slurry too viscous to work with. Proper optimization needs to be done to ensure high-quality parts.

During printing, cured depth and width are critical for final part accuracy. Multiple factors influence cured width, including powder characteristics, particle size and refractive index, resin polymer properties, and ceramic slurry characteristics, such as ceramic volume fraction, interparticle distance, and irradiation wavelength. Maintaining low cured width ensures high resolution and precision in the final part [73]. Achieving high-quality, functional parts via SLA necessitates meticulous optimization of the resin matrix and printing parameters. By carefully managing these variables and selecting suitable ceramic materials, manufacturers can produce

components with desired dimensional accuracy, structural integrity, and surface quality, meeting diverse application requirements.

2.2.3 Post-processing

Post-processing treatment is one of the critical steps that determines the properties of the final part. Different post-processing steps include UV curing to cure the uncured resin, removal of the support structure from the part, and densification. The green parts usually undergo debinding to remove the binder or other organic residue from the printed part. This leaves behind a fragile ceramic structure with poor mechanical properties. Based on the powder sensitivities, the debinding step can be carried out in different environments. In a study utilizing stereolithography of alumina, the samples were debinded in air, argon, and vacuum [157]. The results showed that debinded samples in the air showed better flexural strength and relative density. In the air environment, the exothermic reaction was favored for debinding, while under the argon environment, the endothermic reaction took place, which made a difference in the final properties. After the debinding step, the parts undergo sintering to achieve the desired part with improved densification and mechanical properties. Like debinding, this step is carried out at an elevated temperature, leading to further shrinkage. However, no polymer removal or decomposition occurs. Different sintering approaches include solid-state sintering, liquid-phase sintering, and precursor infiltration [64]. Depending on the material type, part size, solids loading, and particle size, the post-processing steps can vary and, therefore, need proper optimization to ensure defect-free parts [158].

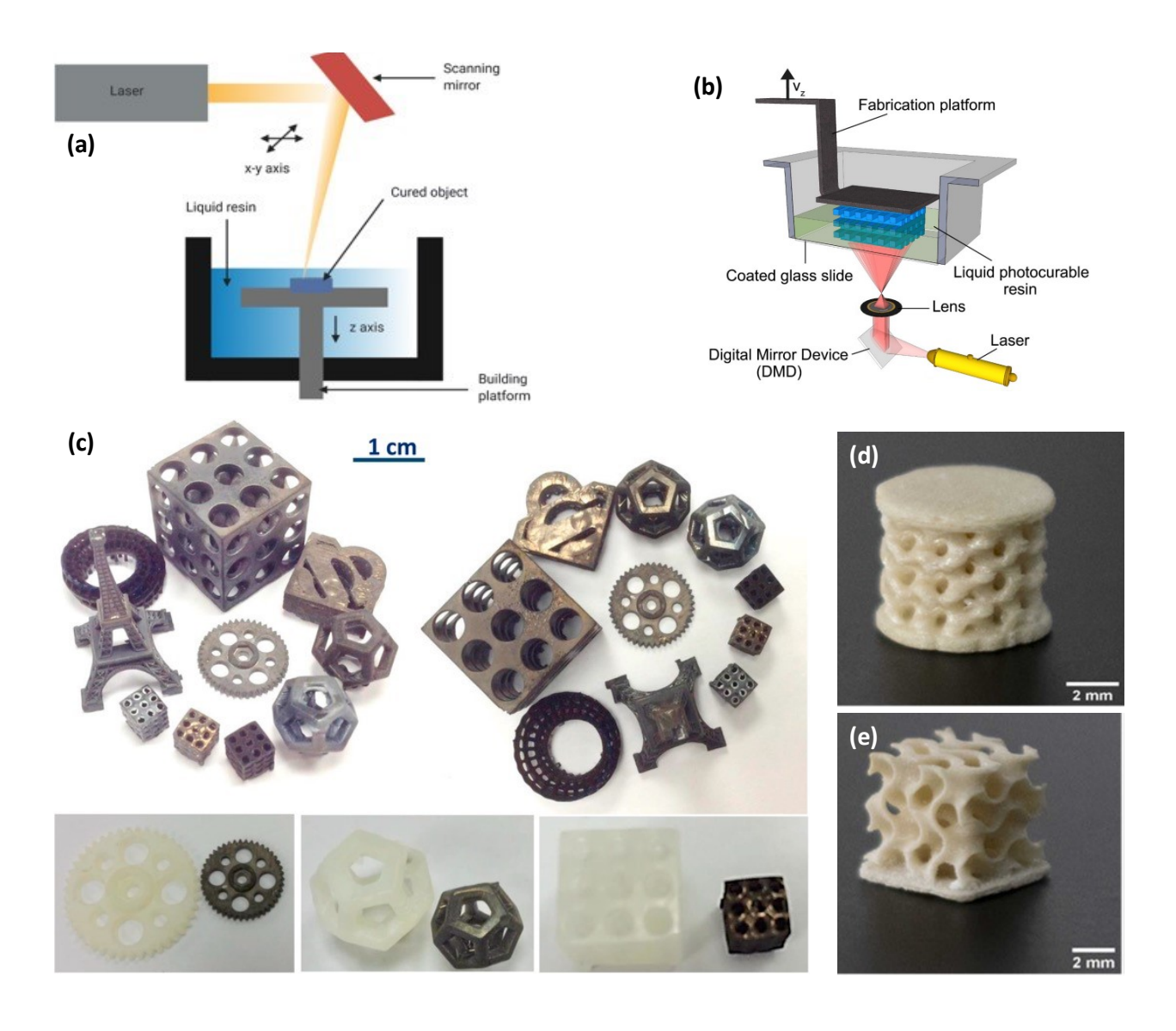


Figure 3. Schematic of (a) point curing by stereolithography [159]. (b) bottom-up digital light processing (DLP)[160] (c) Silicon carbide ceramic part was prepared using stereolithography on a pre-ceramic polymer. Below is a comparison between the green and sintered parts[5]. (d,e) Barium Titanate complex parts are fabricated using digital light processing 3D printing technology [161].

2.3. 3DP of Ceramics from Liquid Precursors

Most 3DP technologies for ceramics are typically based on the use of powders that are either employed to form a dry powder bed, such as in BJ, SLS/SLM or are continuously supplied to a heat source, as in DED or are embedded into solid or liquid polymers/photopolymers to generate filaments or pellets (FFF), tapes (LOM), slurries (IJP) or photocurable slurries (SLA/DLP). The choice of powder characteristics is determined not only by the requirements of the part to be produced but is often influenced by the specific AM technology adopted for the fabrication.

For instance, the use of fine particles that promote sintering and the high particle loading desirable in photocurable slurries in SLA/DLP, TPP result in very high viscosities, requiring the implementation of suitable ways for generating homogeneous thin layers to be cured in the layer-wise process, such as the use of a rotating blade/vat or a tape-casting approach, leading to significantly increased equipment complexity and cost. Moreover, particle stabilization in a non-aqueous medium is often tricky, causing segregation phenomena within the slurry that are incompatible with the long printing times required. Furthermore, the difference in refractive index between the particles and the surrounding liquid leads to the loss of resolution because of scattering and, together with high absorbance for some materials, can significantly reduce the penetration depth of the radiation. When particles have to flow through a nozzle, the maximum particle size determines the minimum acceptable nozzle diameter, thereby limiting the printed part's size and surface quality. Additionally, clogging of the nozzle can often occur.

The presence of particles causes all of the above issues and can be avoided if a liquid precursor is used instead [41]. Such precursors include preceramic polymers [162] and sol-gel solutions [163]. It is noteworthy to observe that they allow for the production not only of

ceramics but also of glasses and glass ceramics and that the transformation from a precursor to a ceramic material occurs via a thermal treatment, typically in a controlled atmosphere. Naturally, the use of fully liquid feedstocks for 3DP of ceramics has its disadvantages; for instance, they cannot be used in BJ, SLS/SLM, DED, or FDM technologies either due to intrinsic limitations in the technologies themselves or because current equipment is not structured to handle liquid systems. Furthermore, the compositional range of the resulting ceramics is somewhat limited when using preceramic polymers since, typically, only silicon-based materials are available. Solgel systems are much more versatile in terms of the ceramic compositions that can be achieved but suffer severely from low strength and drying defects when in the gel stage, making the fabrication of quality parts very challenging.

Preceramic polymer-based, low viscosity, and highly transparent fully liquid photocurable solutions have been successfully employed in a variety of 3DP technologies, such as DLP, TPP, and VAM, enabling the fabrication of defect-free parts with feature sizes in a range from the sub-micron to the hundreds of microns [3]. Photocuring ability can be provided to the precursor by grafting photocurable moieties [164] or blending the preceramic polymer with a photocurable polymer [42]. Click chemistry obtains a high ceramic yield and preceramic thermoset parts using conventional DLP [43] or self-propagating photopolymer waveguide technology [112].

By controlling the rheology of the solution, for instance, adapting the precursor concentration, adding fillers, or exploiting the fast evaporation of a solvent, intricate architectures with spanning features can be manufactured by DIW [52,53] and the use of elastomeric preceramic polymers enables the fabrication of complex 3D structures starting from 2D sheets further processed by origami [43]. The addition of inert/reactive/sacrificial solid

particles or fibers to the all-liquid preceramic polymer solutions allows for the production of parts possessing porous struts [165], CMCs [55], or bioceramics [56]. SiOC, SiC, SiCN, and advanced oxide ceramic parts have been obtained employing the above AM approaches. Some examples of parts produced using preceramic polymer-based feedstocks and the different technologies above are reported in **Figure 4**.

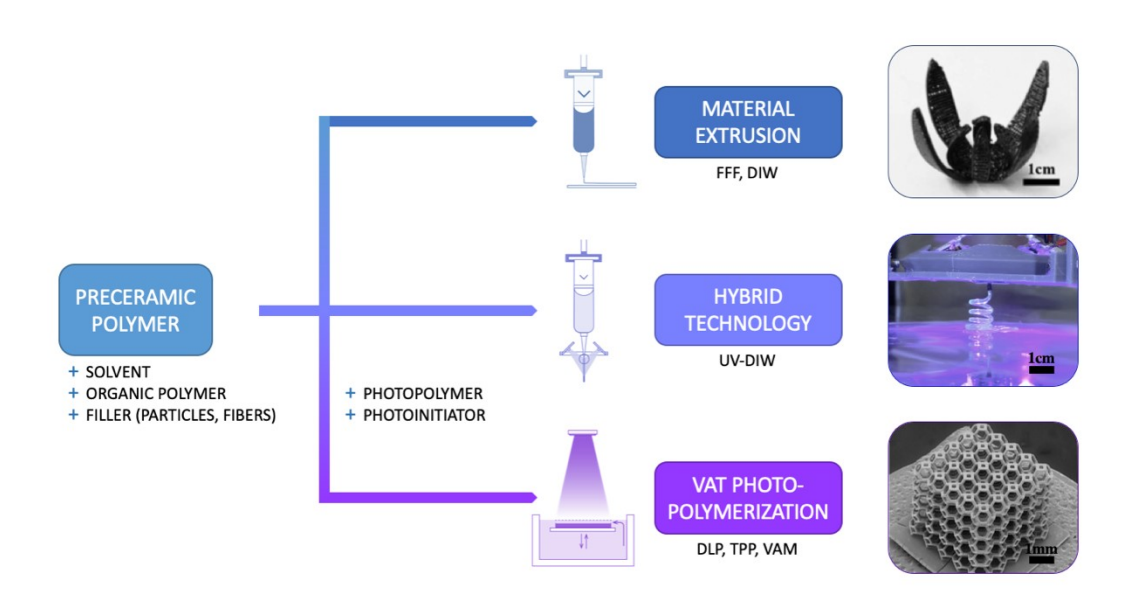


Figure 4. Flowchart of the fabrication of preceramic polymer-derived parts using different AM technologies - material extrusion [54], vat photopolymerization [42], and a novel hybrid approach [41].

The use in 3DP technologies of sol-gel solutions, either based on alkoxides or salts, has been so far limited to very few examples, such as glass [44,45], mesoporous silica [61], yttrium aluminum garnet [46], barium titanate [47] and titanium carbide [41] for DLP. Moreover, organic-inorganic hybrid materials can also be obtained [48], further extending the range of applicability of the approach. DIW has also been successfully used to produce silica, silica-titania, and silica-

germania glasses [57,166,167]. The complex microstructural development of titania sol-gel inks during printing has been investigated *in situ* [58]. It has been demonstrated that sol-gel precursors, particularly silicon alkoxides, can undergo thermal crosslinking and develop glass phases also without previous hydrolysis and condensation; therefore, they have been embedded in DLP inks [49] as well as in colloidal suspensions for spatial UV-assisted DIW, where they act both as rheology and sintering aids [59]. **Figure 5** highlights the versatility of the feedstocks containing sol-gel precursors in terms of applicable technologies and different compositions that can be produced.

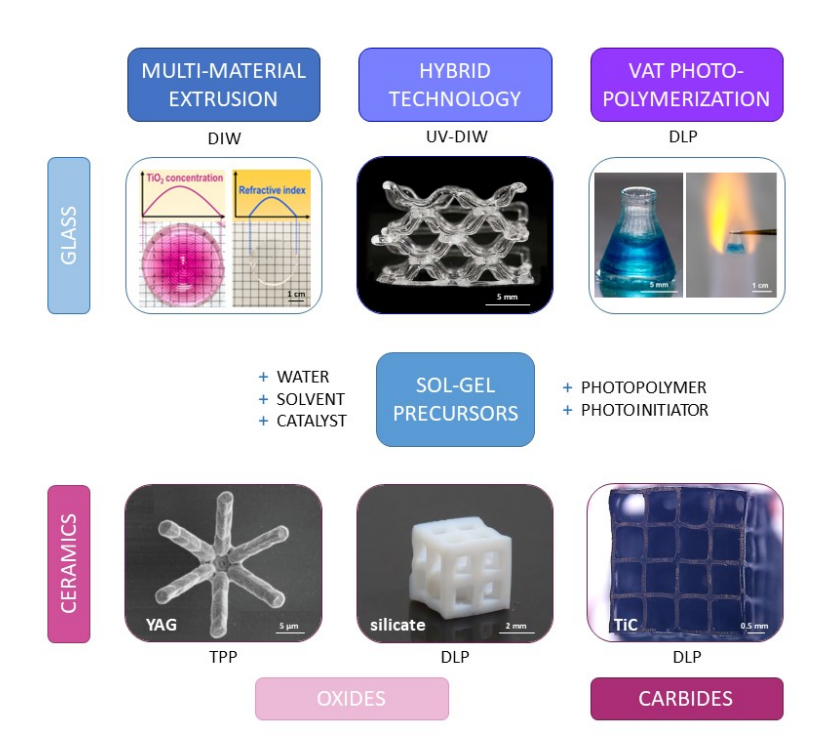


Figure 5. Examples of parts fabricated from feedstocks containing sol-gel precursors using different AM technologies include glass [44,57,59] and ceramic compositions [41,46,47].

There has been an increasing wealth of investigations concerning the 3D printing of ceramics using precursors, testifying to the considerable scientific and technological interest in

this specific field, although some challenges remain to be addressed. The primary issue is that converting from precursor to ceramic occurs with weight loss, gas evolution, and significant shrinkage. On the one side, this limits the maximum thickness achievable after firing to a few millimeters and becomes problematic, especially when the architecture of the part is anisotropic [168]. On the other side, however, the significant change in volume increases the resolution that can be achieved, enabling it to go beyond the limitations in the minimum feature size realizable that are typical of the specific 3DP technology employed.

Future directions for the research on 3DP using precursors will undoubtedly take further advantage of the main positive characteristics of the approach, namely the high transparency of the formulations and rheology controllable in a wide range of values. Indeed, this enables printing using approaches that require a significant penetration depth for the radiation, such as TPP and VAM, and some examples have already been recently published in the literature [65,169–172]. Moreover, for TPP, particle-free resins remove the limit in the printing resolution of features, which is given by the length scale of the dispersed particles. Furthermore, the lack of particles in the feedstock should also make it possible to reduce the nozzle size in DIW significantly, thereby increasing the resolution achievable and providing significantly higher strength (or strength-to-density ratios) for parts with cellular architectures. At the same time, using a photocurable solution as the ink enables the free forming of complex structures by DIW coupled with UV irradiation, which could be further enhanced using advanced AM technologies, such as RAM.

2.4. Direct Ink Writing (DIW)

Direct ink writing (DIW) is a filament deposition method involving extruding powder-loaded suspensions or inks through a nozzle. By guiding the path of the nozzle (**Figure 6a**) [66] using a robot, gantry, or mechanized system. Among the first to realize the great potential of this 3DP technique for ceramics was a team from Sandia National Labs led by Joseph Cesarano III [81]. While extrusion-based AM methods are being explored across different material classes, including constructing large-scale concrete structures, the primary focus of this article addresses the DIW of inks of sub-micron ceramic powders followed by sintering. Discussed presently is a brief overview of DIW, recent highlights, and a discussion of challenges and opportunities. More extensive review articles on DIW are available [82–85].

DIW has found great utility for the 3DP of ceramics for several reasons. First, much is known about preparing high-solids and stable colloidal suspensions of ceramic powders, an outgrowth of basic ceramic research that recognized the need to control interparticle forces to reduce processing defects and increase green-body densities [173]. Using dispersants in water-based suspensions to create repulsive forces between powders, inks with powder loadings of greater than 50 vol.% are not uncommon, with some inks approaching 60 vol.% solids [25]. Maximizing the powder loading increases the green body density after drying, reducing the porosity that must be removed during sintering. Second, by adjusting dispersant amounts, the pH of the water, ceramic powder volume loadings, and adding 1-5 vol.% organic polymers, it is possible to create inks with yield-pseudoplastic rheology. Inks with this rheological behavior possess yield stress, DIW printing requirements, and shear thinning. The yield stress is essential as it provides structure to the printed part after the shear stress is removed and supports subsequent printed layers, while shear thinning helps extrudability through small nozzles. Third,

the high melting temperature of ceramics makes 3DP techniques often used for direct printing of metals, where the powder is melted via a laser, less valuable due to large thermal gradients and the development of residual stresses during cooling. Combined with the low fracture toughness of ceramics, these residual stresses often lead to printed parts cracking. In DIW, printing occurs at or near room temperature; typically, the only residual stresses in the printed parts occur during drying. These can be managed by controlled-rate water removal in a humid atmosphere. After drying, the part is sintered in a second processing step to remove porosity. Thus, DIW is an indirect 3DP process.

Early DIW work focused on printing alumina powders as a model material due to low cost, ease of stabilization in water-based inks, and simple sintering protocols. As an example of a successful DIW ink composition, 55 vol.% submicron alumina powders with an anionic dispersant (Darvan 821a), 5 vol.% 55k g/mol molecular weight polyvinylpyrrolidone, and balance water were successfully printed through a 1.25 mm nozzle at a shear rate of ~20 s⁻¹ [95]. The static yield strength of this ink was 157 Pa; yield strengths below 100 Pa were too low to support subsequent layers, while inks with strengths above 250 Pa did not flow nicely out of the nozzle. B₄C [174], SiC [86], ZrO₂ [175], and other essential ceramics have also been used in DIW. Recently, Si₃N₄ inks have been printed successfully with ~46 vol.% powder loading (**Figure 6b**)[66].

One of the most significant advantages of DIW relative to other ceramic 3DP methods is the ability to orient high aspect ratio (HAR) phases such as chopped fibers, whiskers, and platelets in the extrusion direction during layer buildup [86,176]. High-aspect ratio phases are added to manipulate properties such as strength, toughness, thermal conductivity, etc. HAR phase alignment occurs due to the high shear stresses generated near the nozzle walls (**Figure**

6c). Cox [177] recently printed a 10 vol.% carbon fiber (C_f)/45 vol.% SiC powder ceramic matrix composite (CMC) that was pressureless sintered to 96% relative density. The average 4-pt bend strength of this DIW CMC was 343 MPa, with a Weibull modulus of 10.7. Similarly, dense monolithic SiC-only samples demonstrated a 4-point bend strength of 351 MPa with a Weibull modulus of 7.4. Beyond the high strength and narrower distribution of strengths, fiber pullout (Figure 6d) and non-catastrophic failure behavior (Figure 6e) were observed, demonstrating that 3DP approaches such as DIW can be used to prepare CMC materials.

Challenges and opportunities for DIW-based 3DP

CMCs have found commercial success in the aviation industry [178] and are being considered for emerging opportunities in hypersonic flight. C_f/SiC and SiC_f/SiC CMCs have a long history of process development [179,180]. Much is known about, for example, how to fabricate CMC composites, including the layup of plies, matrix densification steps, BN and pyrolytic graphite debond coatings, etc. However, the high processing costs and long lead times associated with CMC part production make the discovery and maturation of alternative processing approaches for the fabrication of CMCs attractive. It is believed that DIW is a fully matured processing approach that could reduce costs and shorten the lead times of traditional 2D CMC processing routes while also providing the requisite mechanical properties for high-temperature applications. As such, there is an opportunity for the DIW scientific community to move this AM technology toward that goal.

There are many advantages to using DIW for the production of CMCs. First, it would afford new matrices to be explored by simply developing inks with other high-temperature

ceramic powders such as ZrB₂ and HfB₂ and non-SiC carbides such as ZrC and HfC. Secondly, unlike traditionally processed CMCs, where the fibers are oriented by hand placement of the individual plies, the orientation of the fibers is controlled by the flow of the colloidal slurry through the nozzle during the writing process. Traditional composite architectures such as 0°, 0°/90° (Figure 6f), quasi-isotropic, etc., can be prepared by changing the write direction.

However, as the technique matures, more complicated designs, including the internal structure, could be developed, which are complicated with current processes. Third, the matrix phase in DIW CMCs can be formed and densified in one step, implifying matrix densification approaches (e.g., polymer infiltration and pyrolysis, liquid silicon infiltration, or chemical vapor infiltration) used in traditionally processed CMCs. Furthermore, there is an opportunity to reduce the tooling costs associated with traditional CMC forming. Rather than starting with, for example, a wedgeshaped tool and the lay-up of plies on its surface, DIW CMCs could be printed directly into the desired wedge-shaped part. These are just a few advantages of using DIW as a processing route for making CMC materials.

Despite successes using fiber- and powder-loaded inks to fabricate DIW CMCs, there are many challenges. First, there are limitations to the volume loading and length of fiber that can be incorporated into inks while retaining its extrudability. For example, Croom et al. [181] studied the mechanics of nozzle clogging using computed tomography for SiC fiber volume loadings up to 5.75% (no ceramic powders were added), noting several contributing mechanisms. Of these, upstream fiber entanglement and accumulation of fibers near the nozzle exit are most important as the fiber volume increases (see Figure 6g). Preparation of inks with higher fiber loadings will be essential as the fiber phase has been shown to change the crack path during failure via fiber pullout and should carry more load. Those variables that govern interactions between the fiber

and powder as they move relative to one another in shear and through a narrowing nozzle are crucial for enabling DIW of CMCs and should be investigated as little is known fundamentally about these composite fluids. Interactions of the fiber and powder during sintering may also be challenging, and coating systems may need to be developed to preserve the fiber morphology. Developing DIW methods to incorporate continuous fibers could also move this processing approach forward; however, nearly all continuous fiber 3DP research is on polymer matrix composites. Second, fiber loading strongly influences the sinterability of the DIW parts. For example, carbon fiber volume loadings of 15 vol.% caused the overall densification of the SiC powders to fall below 90% relative density [80]. While exhibiting minimal to no change in length during the sintering process, the fibers negatively influence how much the SiC powders shrink during sintering. Fibers hindering shrinkage in DIW printed ceramics has been noted as a problem before [182]. Thus, understanding and controlling the local sintering dynamics will be critical. Third, different drying behaviors, coefficients of thermal expansion, and elastic modulus between the fiber and the matrix can cause distortion and cracking of the dried and sintered bodies in some composite architectures. Scaling laboratory-sized parts to larger ones will likely reveal particular challenges centered around drying. Understanding the development of drying stresses as a function of part thickness, fiber loading and orientation, and powder loading will be key. Thus, it is evident that understanding the development of residual stresses that develop between fiber and matrix during printing, drying, and sintering is critical. With a thorough scientific understanding of the processing variables, it should be possible to mature the DIW process to produce high-performing structural ceramic parts and enable lower cost and significantly increased complexity in design.

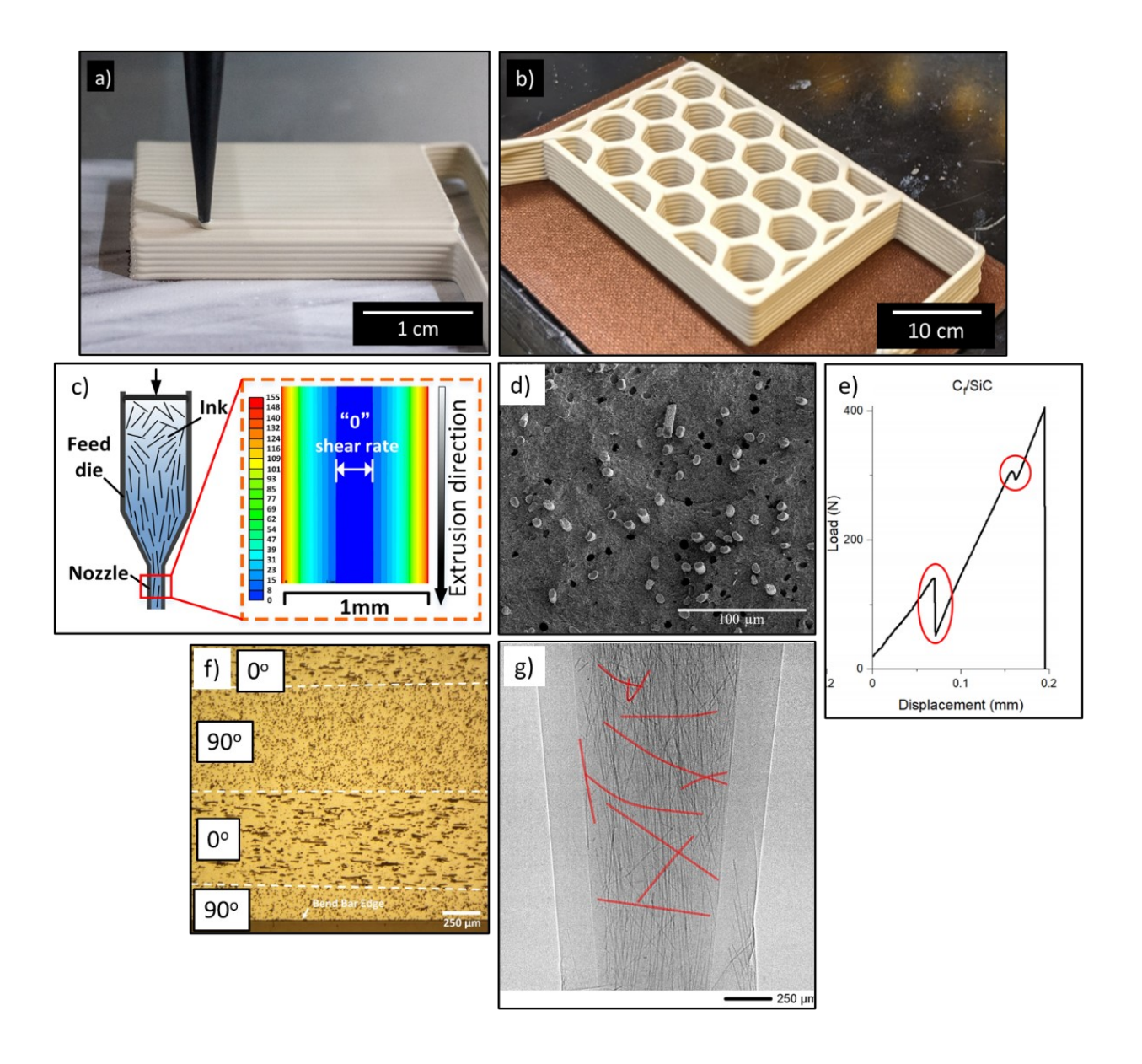


Figure 6. (a) Direct ink written 46.5 vol.% Si₃N₄ ink, extruded through a rastering 1 mm nozzle [66]; (b) printed lattice of a 46.5 vol.% Si₃N₄ ink [66]; (c) schematic showing the alignment of short fibers through a nozzle during extrusion and an adjacent image showing the local shear stress through a 1 mm orifice [86]; (d) SEM micrograph of a failed DIW 0° C_f/SiC CMC near the tensile axis showing fiber pullout [80]; (e) Load versus deflection plot of a DIW 0° C_f/SiC CMC showing cracking events (circled) and reloading before failure [80]; (f) DIW C_f/SiC CMCs with a 0°/90° orientation of the fibers, and (g) in situ synchrotron X-ray imaging during printing of

SiC fiber & epoxy ink, showing the presence of many highly-misoriented and bent fibers in ink. The nominal extrusion speed was 2 mm/s. The image was obtained from Dr. Croom.

2.5. Extrusion-based 3DP of Ceramics

The fused deposition of ceramicsTM (FDCTM) process (**Figure 7a**) was developed at Rutgers University (NJ, USA) and patented by Safari and Danforth et al. [183,184], and was implemented to fabricate functional materials, including electromechanical actuators and sensors. The FDCTM process is an independent offshoot of the Fused Deposition Modeling (FDMTM) process, which uses a thermoplastic polymer as filament feedstock, the details of which can be found elsewhere [184]. The FDMTM process is limited to the fabrication of parts and components that are based on polymer materials. The FDCTM process is a 3DP method that lends itself to print ceramics [185].

The breakthrough of the FDCTM process is the successful development of four different binder formulations for the uniform dispersion of any chosen ceramic powder in the thermoplastic polymer [186,187]. The ceramic-polymer mixture is then extruded into a filament feedstock (35-65 vol% solids loading) (**Figure 7a**) and then fed into the liquefier of the FDCTM system (**Figure 7b**). The fabricated part is then subjected to a thermal cycle to remove the mixture's polymer (4-component binder) phase, leaving behind a ceramic preform [185,186]. Upon sintering, a highly dense 3D ceramic object is obtained in a free-form fashion. The Rutgers group also developed a multi-head (MH-FDC) (**Figure 7c**) system capable of building a 3D object made of distinct materials by co-deposition. The MH-FDC system also has a built-in printing flaw detection feedback circuit. Multi-material piezoelectric actuators comprised of soft

and hard Pb(Zr_{0.5}, Ti_{0.5})O₃ (PZT) (**Figure 7d**), and metal electrodes were successfully demonstrated using MH-FDC [188,189].

2.5.1. Electromechanical Actuators by FDCTM

An electromechanical actuator converts electrical energy to mechanical energy via first-order (piezoelectricity) and second-order (electrostriction) effects[190] Such actuators, single phase or their composites, produce exact motion in the ~1-100 µm and can generate high force, making them very versatile devices in various engineering systems. Such electromechanical devices can also be sensors where a mechanical stimulus produces an electrical response[190].

The FDCTM process surpasses the limitations of conventional fabrication methods for electromechanical actuators [191]. As such, one can accomplish form factor engineering (**Figure 7e-i**), where one utilizes the design of the transducer to amplify its displacement [87–89]. The contribution of a novel design to the displacement is additive to the intrinsic response of the material, providing much-needed amplification of the mechanical output. The FDCTM process allows one to create complex-shaped ceramic transducers and fabricate complex-shaped polymer matrix electromechanical diphasic composites by a two-step process [90]. The FDCTM process also enables one to create monolithic ceramic-ceramic composites of any arbitrary shape[87–89].

The Rutgers group has demonstrated the effectiveness of the FDCTM process by developing novel actuators like spiral, telescoping, dome, tube, curved and multilayered tubes, bellows, oval actuators, ladder structure, serpentine, rhombohedral-lattice among others (**Figure 7e-j**) [87–89]. Spiral actuators (**Figure 7j**) exhibit large field-induced displacement because both tangential and radial displacements are triggered, with the tangential displacement being dominant [91]. The

tangential displacement reaches 1.9 mm at 11.6 kV/cm, twelve times that of a PZT strip of the same dimensions (**Figure 7k**). The blocking force is 0.8 N for driving fields of 1.3 to 3.3 kV/cm as it is inversely proportional to the displacement[91]. Bilayer actuators, comprised of piezoelectric 0.65Pb(Mg_{1/3},Nb_{2/3})O₃-0.35PbTiO₃ and electrostrictive 0.90Pb(Mg_{1/3},Nb_{2/3})O₃-0.10PbTiO₃, were also fabricated. Bilayer spirals demonstrate increased tangential displacement attributed to the strain differential induced by the electric field across the interface of the piezoelectric and electrostrictive materials. The co-firing process was conducted at 1250°C for 1h, adjusting filament properties and integrating two distinct materials. These bilayers demonstrated a tangential displacement of 510 μm at an electric field strength of 500 V/cm, surpassing the 200 μm displacement observed in single-material actuators under the same electric field conditions [92].

The fabrication of monolithic multi-material monomorphic actuators using the same materials as in the spiral follows the same approach (the interface and the bilayers are depicted in **Figure 7I**)[93,94]. The monomorphic devices are planar, while the exact mechanism of the bilayer spiral amplifies the tip displacement (x). However, the x depends on the polarity of the applied electric field (E), i.e., x(E)>x(-E) (**Figure 7m**) [93,94]. In other words, the displacement is asymmetric. The degree of symmetry can be fine-tuned by the judicious choice of piezoelectric and electrostrictive layer thickness, which is relatively straightforward using the FDCTM process (**Figure 7m**)[93,94].

Novel PZT ceramic-polymer composites and rhombohedral-lattice structures, with various orientations of the ceramic phase to the poling direction, were also demonstrated with the FDCTM process using a two-step process (**Figure 7f**). The orientation angle (θ) of the ceramic phase was varied from 0° and 75° with 15° increments. The ceramic structures fabricated by

FDCTM were embedded in hard epoxy. Owing to the transverse coefficient (d_{32}) becoming a positive quantity ($d_{31} > 0$) where $dh = d_{33} + d_{31}$, these composites demonstrate an effective hydrostatic piezoelectric coefficient (d_h) [192].

2.5.2. Alternate 3DP Processes for Electromechanical Actuators and Sensors

Other 3DP processes were implemented for the fabrication of objects that are based on functional ceramics. For instance, the direct-write MicroPenTM process was adapted by the Rutgers group for the printing of quasi-planar devices [193]. General Electric adopted a digital microprinting process to fabricate piezoelectric transducers for medical ultrasound imaging, including matching and backing layers and the adhesive joints connecting the transducer [194]. Robocasting has proven to be a highly effective 3DP method in developing PZT composites comprising a 3D ladder structure with solid PZT caps[195,196]. Such composites have high hydrostatic piezoelectric coefficients, making them attractive for sensor applications. Moreover, using barium titanate ceramic suspension to fabricate a piezoelectric part using projection-based stereolithography enables one to develop conformal components for cornea imaging in ophthalmological applications [197,198]. Freeform Injection Molding (FIM), a hybrid 3DP, was an effective method for fabricating conformal and air-ceramic composite piezoelectric structures [199]. Reactive-colloidal inks were demonstrated for 3D printing by robocasting of BaTiO₃based ceramics [200]. Tunable 3D-printed PVDF-TrFE piezoelectric arrays were in-situ polarized recently [201].

2.5.3. Prospective Developments in 3DP of Electromechanical Transducers

Various 3DP processes open new avenues for developing unprecedented composite, multimaterial, and multifunctional transducers. Essentially, one can develop artificial macro-crystals
that conventional processing methods could not obtain. For instance, a multi-material system
with a specific connectivity pattern can be fabricated to induce cross-coupling between disparate
phenomena such as ferroelectricity and ferromagnetism or magnetostrictivepiezoelectric/electrostrictive coupling, flexoelectric composite, among others. We believe a
major future direction seems to be 3D printing under applied fields (primarily electrics,
magnetic, and thermal fields) that will enable one to obtain nano- and microscale scale ordering
in the final 3D composite. Such ordering would then serve to obtain the desired nano- and
microstructures. We also anticipate that electroactive polymer matrix composites with ceramic
particles dispersed in the polymer will find significant applications in energy storage applications
where 3DP will play a significant role.

However, some challenges exist requiring resolution. The layer thickness in 3DP must be reduced to at least $5-10 \mu m$. This can only be obtained with unique feedstock in which colloidal control is necessary to disperse $\sim 100-200 \mu m$ particles in a polymer matrix. Secondly, hardware capable of depositing such thin layers needs to be developed. Thirdly, the resolution of the spatial displacement of the hardware needs to be improved. Advances in the above direction will likely pay dividends one cannot fully predict.

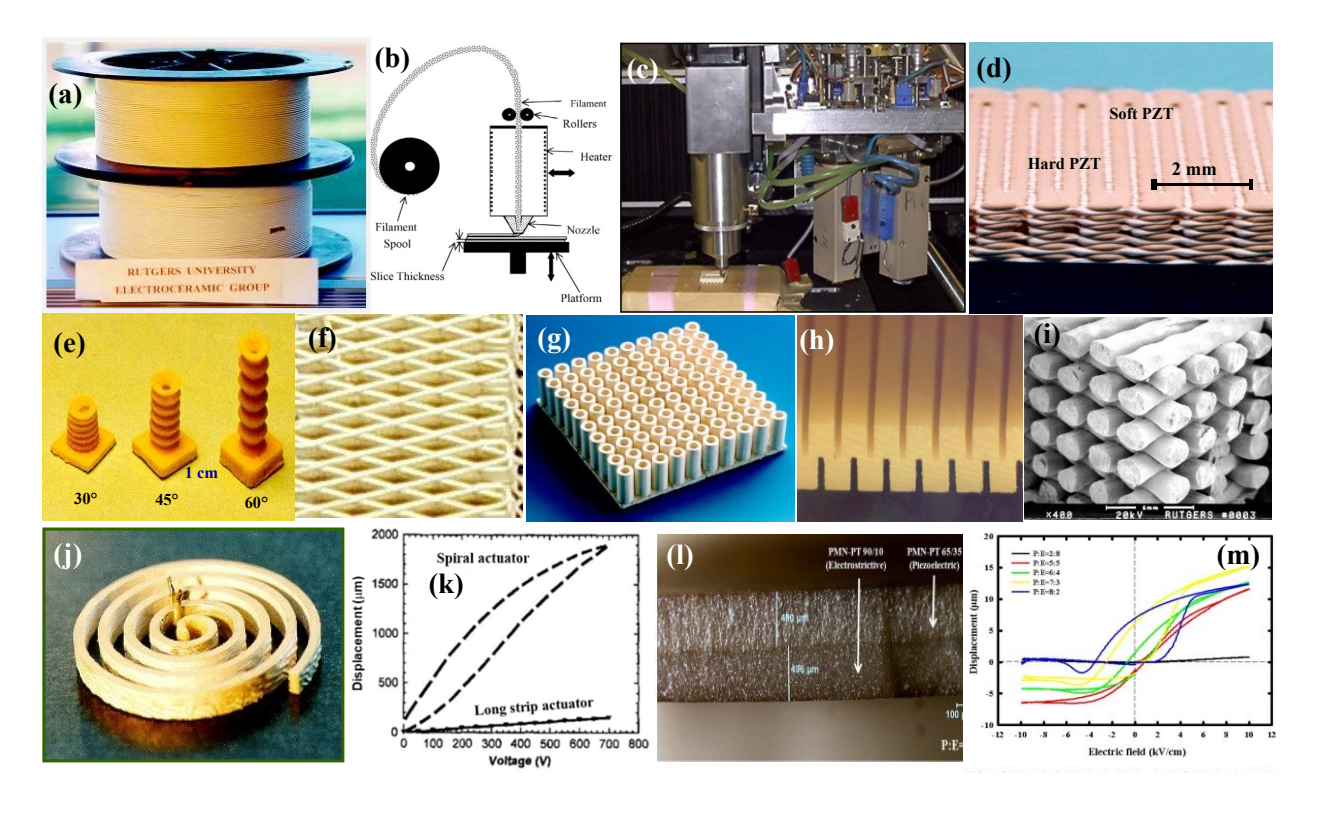


Figure 7. (a) Polymer (thermosetting) matrix - ceramic reinforced FDCTM filament feedstock of 1.9 mm diameter. The filament is comprised of the 4-component binder. Solids loading varies from 35-65%. (b) Schematic of the FDCTM process showing the liquefier. The thermosetting polymer containing the ceramic materials is molten and deposited on an xyz stage where the 3D object solidifies. (c) The multi-head FDCTM (MH-FDC) system enables one to fabricate 3D parts using distinct materials by co-deposition. The system also has a flaw monitoring system. (d) A ceramic-ceramic composite transducer comprised of hard and soft Pb(Zr_{0.5},Ti_{0.5})O₃ (PZT) as fabricated by MH-FDC. (e) PZT-based piezoelectric below actuators by FDCTM. (f) PZT-based rhombohedral lattice structured piezoelectric actuator by FDCTM. (g) PZT-based tube array piezoelectric actuator by FDCTM. (h) PZT-based serpentine piezoelectric actuator by FDCTM. (j) PZT-based spiral piezoelectric actuator by FDCTM. (k) Comparison of tip displacement between spiral and strip actuators as a function of applied voltage, showing the displacement amplification due to the

"shape effect". (I) Cross-sectional scanning electron microscope image of a co-sintered bi-layer electromechanical bending actuator by FDCTM. Top layer is piezoelectric 0.65Pb(Mg_{1/3},Nb_{2/3})O₃-0.35PbTiO₃ (~480 μm); bottom later is electrostrictive 0.90Pb(Mg_{1/3},Nb_{2/3})O₃-10PbTiO₃. (m) The comparison of the electric field response of the co-sintered bi-layer electromechanical bending actuator by FDCTM shows the effect of the piezoelectric-electrostrictive layer thickness ratio on tip displacement. Also shown is the asymmetry of the tip displacement as a function of the applied voltage's polarity.

The 3D printing approach was successfully extended to microelectronics [202] and similar applications using ink [203] and aerosol-based [204] feedstock, enabling one to develop devices on suitable substrates. Hence, 3D Printing has the potential to impact surface acoustic wave (SAW) devices and micromechanical electro-mechanical systems (MEMS) [202,204] among others.

2.6. 3D Printing of melt growth ceramics by Laser Directed Energy Deposition (LDED)

Melt growth ceramics (MGCs), obtained directly by melting and solidification of pure raw materials, are famous for their ultra-high-temperature properties and microstructural stability that develop as a response to clean and high-strength bonding interface shared by atoms [205–207]. The main preparation methods, including directional solidification methods, such as Bridgman, laser-heated float zone, and non-directional solidification methods, such as combustion or explosion synthesis, generally have long preparation periods, large subsequent

machining allowance, and challenges in preparing complex structures [208,209]. Therefore, for efficient and high-quality MGC fabrication, developing effective near-net-shaping techniques is of prime importance. Schematic of the LDED system and typical deposition structures are shown in **Figure 8**.

Laser-directed energy deposition (LDED), also known as laser-engineered net shaping (LENS), is a kind of 3D Printing technology based on synchronous feeding. LDED uses a high-energy laser beam to melt high-purity ceramic powders completely, directly shaping 3D structures by *in situ* deposition of the melted materials. Synchronous feeding and *in situ* deposition impart significant advantages in the parts manufacturing cycle, material composition, and utilization. Furthermore, the bottom-up and layer-by-layer deposition methods in LDED remove roadblocks due to mold restrictions, allowing it to fabricate ceramic parts with arbitrary shapes and sizes. Since it was first successfully applied to the preparation of Al₂O₃ MGCs by Balla et al. [30], various MGCs, including single-phase, composite, and gradient ceramics, have been successfully achieved.

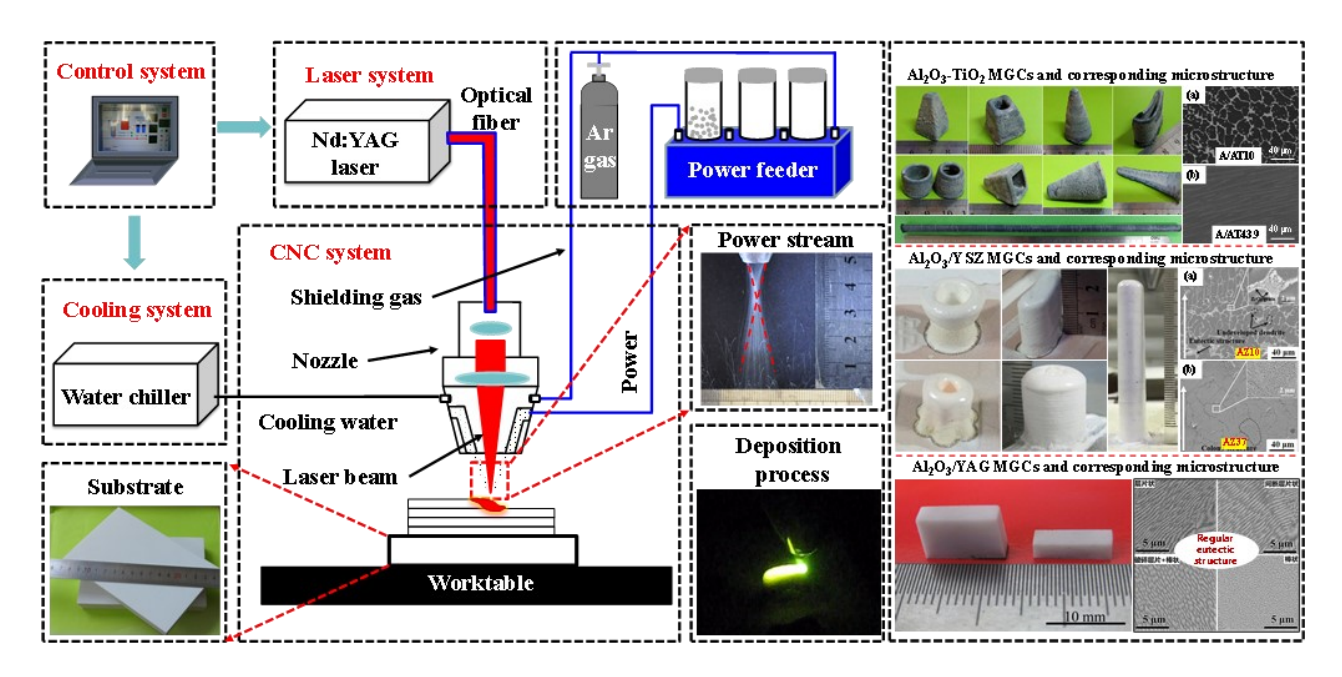


Figure 8. Schematic of the LDED system and typical deposition structures.

LDED technology, characterized by a high energy density heat source and no need for sintering agent doping, provides excellent convenience for preparing single-phase ceramics with high-purity and high melting points. Balla et al. [30] shaped dense Al₂O₃ bulks with sizes up to 25 mm under optimized process conditions using a continuous wave Nd:YAG laser. Cong et al. [210] studied the influence of critical process parameters on the shaping quality of Al₂O₃ MGCs and finally obtained the optimized processing window. Niu et al. [211] established a mathematical model that considers process parameters and material's physical properties based on energy conservation. Al₂O₃ MGCs prepared by LDED are generally composed of coarse columnar crystals along the build direction, mainly attributed to the solidification condition of near one-dimensional heat dissipation during deposition [30,210–213]. Fan et al. [214] also deposited yttria-stabilized zirconia (YSZ) thin wall structures with a relative density of 98.7% and found that the m-ZrO₂ in the raw material transformed into t-ZrO₂ and c-ZrO₂.

Compared with single-phase ceramics, LDED of Al₂O₃-based composite ceramics has attracted more attention due to their diversified properties. Reasonable composition design allows composite ceramics to inherit the high strength of Al₂O₃ while absorbing the unique properties of other composites. Al₂O₃/YSZ MGCs have been proved to possess better microstructure and mechanical properties than pure Al₂O₃ or YSZ [215–220]. The Al₂O₃/YSZ MGCs with different composition ratios are composed of primary Al₂O₃ phase or ZrO₂ and intergranular eutectic matrix, but the content of each phase is different, which also leads to the difference in properties. Accordingly, Niu et al. [221–223] realized the real-time preparation of Al₂O₃/YSZ, Al₂O₃-TiCp, and Al₂O₃/YSZ-TiCp gradient ceramics by changing the composition ratio during the LDED process. Compared with the direct transition, the gradient transition alleviates the stress, and the crack problem at the interface is solved. In particular, the interface's element distribution and mechanical properties also change from step transition to near linear smooth transition.

In addition to the macroscopic composite of materials similar to Al₂O₃/YSZ MGCs, some composites even react *in situ* under a high-temperature melt state, thus obtaining new phases, unique microstructure, and properties. Huang et al. [224,225] confirmed that aluminum titanate (Al_xTi_yO_z, AT) with a thermal expansion coefficient close to zero was synthesized *in situ* from Al₂O₃ and TiO₂. The continuous AT matrix effectively alleviates the destructive effect of high thermal stress generated during LDED on MGCs. Correspondingly, a significant crack suppression effect was found, and some crack-free A/AT irregular structures with cross-sectional dimensions of 20~30 mm were achieved [226,227]. Similarly, SiO₂, Y₂O₃ and MgO were also used to synthesize Al₂O₃/mullite [228,229], Al₂O₃/Y₃Al₅O₁₂ [230,231] and MgAl₂O₄ [232,233] MGCs with Al₂O₃, respectively. The doping of rare earth oxides, such as Er₂O₃ and GdO₂, has

also achieved remarkable results [234–238]. Su et al. [234] realized the large-scale Al₂O₃/GdAlO₃/ZrO₂ cylindrical structures with fine and uniform microstructure by using LDED. Fan et al. [236] prepared high-density Al₂O₃/Y₃Al₅O₁₂/ZrO₂ MGCs with finer microstructure and better properties than Al₂O₃/Y₃Al₅O₁₂ through LDED.

Undeniably, the unique advantages of simple processes and high manufacturing flexibility of LDED provide a new technical scheme for rapid and low-cost preparation of MGCs. However, MGCs are subjected to complex and high thermal stress caused by a high-temperature gradient, much higher than their fracture strength. Therefore, severe cracking is the most essential problem restricting the engineering application of LDED in MGC preparation. Although a series of methods, including process optimization [30,210,211,226–228] and external-field assistance [215,216,230,239,240], have been applied to improve the shaping quality, the cross-section size of crack-free MGCs has not been effectively broken through. In addition, the secondary problems associated with rapid solidification, such as heterogeneity of microstructure and properties, pore defects, etc., have not been completely solved.

It is believed that further research is needed in the following key areas to promote the eventual application of LDED in MGCs. It is necessary to accurately grasp the cracking mechanism of MGCs in the LDED process and develop effective thermal stress control methods to achieve low-stress direct AM of large-scale MGCs. More in-depth understanding of ceramic melts' solidification behavior and microstructure formation mechanism during LDED, laying a theoretical foundation for developing integrated regulation methods for microstructure and properties. Designing unique raw materials suitable for LDED is also a breakthrough in solving microstructural defects and properties. Research on the processing and post-treatment process systems for different MGCs also deserves further attention.

2.7. Powder bed fusion (PBF) processing of ceramics

The powder bed fusion (PBF) technique requires layer-wise ceramic powders to undergo high laser heating. PBF can be further classified into two main categories: Selective Laser Sintering (SLS) and Selective Laser Melting (SLM). In contrast to binder jetting, most components processed through SLS/M typically do not require an additional step of binder burnout and sintering. SLS involves sintering ceramic particles at a temperature lower than their melting point. This process relies on the solid-state diffusion of powder particles across grain boundaries and their subsequent coalescence. The sintering temperature, though insufficient to induce complete melting, fosters the formation of strong bonds between adjacent particles. In contrast, SLM entails completely melting ceramic powder particles, transitioning them from a solid to a liquid phase, followed by rapid cooling. This comprehensive melting and solidification process leads to the formation of fully dense components with intricate geometries. Unlike SLS, SLM involves a higher energy input, resulting in the complete melting and fusion of the ceramic powder. The rapid cooling phase generates fine microstructures and can enhance specific material properties. SLS and SLM offer unique advantages in terms of speed, precision, and achievable complexity of designs. The choice between the two methods often depends on the specific material requirements and the desired characteristics of the final ceramic component. An overview of the SLS/M process and various parts fabricated via SLS/M are shown in Figure 9.

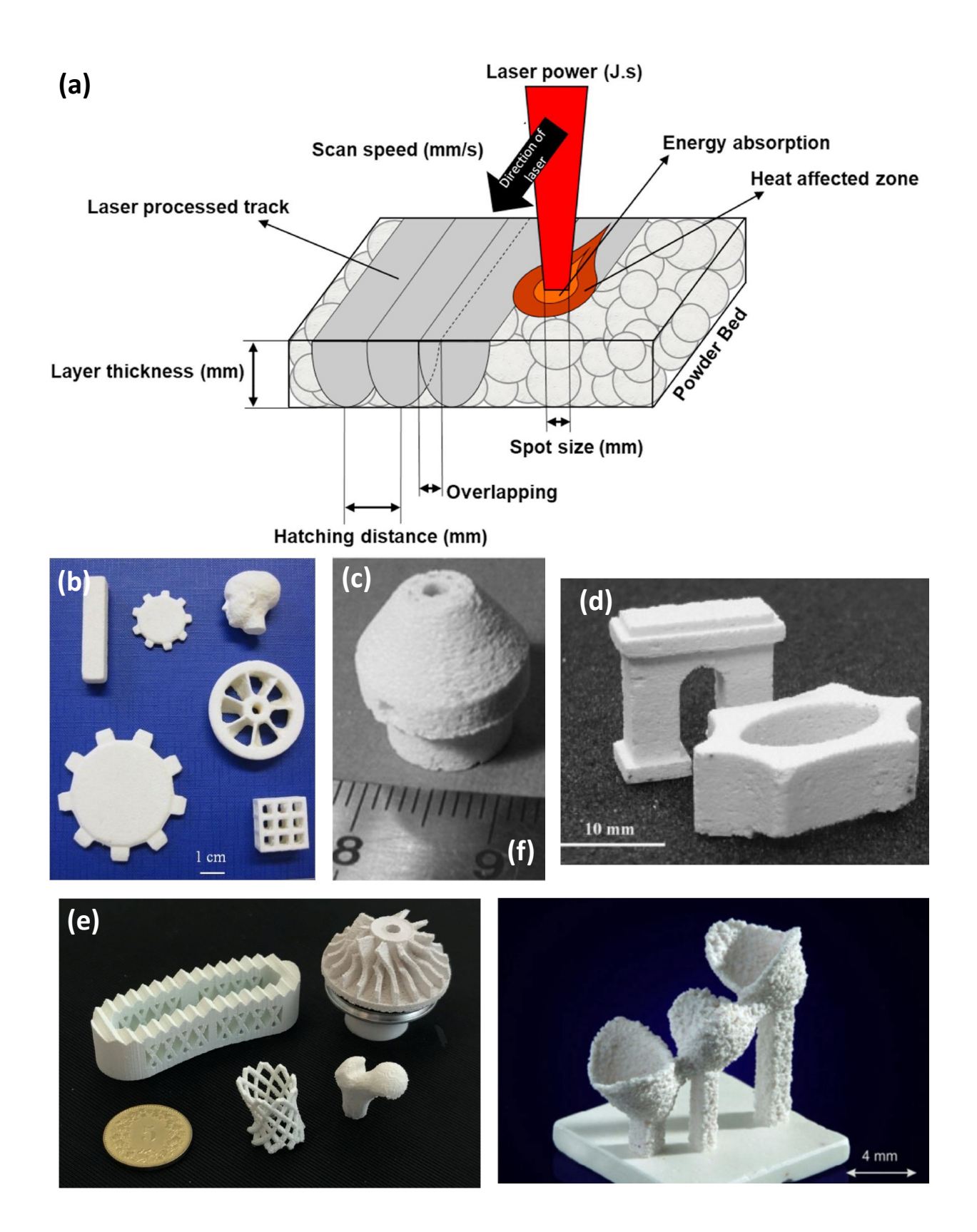


Figure 9. An overview of the SLS/M process and various parts fabricated via SLS/M. (a) Process schematic of the powder bed-based laser operation of ceramics [241]; (b) Complex alumina parts made using selective laser sintering [242]; (c) pure ZrO₂ processed via SLS/M [99]; (d) parts processed via SLM composed of ZrO₂ [28];(e) complex and porous shapes made of Al₂O₃ toughened ZrO₂ [105];(f) dental restoration bridge processed via SLS of Al₂O₃ and ZrO₂ mixture [100].

2.7.1. Selective laser sintering (SLS)

SLS uses a pulsed laser to sinter fine ceramic particles [101]. The origins of this technology can be traced back to the University of Texas at Austin [102]. The subsequent commercialization of SLS took shape in 1992 by DTM Corporation, eventually acquired by 3D Systems in 2001. The SLS process resembles the binder jet operation, with a notable deviation – using a laser instead of a printhead with the binder. In SLS, ceramics undergo direct sintering in the powder bed stage, eliminating the need for a separate sintering cycle. Ceramic powders are preheated below the melting point or the glass transition temperature to mitigate thermal distortions. The print chamber is purged with nitrogen or argon to prevent ceramic degradation at elevated temperatures. In each layer of powder spread onto the build stage, a laser sinters the ceramic powders according to the CAD file. Post-printing, the part can cool down to room temperature to prevent distortions. SLS of ceramics, however, presents challenges. The inherently high melting point of ceramics necessitates substantially high laser power for the printing operation. Using high-energy lasers, coupled with the elevated temperature of the powder supply stage and extended cooling times, renders SLS less efficient and cost-effective. Ceramics can be processed via direct SLS, involving the direct sintering of ceramic surfaces, or via indirect SLS, which entails coating ceramic powders with an organic phase possessing a lower melting point than the ceramic itself. Despite these challenges, SLS of ceramics remains a

promising avenue, unlocking opportunities for intricate and functional ceramic components, particularly when tailored to specific material requirements and design complexities.

Direct SLS employs a high-energy focused laser beam on ceramic particles, inducing sintering at elevated temperatures. This method can be further classified into two distinct categories: powder-based and slurry-based direct SLS. In powder-based SLS, ceramic powders are meticulously layered onto the build stage through a feeding mechanism while the laser operates. This process necessitates a uniform spread of the powder layer with high packing density. Insufficient packing density leads to lower sintered density and distorted parts.

Shishkovsky et al. successfully demonstrated the SLS fabrication of an alumina and zirconia composite mixture, showcasing potential insulators and coatings applications [28]. Wang et al. extended the applications of powder-based SLS, showcasing the successful processing of alumina-zirconia-silica glass-ceramic compositions tailored for dental applications [243].

A slurry-based direct SLS utilizes a homogeneous slurry instead of individual ceramic powders. A doctor blade spreads the slurry onto the build stage, followed by a drying process and subsequent laser operation [244]. This approach allows for finer ceramic particles, resulting in higher-density final parts [97,245]. However, mechanical properties may be compromised, and the potential for thermal cracking arises due to microstructural inhomogeneities [246]. The choice between powder-based and slurry-based direct SLS depends on specific application requirements, considering factors such as desired mechanical properties, thermal performance, and the complexity of the final part. Both methodologies, despite their respective challenges, contribute significantly to the advancement of ceramics processing through SLS, offering diverse possibilities for applications in insulation, coatings, and dental components.

Indirect SLS involves the utilization of ceramic particles coated with an organic or polymeric material. The process involves melting and fusing the polymeric surface on the ceramic particles through laser operation [247]. While this method eliminates the need for high-power lasers during the initial process, an additional step of binder removal and sintering of the ceramics is essential to achieve high-density functional parts. The advantage of using an organic or polymeric coating is its lower melting temperature than ceramics, making high-power lasers unnecessary. This characteristic renders indirect SLS more versatile than direct SLS. A semicrystalline polymer as a binding agent is often preferred due to its higher density than amorphous polymers [248]. However, challenges may arise from distortions caused by the high shrinkage characteristics of semicrystalline polymers. A range of polymeric binders is employed in indirect SLS, including epoxy resins, polymethacrylates, acrylic binders, polypropylene, and more [249–252]. Each binder offers unique properties, influencing the final characteristics of the sintered ceramic part. Indirect SLS, with its versatility and varied binder options, provides a flexible approach to ceramic processing.

2.7.2. Selective laser melting (SLM)

In contrast to SLS, the SLM process involves melting ceramic particles in a layered powder bed state. Given the high melting points of ceramics, the SLM operation requires high-power lasers. Once the ceramic powders are melted, they undergo rapid solidification. Laser absorption, an inherent property of the ceramic composition used, is a critical criterion for the SLM process. For instance, alumina and silica exhibit less than 10% laser absorption towards Nd:YAG lasers (1.06 µm wavelength) but display high laser absorption (96%) towards CO₂ lasers with a higher wavelength (10.6 µm wavelength) [253]. Conversely, silicon and tungsten

carbide show 75-85% laser absorption towards Nd:YAG and 48-66% absorption towards CO₂ lasers [253]. SLM is advantageous for processing high-density parts with favorable mechanical properties [104]. However, the process involves melting ceramics and rapid cooling, leading to phase changes due to non-equilibrium processing conditions [254]. Wilkes et al. have demonstrated a dual laser system for SLM operations on a zirconia and alumina mixture—a CO₂ laser for preheating the powder and an Nd:YAG laser for selective melting. Their work demonstrated that higher surface resolution was achieved without preheating powders, resulting in a loss of mechanical strength in the parts [98]. Yves-Christian reported the potential of SLM by achieving close to 100% dense zirconia-alumina parts with 500 MPa of flexural strength [106]. With its ability to achieve high-density parts and favorable mechanical properties, SLM in ceramics presents a promising avenue for advanced manufacturing applications.

3.0 Applications of 3D Printing of Ceramics

3.1. Structural ceramics

Two potential routes for exploring advanced manufacturing of functionalized ceramics were identified and pursued. Direct-ink writing (DIW) was selected for its capability to mix two or more inks *in situ* dynamically before extrusion [96]. DIW produced functionally graded B4C-SiC multi-material ceramics. As a complementary research effort, ceramics with microstructural texture were printed using shear alignment on a stereolithography-based Admaflex 130 system [255], similar to efforts by other groups on DIW of chopped fiber composites [256] and textured barium titanate [257]. In the long term, combining these research efforts would enable multi-scale microstructure tailoring through composition grading with platelet or fiber-seeded inks.

DIW of functionally graded B4C-SiC ceramics was performed using a custom-built system based on a Taz 6 Lulzbot fused filament fabrication 3D printer modified to print aqueous ceramic ink with multi-material and in-line shear mixing capabilities (**Figure 10a**) [96]. The Taz 6 firmware was modified to remove temperature-related errors, print head spatial variations, and custom tool path modifications. Slic3r [258], a 3D slicing engine, prepared the G-code and sent it to Taz. The composition was controlled by parameters manually added into the G-code to control the ratio of ceramic inks mixed in the auger.

B4C (mean particle size $\sim 0.8~\mu m$) and SiC (mean particle size $\sim 0.7~\mu m$) powders were processed into high ceramic content aqueous ink formulations. The rheological behavior was controlled using mixtures of organic binders and dispersants and deionized water. Ink formulations were mixed using a DAC 400 VAC SpeedMixer (Flacktek, Landrum, SC) at speeds up to 2000 RPM. Continuous and discrete B4C/SiC composites were printed with this system and sintered to >98% theoretical density by hot pressing at 1950°C and 35MPa for 2 h. Microstructural characterization was performed via scanning electron microscopy (SEM) on cross-sectioned and polished specimens, highlighting controlled interfaces between B4C and SiC layers (Figure 10b) and the presence of residual stress cracking in specimens with sharply graded interfaces (Figure 10c).

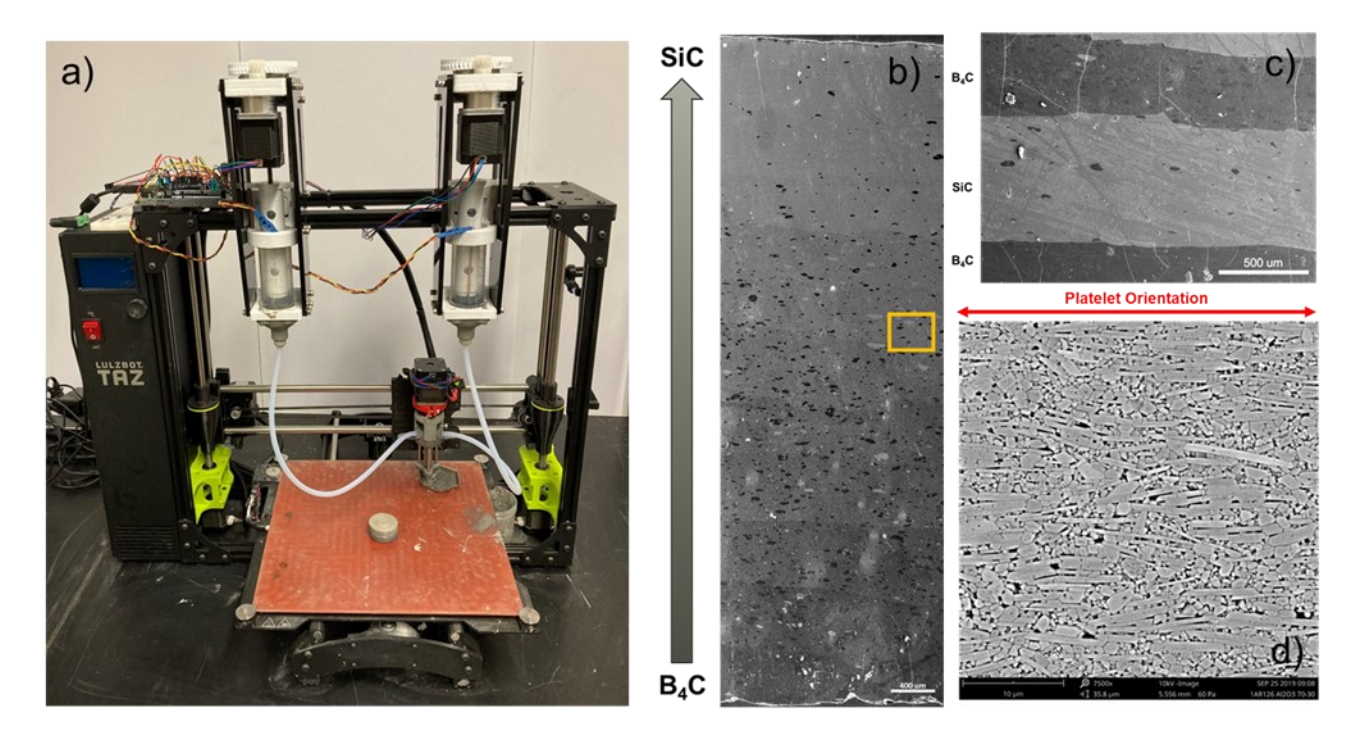


Figure 10. (a) Modified TAZ Lulzbot setup with dual B4C/SiC feed system. (b) Continuously graded DIW and hot-pressed B4C-SiC part. (c) Hot pressed discretely graded B4C – SiC DIW part showing residual stress cracking. (d) Hot-pressed textured alumina microstructure produced via SLA.

SLA of textured ceramics was performed with an Admaflex 130 using a customized photocurable ceramic feedstock based on Tethon Genesis resin (Tethon 3D, Omaha, NB) containing alumina powder (A16, Almatis, D50=0.4μm) and alumina platelets (Alusion, D50=7.9μm, mean thickness = 200nm) [255]. The resin's shear viscosity increased with solids loading up to a maximum usable viscosity of 500Pa·s at 40 vol.% solids loading. The platelet fraction of ceramic also influenced viscosity, with platelet fractions of 30% and 50% reducing viscosity while increasing the flow index, weakening the shear-thinning behavior of the ink. Platelet fractions above 50% were unattainable due to high viscosity during mixing.

The resin containing 35 vol.% solids loading, with the ceramic solids having a platelet fraction of 15%, was successfully printed on an Admaflex 130 printer. Shear alignment was characterized with SEM (Figure 10d) and measured as 0.045 and 0.114 pre- and post-sintering using Lotgering factors calculated from XRD scans. Both specimens were sintered by hot pressing to >99% theoretical density as measured by areal analysis. A minimal grain growth with submicron grain size and 10:1 platelet aspect ratio was confirmed via stereographic analysis. Indentation toughness testing observed no significant impact of the microstructural texture on toughness or crack deflection. This was attributed to the strong interfacial bonding between alumina grains and demonstrates the additional need for interfacial property control to realize the toughness properties of textured microstructures.

3.2. 3D Printed transparent ceramics for future laser gain media

Since the invention of translucent Al₂O₃ ceramics for streetlamp envelopes made by General Electric in the 1950s, transparent ceramic materials have improved in optical clarity and are starting to be implemented in several essential applications. While typically more costly to fabricate than traditional glass or single-crystal optics, transparent ceramics can sometimes offer a solution where other optical materials cannot fulfill the performance requirements. The most widely deployed example of such an application is using MgAl₂O₄ spinel for armored bullet-proof windows due to the extreme strength-to-weight ratio compared with traditional glass [259]. Similar high-performance optical applications where ceramics offer a benefit include laser gain media with higher and more uniform doping than some hard-to-grow single crystals and radiation detectors able to be produced in large sizes impossible to grow as single crystals while still maintaining high detector performance [260–262].

One application in which ceramic optics can offer a unique solution and is particularly difficult and costly using traditional glass or single crystal materials is composite optics, i.e., components consisting of multiple regions with different compositions, doping, index of refraction, etc., within a single optical material. Owing to the all-solid-state fabrication from green body to sintered structure, ceramics are particularly amenable to fabrication where a predetermined tailored structure remains intact, which is impossible to achieve via melt-growth techniques. This fabrication advantage has allowed optical ceramics to develop a new functional role as composite laser gain media [263].

Solid-state laser gain media currently employ standard geometries, including rods, waveguides, disks, and slabs (**Figure 11**). However, in attempts to improve thermal management, beam quality, and energy storage, more advanced laser gain media design requires incorporating features such as undoped edge cladding, doping gradients, index control, and saturable absorbers. Some composite optics, such as endcaps, can be made by diffusion bonding single crystals, but this process is complicated and only available in simple geometries [264]. More complex shapes, such as edge cladding, have been fabricated by assembling pre-sintered ceramic structures and forming the optical bond during the final stages of sintering [265]. More recently, with the improved development of 3D ceramics printing, more complex optical structures are being created for use as laser gain media.

DIW of ceramic slurries was combined with transparent ceramic processing to create an Nd-doped YAG core laser rod with an undoped cylindrical cladding along the full length of the rod [266,267]. This work showed the feasibility of printing complex doping profiles in optical ceramics, including a radial gradient; however, it also highlighted the difficulty in achieving a uniform index of refraction suitable for the propagation of a coherent laser beam. Inert dopants

(e.g., Lu) were used in the clad region to compensate for the index change induced by the core's active ion dopant (Nd). Even when the index was matched perfectly for these two regions, unequal dopant diffusion across the interface can create up to several hundred ppm index fluctuation [268]. Using Gd as a compensating dopant with more similar diffusion kinetics to Nd improved the index homogeneity. Additionally, the design of a gradient doping profile rather than a sharp compositional interface relaxed some precision and resolution requirements. Therefore, improved design, printing, and processing parameters are needed to take full advantage of these composite structures.

While DIW effectively builds advanced 3D structures, it is inherently limited in resolution. Nozzle sizes for DIW of ceramic particle-based slurries are typically greater than 500 microns. Attempts to use smaller nozzles require low-viscosity inks and are subject to frequent clogs. Collectively jetting discrete droplets onto a substrate is another 3DP technique or printing spatially tailored geometries into a ceramic green body [269]. This method requires low-solids-loading inks but can print smaller feature sizes owing to the small 0.5nL droplet size. Particularly suited for printing thin layers of material, this method was used to successfully print planar waveguide structures with thicknesses ranging from 25 to 400 microns. Optical properties, including laser mode control, can be optimized by printing specific layer thicknesses and controlling the change in index between the waveguide core and clad; however, layer uniformity and interface roughness must be perfected to minimize optical scatter.

Similar developments in new printing styles and other ceramic 3D printing techniques of green bodies are currently being pursued to fabricate thin disk and slab laser geometries.

Transparent ceramics are a relatively uncommon form of optical material but have a few specific advantages in applications where traditional glass or single crystals can't be used. Specifically,

when used in conjunction with the ever-improving 3D Printing techniques, optical ceramics have the potential to open a new dominion of solid-state laser design.

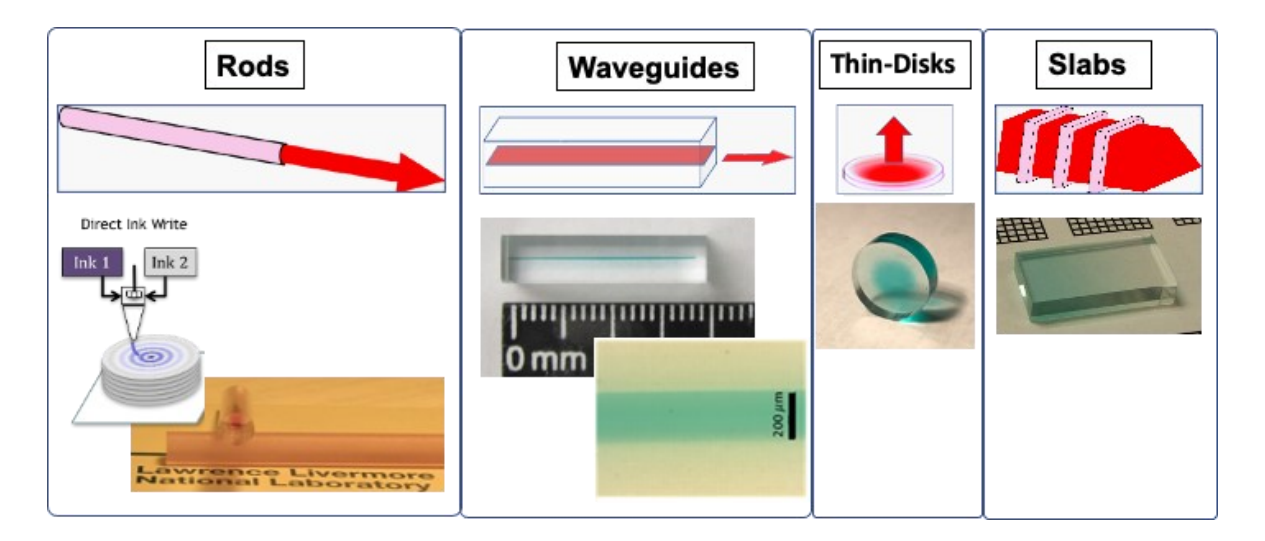


Figure 11. Several standard laser gain media geometries and examples of how 3D Printed ceramics can offer unique solutions and design advantages.

3.3. Biological applications of 3D Printing of ceramics

Replicating nature's intricate structures and compositions poses a considerable challenge, especially in biomedical research, where everyone's unique anatomy adds complexity. However, 3D printing has emerged as a transformative tool, showing potential in creating patient-specific implant structures that closely match the shape and size of the human bone to be replaced. This reduces post-operative complications and facilitates faster healing for the patient [270]. 3D printing enables the fabrication of site-specific structures with variations in functional gradient density, toughness, strength, and composition [271]. Among the materials that closely resemble the composition of natural bone, bio-ceramic materials such as alumina, zirconia, and calcium phosphates have demonstrated favorable biological interactions with tissues, **Figure 12**. 3D printing, coupled with bio-ceramic fabrication, has opened numerous opportunities in developing

materials for bone tissue engineering. Despite the promising potential, challenges persist in the manufacturing techniques employed for bio-ceramics, primarily due to their high melting points and inherent brittleness. However, due to the excellent bioactive nature of these materials, they have found applications in biomedical implants. The synergistic approach of 3D printing and bio-ceramics exemplifies a promising avenue in bone-tissue engineering.

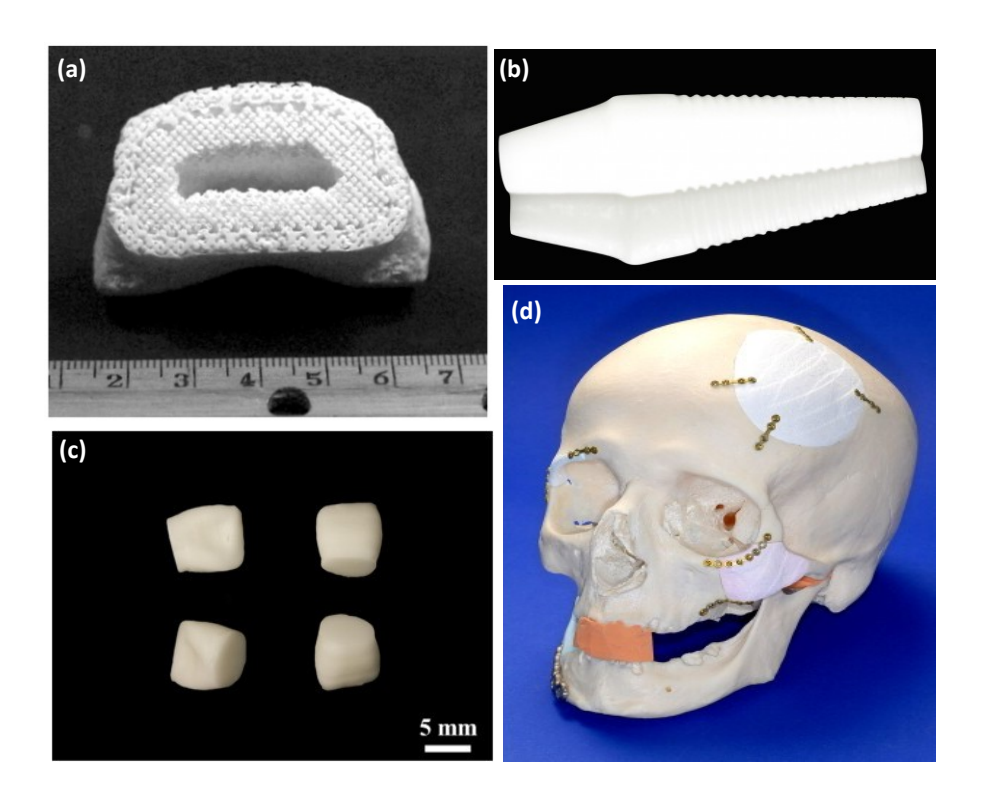


Figure 12. 3D Printed bio-ceramic implants (a) Alumina bone graft with gradient porosity [60]; (b) Monolithic zirconia dental screw processed via SLA-based DLP technique [50]; (c) ZrO2-Al2O3 dental implants prepared by SL technology [272]. (d) Patient-specific 3D printed calcium phosphate cranial implants [63].

3.3.1. Alumina ceramics

The utilization of alumina as a clinical biomaterial dates back to the 1970s, marking over two decades of its prominent role in dental and orthopedic applications [273]. Alumina, a bioinert material known for its exceptional mechanical strength, wear resistance, and biocompatibility, has become a cornerstone in various medical contexts. Notably, its outstanding tribological properties have led to its widespread adoption as the articulating surface in total hip arthroplasty (THR) implants [274,275]. The innate bio-inertness of alumina surfaces has spurred efforts to enhance osteogenesis within the alumina matrix. Techniques such as introducing dopants like Ca, Mg, and Si have been explored. Howlett et al. investigated the impact of Mg-doped alumina, revealing a significant improvement in the adhesion of human bone-derived cells compared to monolithic Al₂O₃ [276]. Similarly, Pabbruwe et al. explored the effects of Ca, Mn, and Cr dopants in alumina, each contributing to enhanced biological performance: Ca promoted hypertrophic bone formation, Cr enhanced bone remodeling, and Mn demonstrated a capacity to promote osteogenesis [277].

Surface modification strategies, including the introduction of amino ion groups, have demonstrated enhanced osteogenesis compared to plain alumina compositions [278]. Alumina surfaces are often coated with bioactive ceramics such as hydroxyapatite (HA), tricalcium phosphate (TCP), and bioglass. These coatings, enriched with osteogenic, angiogenic, and antibacterial dopants, aim to induce specific biological functionalities [279,280]. In dental implants, alumina's high strength positions it prominently in applications like dental crowns, bridges, and endodontic posts [281]. Dehurtevent et al. have successfully made alumina dental crowns using the stereolithography technique and studied the effect of the different building orientations on the mechanical and physical properties of the crown [282]. It was found that ZY-

oriented print with the smallest number of layers showed the best behavior. Griffith et al. also showed successful freeform alumina fabrication with stereolithography using fine powder suspension in photopolymerizable media [21]. Aqueous acrylamide-based suspension was used for alumina with viscosity below 500 mPa/s and cure depth above 300 μm, having a dose of 1500 mJ/cm². These alumina dental implants have recently been made using fused deposition modeling or fused deposition with glass infiltration [77]. These glass-infiltrated samples showed enhanced mechanical strength for 260 MPa, similar to leucite-type glass ceramics.

Alumina could also be employed as a porous scaffold with interconnected porosity for bone tissue engineering applications [283]. In one of the studies, controlled porosity 3D-honeycomb alumina scaffolds were made using an indirect fused deposition process, showing control over the shape of both internal architecture and the part [284]. The study showed that as the porosity amount increases, the strength of the alumina ceramics starts to decrease exponentially. Stringent guidelines from the US Food and Drug Administration (FDA) emphasize the implementation of only high-purity alumina for such critical applications [285]. The journey of alumina in biomedical applications has witnessed remarkable evolution. From initial uses with a 13% failure rate to modern advancements reducing failures to less than 5%, alumina manufacturing has entered a new era with the development of a third generation marked by high purity and high density [281,286,287].

3.3.2. Zirconia ceramics

Introduced as a dental material in the early 1990s, zirconia has emerged as a polymorphic ceramic with exceptional properties, surpassing even alumina in flexural strength [288]. Its

remarkable strength, bio-inert characteristics, and excellent corrosion and wear resistance position zirconia as a versatile material for various applications, spanning dental and orthopedic restorations [289–291]. Zirconia is often stabilized in the cubic or tetragonal phase through the addition of stabilizing dopants such as yttria (Y₂O₃), magnesia (MgO), ceria (CeO₂), or calcium oxide (CaO) [292,293]. Dental applications commonly involve using zirconia doped with three mol.% yttria [294]. The first 3D-printed zirconia dental implant was made in 2009 using direct inkjet printing [295]. Osman et al. also showed the printing of zirconia dental implants using stereolithography with accurate dimensions and close mechanical properties compared to conventional implants [296]. Many recent studies have also reported successful fabrication of zirconia full contour crowns and bridges [297–299]. Lu et al. have reported that yttria-stabilized tetragonal zirconia polycrystal (Y-TZP) made using digital light processing (DLP) acquires flexural strength compared to conventional subtractive manufacturing. While the uniaxial and biaxial strength shown by Y-TZP using subtractive manufacturing was 1171 MPa and 984 MPa, the DLP fabricated part showed uniaxial and biaxial strength of 1004 MPa and 742 MPa, respectively. 3D printing Zirconia is also utilized to fabricate ultra-thin veneers to treat worn-out or abrasive tooth substances [300]. Surface functionalization treatments are pivotal in inducing bioactivity and promoting host bone affinity for zirconia implants. Strategies include depositing phosphosilicate glasses, HA, or fluorapatite layers and the surface attachment of hydroxyl groups. These approaches have proven effective in enhancing biological activity at the host bone and implant interface compared to pure zirconia [301–304]. Beyond its dental applications, zirconia's excellent wear rates position it as a compelling choice as hip prosthesis material due to its biocompatibility and wear resistance. Studies have demonstrated low wear rates on both hip and knee simulators, further establishing the credibility of zirconia in orthopedic settings [305].

Zhu et al. made zirconia-based implants for the hip joint using Makerbot Z18 3D Printer and incorporated zinc oxide nanoparticles to induce antibacterial properties [306]. The antibacterial efficacy was studied against *Escherichia coli* and *Staphylococcus aureus* and showed that adding zinc oxide showed anti-bacterial efficacy of 91.7 ± 1.1 % and 99.8 ± 0.25 %, respectively. Further *in vivo* results showed that the implant after 4 weeks did not dislocate from its position and exhibited bone formation. Incorporating zirconia in biomedical engineering underscores its dual role as a material of strength and biocompatibility. With continuous advancements in surface treatments and its proven performance in diverse applications, zirconia stands as a testament to the evolving landscape of biomaterials in pursuing enhanced patient outcomes.

3.3.3. Calcium phosphates ceramics

Due to their remarkable similarity to the natural bone's composition, calcium phosphates (CaP) exhibit exceptional bioactivity and stand as one of the most widely used ceramic materials for bone regeneration and repair. Whether as the primary composition in artificial bone grafts or as coatings on metallic implants, calcium phosphate chemistry, especially hydroxyapatite (HA) and TCP, holds prevalence in biological applications [307,308]. They constitute approximately 60 wt. % of natural bone and 90 wt. % of tooth enamel, calcium phosphates emerge as a fitting material for bone scaffolds and replacement applications.

CaPs typically comprise of calcium ions (Ca²⁺) and orthophosphate ions (PO₄³⁻); the Ca/P atomic ratio influences their properties. Apatites with a Ca/P ratio of 1.5 to 1.67, such as HA, are known for their stability and low resorbability. Pure hydroxyapatites (Ca₁₀(PO₄)₆(OH)₂) with a Ca/P ratio of 1.67 have demonstrated long-term un-resorbed behavior in the body after several

years of implantation [309] and showcased bioactivity and osteoconductivity [310]. Tricalcium phosphate (TCP), such as β -TCP (Ca₃(PO₄)₂) with a Ca/P atomic ratio of 1.5, is known to resorb into the body. The choice between HA and β -TCP depends on the application; for instance, bone scaffolds requiring long-term integrity post-implantation may use HA, while β -TCP is suitable for applications such as bone tissue engineering scaffolds.

Apart from providing support as a bone graft, the 3D Printed CaP can also be a localized delivery vehicle. It can deliver osteogenic drugs, growth factors for bone repair, and antibiotics to treat infections. Oral administration of drugs to treat bone repair has limited overall efficacy due to systemic circulation and low drug concentration at the desired site. Localized drug delivery provides an excellent route by maximizing the dosage amount at the desired site, minimizing side effects to other normal cells, and improving the overall therapeutic efficacy [311]. Some *in vitro* and *in vivo* results of CaP scaffolds for bone tissue engineering are shown in **Figure 13.**

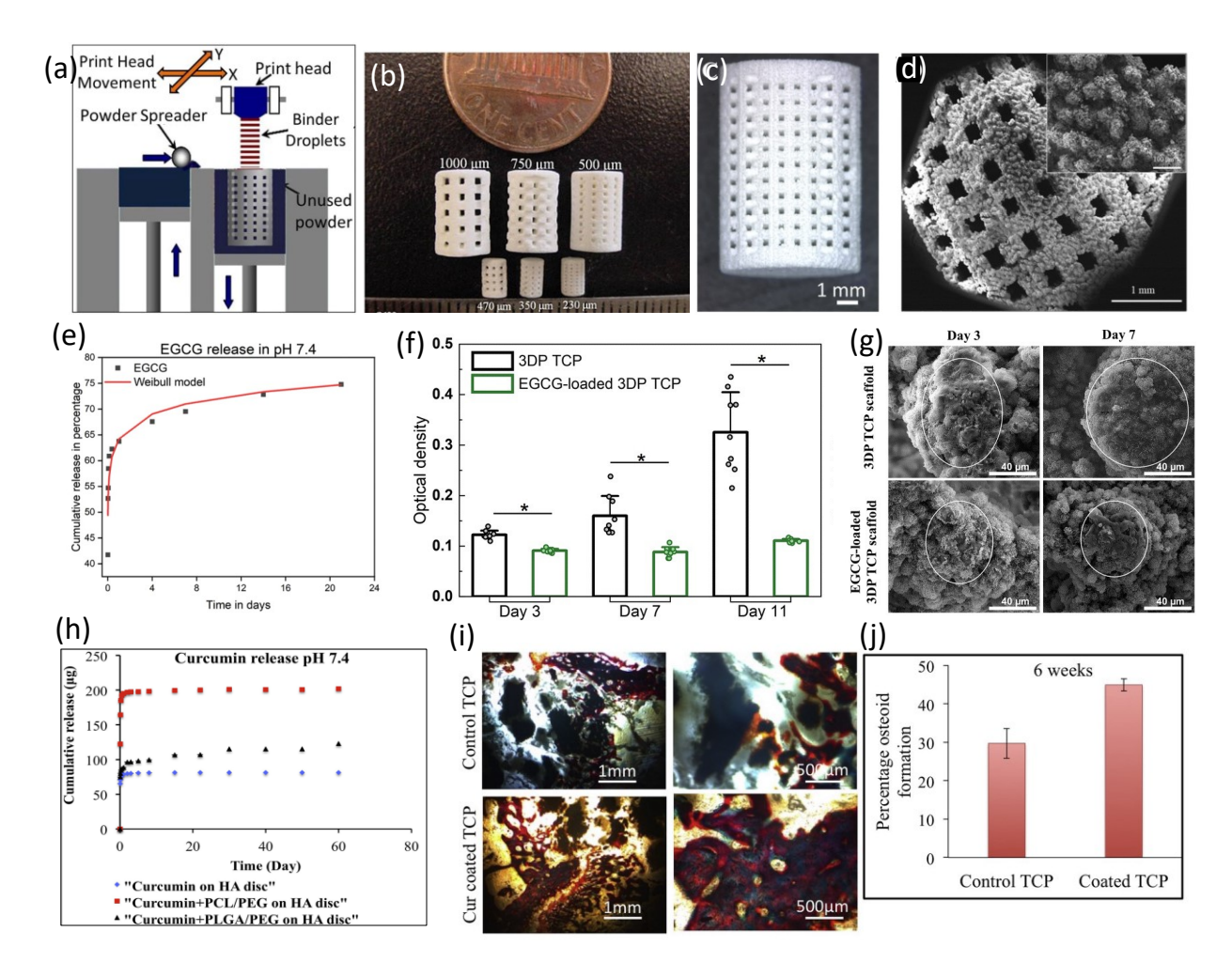


Figure 13. 3D Printed calcium phosphate scaffold for bone tissue engineering. (A) Schematic of binder jet 3D printing [78]; (b) Microwave-sintered 3D printed tricalcium phosphate scaffolds for bone tissue e; (c) and (d) A densified 3DP TCP scaffold with designed porosity of 400 μm after sintering results in reduced pore size with intrinsic residual micropores in the range of 5–20 μm as shown through scanning electron microscopy [79]; (e) *In vitro* release profile of epigallocatechin gallate (EGCG), an extract from green tea, exhibiting a release of 75 % after 21 days from 3DP TCP scaffold [79]; (f) The release of EGCG significantly reduces osteosarcoma growth to 66 % compared to control [79]; (g) Morphology of the cells shows ruptured morphology in the presence of EGCG on day 3 and day 7 [79] (h) Curcumin (an active ingredient from turmeric) release from the scaffold shows 64 % release with the addition of the

PCL-PEG polymer system [312]; (i) The release of curcumin from the 3DP TCP scaffold shows improved bone growth at the tissue-material interface, where the reddish-orange section shows the osteoid-like new bone formation and mineralized bone is shown in green [312]; (j) The histomorphometric analysis by ImageJ shows enhanced bone growth in the curcumin-coated scaffold after six weeks of surgery [312].

Despite their exceptional bioactivity, a drawback of CaPs is their mechanical strength. They exhibit brittleness and low tensile strength, ranging from 6-10 MPa [313]. This restricts their applications to low-load-bearing sites such as cranial and maxillofacial regions or as coatings on Ti-based implant materials for high-load-bearing sites. One of the most promising applications of 3D-printed CaPs lies in bone tissue engineering. 3D printing enables the creation of porous scaffolds with controlled pore architecture and functionalized composition, which can be used to fill bone defects and support the growth of new bone at the implant site [32,123].

4.0 Challenges and future directions

As outlined in this article, research related to 3D printing (3DP) of ceramics started in the early 1990s, and researchers were developing processes for various metal 3DPs around the same time. Yet, in the past three decades, significant development has happened in metal 3DP, widely used in numerous applications, but ceramic 3DP is still in its infancy. In 2022, the American Ceramic Society and the Materials Research Society jointly organized a Webinar to highlight different aspects of 3DP of ceramics. Experts worldwide participated in this Webinar to share

their insights and how they feel the 3DP of ceramics will evolve in the coming days. This Webinar covered various 3DP ceramic processing and applications. This review article is a culmination of that Webinar. Not only do experts from worldwide write each section of this review paper, but it also covers the current technological need, recent developments, and applications of 3D Printed ceramic structures. This review differs from other review articles published in recent years because of the in-depth processing-properties relationships given here, keeping current and future applications in mind. This is only possible because of subject matter experts' commentary, which makes this review possible. This review article is timely and critical for scientists and engineers dealing with ceramics.

3D printing of ceramics is a fast-moving field in which many innovations are currently being developed. However, the 3DP of ceramics is still in its infancy because of significant challenges related to materials development for different 3DP processes, process optimizations, and extensive post-processing requirements. Researchers have published many articles on different ceramic 3DP processes; however, very few commercial systems are available for ceramic 3DP. DIW, ceramic slurry-filled SLA, and binder jetting systems are the most popular for ceramic 3DP, and these technologies are seeing some commercial success. This section outlines some critical issues related to ceramic 3DP processes and potential future directions on how ceramic 3DP can make a difference. We have divided challenges into three categories – pre-processing, processing, and post-processing-related.

Pre-processing challenges: Pre-processing challenges will vary from process to process. For SLA or FDC processes, for example, extensive materials development work is needed to design the ceramic-filled slurry or filaments, respectively. Selecting ideal surfactants to increase the solids loading or a plasticizer to increase the flexibility of the filaments is not trivial. Also, starting powder particle size, distribution, and shape are critical to the process's overall flowability. Interestingly, although most polymer development work is needed during the preprocessing steps to make the 3DP process work, it is vital to remember that all polymers must be removed during the post-processing steps to have a dense ceramic part. Naturally, pre-processing steps require an extensive understanding of processing and post-processing operations. Binders developed during pre-processing are sensitive to materials chemistry. For example, a slurry composition developed for Al₂O₃ may not work directly for SiC powders. Many ceramic powders are moisture-sensitive, and special storage may be required for starting materials. This can make process optimization challenging as the viscosities may change at different times of the year or in different locations with varying humidity. A closed build environment, strict materials storage protocols, and minimum batch-to-batch powder-particle size variations are needed to make ceramic 3DP commercially successful. Finally, the reusability of unused starting materials also requires good scientific understanding and strict protocols to minimize batch-to-batch variations. Standards for usable DIW and SLA inks should be developed to help future researchers more accurately target their compositions. The composition-rheology relationships of inks containing anisotropic particulates are particularly poorly understood. Additional firstprinciples rheological experiments and simulations are needed to determine the relationships between flow properties and particulate morphology, aspect ratio, and size distribution. Such

knowledge will be necessary for developing more advanced inks that reach higher fractions of oriented particulates.

Processing challenges: Processing-related challenges are unique to each 3DP process and have already been discussed in detail. For example, challenges related to melt-cast LDED processes are different from those of slurry-based SLA. However, a few aspects are common for all processes, such as dimensional tolerances, support structures and how to remove them, and part size. Processes like LDED are suitable for small parts with simple shapes, while binder jetting can print large parts with complex shapes. However, extensive process optimization is needed for all processes before reliable and reproducible parts can be 3D printed. Printing of functionalized parts is hampered by the lack of design and control software that enables control over factors other than shape. Additional data had to be manually inserted into the G-code used to execute the print to control composition in the DIW experiments as usable part files. stl format and slicing software only account for shape information.

Post-processing challenges: The main post-processing challenges are removing support structures, binder removal, and densification or sintering. Processes like SLA require additional curing steps, or binder jetting needs drying and depowdering, which are unique. Removing the support structure without damaging the part can be an issue for fused deposition or DIW parts, as those parts do not have high mechanical strength in the green state. Binder removal of SLA or FDC is challenging due to low solids-loading. In most cases, thermal debinding is used, where a slow heating rate removes the binder from the part, followed by high-temperature sintering. If binder chemistry can be designed such that solvent extraction can be used to remove a part of the initial binder volume, then faster heating can be used to remove the remaining binder. Naturally, designing polymer chemistry becomes essential not just for the pre-processing steps but also for

the post-processing. The sintering of 3D-printed parts is sensitive to the materials' chemistry. While the oxide ceramics can be sintered in air, nitrides, carbides, or borides require unique sintering environments to prevent degradation. Unfortunately, cracking, delamination, and warping are common in 3D-printed ceramic parts, which are evident after the sintering cycles. This is not only frustrating but also makes ceramic 3D printing expensive. Sintering multimaterial green bodies requires that the constituents be chemically compatible and have similar densification temperatures. Densification of parts with anisotropic particulates is also challenging due to the anisotropic shrinkage of platelets and fibers and the tendency to create "overhang" porosity. Even when densification can be achieved, residual stresses from the coefficient of thermal expansion mismatches can cause cracking or spallation. Future research should investigate novel co-sintering or additive methods that avoid the need for green body densification to minimize these issues. Methods are also needed to model the residual stresses more accurately when designing and sintering multi-material ceramics. Ceramic 3D printing's future is headed in directions that offer capabilities beyond the traditional shape-control of AM techniques, with increasing demand for and research on capabilities enabling multi-material and microstructurally controlled parts.

Although this manuscript is focused primarily on pure ceramic part fabrication, significant work has been done over the years on ceramic-based composites that involve ceramic Printing. 3DP of metal-ceramic composites where ceramic preforms were infiltrated with liquid metals can enhance the mechanical properties significantly [314]. In recent years, LDED has been used to print ceramic-metal or functionally graded composites offering unique location-specific properties or naturally architected designs [315–317]. Future research with ceramics and composites using 3D printing has the potential to transform ceramic processing as it did to

metals and polymers and is expected to enable innovative product designs offering locationspecific properties and on-demand manufacturing.

5.0 Acknowledgments

Profs. Bandyopadhyay and Bose acknowledge financial support from the National Science Foundation under Grant Number CMMI 1934230. Dr. Seeley acknowledge his part of this work was performed under the auspices of the U.S. Department of Energy by Lawrence Livermore National Laboratory under Contract DE AC52 07NA27344. LLNL-JRNL- 835915.

6.0 Declaration of Competing Interest

The authors declare that they have no known competing financial interests or personal relationships that could have appeared to influence the work reported in this paper.

7.0 Data availability statement

The authors declare that all data supporting the findings of this study are available within the paper.

8.0 References

- [1] Y. Lakhdar, C. Tuck, J. Binner, A. Terry, R. Goodridge, Additive manufacturing of advanced ceramic materials, Prog Mater Sci 116 (2021) 100736. https://doi.org/10.1016/j.pmatsci.2020.100736.
- [2] Z. Chen, Z. Li, J. Li, C. Liu, C. Lao, Y. Fu, C. Liu, Y. Li, P. Wang, Y. He, 3D printing of ceramics: A review, J Eur Ceram Soc 39 (2019) 661–687. https://doi.org/10.1016/j.jeurceramsoc.2018.11.013.
- [3] R.P. Chaudhary, C. Parameswaran, M. Idrees, A.S. Rasaki, C. Liu, Z. Chen, P. Colombo, Additive manufacturing of polymer-derived ceramics: Materials, technologies, properties and potential applications, Prog Mater Sci 128 (2022) 100969. https://doi.org/10.1016/j.pmatsci.2022.100969.
- [4] S. Eqtesadi, A. Motealleh, F.H. Perera, P. Miranda, A. Pajares, R. Wendelbo, F. Guiberteau, A.L. Ortiz, Fabricating geometrically-complex B4C ceramic components by robocasting and pressureless spark plasma sintering, Scr Mater 145 (2018) 14–18. https://doi.org/10.1016/j.scriptamat.2017.10.001.
- [5] Y. de Hazan, D. Penner, SiC and SiOC ceramic articles produced by stereolithography of acrylate modified polycarbosilane systems, J Eur Ceram Soc 37 (2017) 5205–5212. https://doi.org/10.1016/J.JEURCERAMSOC.2017.03.021.
- [6] M. Krinitcyn, Z. Fu, J. Harris, K. Kostikov, G.A. Pribytkov, P. Greil, N. Travitzky, Laminated Object Manufacturing of in-situ synthesized MAX-phase composites, Ceram Int 43 (2017) 9241–9245. https://doi.org/10.1016/j.ceramint.2017.04.079.
- [7] F. Zhang, Z. Li, M. Xu, S. Wang, N. Li, J. Yang, A review of 3D printed porous ceramics, J Eur Ceram Soc 42 (2022) 3351–3373. https://doi.org/10.1016/j.jeurceramsoc.2022.02.039.
- [8] N. Yashiro, T. Usui, K. Kikuta, Application of a thin intermediate cathode layer prepared by inkjet printing for SOFCs, J Eur Ceram Soc 30 (2010) 2093–2098. https://doi.org/10.1016/j.jeurceramsoc.2010.04.012.
- [9] M. C. Leu, B.K. Deuser, L. Tang, R.G. Landers, G.E. Hilmas, J.L. Watts, Freeze-form extrusion fabrication of functionally graded materials, CIRP Ann Manuf Technol 61 (2012) 223–226. https://doi.org/10.1016/j.cirp.2012.03.050.
- [10] W. Wang, L. Zhang, X. Dong, J. Wu, Q. Zhou, S. Li, C. Shen, W. Liu, G. Wang, R. He, Additive manufacturing of fiber reinforced ceramic matrix composites: Advances, challenges, and prospects, Ceram Int 48 (2022) 19542–19556. https://doi.org/10.1016/j.ceramint.2022.04.146.

- [11] A. Zocca, P. Colombo, C.M. Gomes, J. Günster, Additive Manufacturing of Ceramics: Issues, Potentialities, and Opportunities, Journal of the American Ceramic Society 98 (2015) 1983–2001. https://doi.org/10.1111/jace.13700.
- [12] C. L. Cramer, E. Ionescu, M. Graczyk-Zajac, A.T. Nelson, Y. Katoh, J.J. Haslam, L. Wondraczek, T.G. Aguirre, S. LeBlanc, H. Wang, M. Masoudi, E. Tegeler, R. Riedel, P. Colombo, M. Minary-Jolandan, Additive manufacturing of ceramic materials for energy applications: Road map and opportunities, J Eur Ceram Soc 42 (2022) 3049–3088. https://doi.org/10.1016/j.jeurceramsoc.2022.01.058.
- [13] T. G. Aguirre, C.L. Cramer, D.J. Mitchell, Review of additive manufacturing and densification techniques for the net- and near net-shaping of geometrically complex silicon nitride components, J Eur Ceram Soc 42 (2022) 735–743. https://doi.org/10.1016/j.jeurceramsoc.2021.11.001.
- [14] H. L. Marcus, J.J. Beaman, J.W. Barlow, D.L. Bourell, Solid freeform fabrication. Powder processing, American Ceramic Society Bulletin 69 (1990) 1030–1031.
- [15] H. L. Marcus, J.W. Barlow, J.J. Beaman, D.L. Bourell, From computer to component in 15 minutes: The integrated manufacture of three-dimensional objects, JOM 42 (1990) 8–10. https://doi.org/10.1007/BF03220915.
- [16] E. Sachs, M. Cima, J. Cornie, Three-Dimensional Printing: Rapid Tooling and Prototypes Directly from a CAD Model, CIRP Annals 39 (1990) 201–204. https://doi.org/10.1016/S0007-8506(07)61035-X.
- [17] U. Lakshminarayan, H.L. Marcus, Microstructural and Mechanical Properties of Al2O3/P2O5 AND Al2O3/B2O3 Composties Fabricated by Selective Laser Sintering, International Solid Freeform Fabrication Symposium (1991) 205–212.
- [18] E. Sachs, M. Cima, P. Williams, D. Brancazio, J. Cornie, Three Dimensional Printing: Rapid Tooling and Prototypes Directly from a CAD Model, Journal of Engineering for Industry 114 (1992) 481–488. https://doi.org/10.1115/1.2900701.
- [19] P. F. Blazdell, J.R.G. Evans, M.J. Edirisinghe, P. Shaw, M.J. Binstead, The computer aided manufacture of ceramics using multilayer jet printing, J Mater Sci Lett 14 (1995) 1562–1565. https://doi.org/10.1007/BF00455415.
- [20] M.L. Griffith, J.W. Halloran, Ultraviolet Curing of Highly Loaded Ceramic Suspensions for Stereolithography of Ceramics, Solid Freeform Fabrication Symposium (1994) 396–403. http://www.dtic.mil/cgi-bin/GetTRDoc?AD=ADA290949#page=405.
- [21] M. L. Griffith, J.W. Halloran, Freeform Fabrication of Ceramics via Stereolithography, Journal of the American Ceramic Society 79 (1996) 2601–2608. https://doi.org/10.1111/J.1151-2916.1996.TB09022.X.

- [22] C. Griffin, J. Daufenbach, S. McMillin, Solid Freeform Fabrication of Functional Ceramic Components Using a Laminated Object Manufacturing Technique, Solid Freeform Fabrication Conf. (1994) 17–24.
- [23] C. Griffin, D. Bautenbach, S. McMillin, Desktop manufacturing. LOM vs pressing, American Ceramic Society Bulletin 73 (1994) 109–113.
- [24] M. K. Agarwala, A. Bandyopadhyay, R. van Weeren, P. Whalen, A. Safari and S. C. Danforth, "Fused Deposition of Ceramics: Rapid Fabrication of Structural Ceramic Components," *Ceramic Bulletin*, **11**, 60-65, (1996).
- [25] J. Cesarano, R. Segalman, P. Calvert, Robocasting provides moldless fabrication from slurry deposition, Ceramic Industry 148 (1998) 94–100.
- [26] M. Zhou, W. Liu, H. Wu, X. Song, Y. Chen, L. Cheng, F. He, S. Chen, S. Wu, Preparation of a defect-free alumina cutting tool via additive manufacturing based on stereolithography Optimization of the drying and debinding processes, Ceram Int 42 (2016) 11598–11602. https://doi.org/10.1016/j.ceramint.2016.04.050.
- [27] T. A. Pham, D.P. Kim, T.W. Lim, S.H. Park, D.Y. Yang, K.S. Lee, Three-dimensional SiCN ceramic microstructures via nano-stereolithography of inorganic polymer photoresists, Adv Funct Mater 16 (2006) 1235–1241. https://doi.org/10.1002/adfm.200600009.
- [28] I. Shishkovsky, I. Yadroitsev, P. Bertrand, I. Smurov, Alumina-zirconium ceramics synthesis by selective laser sintering/melting, Appl Surf Sci 254 (2007) 966–970. https://doi.org/10.1016/j.apsusc.2007.09.001.
- [29] J. Deckers, S. Meyers, J.P. Kruth, J. Vleugels, Direct selective laser sintering/melting of high density alumina powder layers at elevated temperatures, Phys Procedia 56 (2014) 117–124. https://doi.org/10.1016/j.phpro.2014.08.154.
- [30] V. K. Balla, S. Bose, A. Bandyopadhyay, Processing of Bulk Alumina Ceramics Using Laser Engineered Net Shaping, Int J Appl Ceram Technol 5 (2008) 234–242. https://doi.org/10.1111/J.1744-7402.2008.02202.X.
- [31] S. Bose, D. Ke, H. Sahasrabudhe, A. Bandyopadhyay, Additive manufacturing of biomaterials, Prog Mater Sci 93 (2018) 45–111. https://doi.org/10.1016/j.pmatsci.2017.08.003.
- [32] S. Bose, S. Vahabzadeh, A. Bandyopadhyay, Bone tissue engineering using 3D printing, Materials Today 16 (2013) 496–504. https://doi.org/10.1016/J.MATTOD.2013.11.017.

- [33] A. Zocca, C. Gomes, U. Linow, H. Marx, J. Melcher, P. Colombo, J. Günster, Structural optimization of printed structures by self-organized relaxation, Rapid Prototyp J 22 (2016) 344–349. https://doi.org/10.1108/RPJ-07-2014-0087.
- [34] W. Wang, X. Bai, L. Zhang, S. Jing, C. Shen, R. He, Additive manufacturing of Csf/SiC composites with high fiber content by direct ink writing and liquid silicon infiltration, Ceram Int 48 (2022) 3895–3903. https://doi.org/10.1016/j.ceramint.2021.10.176.
- [35] H. Mei, Y. Yan, L. Feng, K.G. Dassios, H. Zhang, L. Cheng, First printing of continuous fibers into ceramics, Journal of the American Ceramic Society 102 (2019) 3244–3255. https://doi.org/10.1111/jace.16234.
- [36] Z. Zhao, G. Zhou, Z. Yang, X. Cao, D. Jia, Y. Zhou, Direct ink writing of continuous SiO2 fiber reinforced wave-transparent ceramics, Journal of Advanced Ceramics 9 (2020) 403–412. https://doi.org/10.1007/s40145-020-0380-y.
- [37] C.S. Chua, S.Y. Ow, S.L. Liew, J. Liu, C.B. Soh, L. Shen, S. Wang, 3D printing of fibre-reinforced ceramic composites with hierarchical structure, Advances in Applied Ceramics 121 (2022) 46–51. https://doi.org/10.1080/17436753.2021.2014276.
- [38] X. Fu, B. Zou, H. Xing, L. Li, Y. Li, X. Wang, Effect of printing strategies on forming accuracy and mechanical properties of ZrO2 parts fabricated by SLA technology, Ceram Int 45 (2019) 17630–17637. https://doi.org/10.1016/J.CERAMINT.2019.05.328.
- [39] K. Li, Z. Zhao, The effect of the surfactants on the formulation of UV-curable SLA alumina suspension, Ceram Int 43 (2017) 4761–4767. https://doi.org/10.1016/J.CERAMINT.2016.11.143.
- [40] X. Shuai, Y. Zeng, P. Li, J. Chen, Fabrication of fine and complex lattice structure Al2O3 ceramic by digital light processing 3D printing technology, J Mater Sci 55 (2020) 6771–6782. https://doi.org/10.1007/S10853-020-04503-Y/TABLES/2.
- [41] G. Franchin, H. Elsayed, R. Botti, K. Huang, J. Schmidt, G. Giometti, A. Zanini, A. De Marzi, M. D'Agostini, P. Scanferla, Y. Feng, P. Colombo, Additive Manufacturing of Ceramics from Liquid Feedstocks, Chinese Journal of Mechanical Engineering: Additive Manufacturing Frontiers 1 (2022) 100012. https://doi.org/10.1016/j.cjmeam.2022.100012.
- [42] J. Schmidt, P. Colombo, Digital light processing of ceramic components from polysiloxanes, J Eur Ceram Soc 38 (2018) 57–66. https://doi.org/10.1016/j.jeurceramsoc.2017.07.033.
- [43] X. Wang, F. Schmidt, D. Hanaor, P.H. Kamm, S. Li, A. Gurlo, Additive manufacturing of ceramics from preceramic polymers: A versatile stereolithographic approach assisted by thiol-ene click chemistry, Addit Manuf 27 (2019) 80–90. https://doi.org/10.1016/j.addma.2019.02.012.

- [44] I. Cooperstein, E. Shukrun, O. Press, A. Kamyshny, S. Magdassi, Additive Manufacturing of Transparent Silica Glass from Solutions, ACS Appl Mater Interfaces 10 (2018) 18879–18885. https://doi.org/10.1021/acsami.8b03766.
- [45] J. Wang, B. Zheng, P. Wang, 3D printed Er3+/Yb3+ co-doped phosphosilicate glass based on sol-gel technology, J Non Cryst Solids 550 (2020) 120362. https://doi.org/10.1016/j.jnoncrysol.2020.120362.
- [46] I. Cooperstein, S.R.K.C. Indukuri, A. Bouketov, U. Levy, S. Magdassi, 3D Printing of Micrometer-Sized Transparent Ceramics with On-Demand Optical-Gain Properties, Advanced Materials 32 (2020) 1–8. https://doi.org/10.1002/adma.202001675.
- [47] T. Rosental, S. Mizrahi, A. Kamyshny, S. Magdassi, Particle-free compositions for printing dense 3D ceramic structures by digital light processing, Virtual Phys Prototyp 16 (2021) 255–266. https://doi.org/10.1080/17452759.2021.1922121.
- [48] E. Shukrun, I. Cooperstein, S. Magdassi, 3D-Printed Organic–Ceramic Complex Hybrid Structures with High Silica Content, Advanced Science 5 (2018) 1–7. https://doi.org/10.1002/advs.201800061.
- [49] D. G. Moore, L. Barbera, K. Masania, A.R. Studart, Three-dimensional printing of multicomponent glasses using phase-separating resins, Nat Mater 19 (2020) 212–217. https://doi.org/10.1038/s41563-019-0525-y.
- [50] R. B. Osman, A.J. van der Veen, D. Huiberts, D. Wismeijer, N. Alharbi, 3D-printing zirconia implants; a dream or a reality? An in-vitro study evaluating the dimensional accuracy, surface topography and mechanical properties of printed zirconia implant and discs, J Mech Behav Biomed Mater 75 (2017) 521–528. https://doi.org/10.1016/J.JMBBM.2017.08.018.
- [51] L. Zhao, Y. Zhang, L. Wu, Z. Zhao, Z. Men, F. Yang, Developing the optimized control scheme for continuous and layer-wise DLP 3D printing by CFD simulation, International Journal of Advanced Manufacturing Technology 125 (2023) 1511–1529. https://doi.org/10.1007/S00170-022-10658-6/METRICS.
- [52] G. Pierin, C. Grotta, P. Colombo, C. Mattevi, Direct Ink Writing of micrometric SiOC ceramic structures using a preceramic polymer, J Eur Ceram Soc 36 (2016) 1589–1594. https://doi.org/10.1016/j.jeurceramsoc.2016.01.047.
- [53] K. Huang, H. Elsayed, G. Franchin, P. Colombo, Additive manufacturing of SiOC scaffolds with tunable structure-performance relationship, J Eur Ceram Soc 41 (2021) 7552–7559. https://doi.org/10.1016/j.jeurceramsoc.2021.08.043.

- [54] K. Huang, H. Elsayed, G. Franchin, P. Colombo, Complex SiOC ceramics from 2D structures by 3D printing and origami, Addit Manuf 33 (2020) 101144. https://doi.org/10.1016/j.addma.2020.101144.
- [55] G. Franchin, H.S. Maden, L. Wahl, A. Baliello, M. Pasetto, P. Colombo, Optimization and characterization of preceramic inks for Direct Ink Writing of Ceramic Matrix Composite structures, Materials 11 (2018) 1–14. https://doi.org/10.3390/ma11040515.
- [56] H. Elsayed, M. Sayed, S.M. Naga, P. Rebesan, C. Gardin, B. Zavan, P. Colombo, E. Bernardo, Additive manufacturing and direct synthesis of sphene ceramic scaffolds from a silicone resin and reactive fillers, J Eur Ceram Soc 42 (2022) 286–295. https://doi.org/10.1016/j.jeurceramsoc.2021.10.001.
- [57] R. Dylla-Spears, T.D. Yee, K. Sasan, D.T. Nguyen, N.A. Dudukovic, J.M. Ortega, M.A. Johnson, O.D. Herrera, F.J. Ryerson, L.L. Wong, 3D printed gradient index glass optics, Sci Adv 6 (2020) 1–8. https://doi.org/10.1126/sciadv.abc7429.
- [58] M. A. Torres Arango, Y. Zhang, R. Li, G. Doerk, A. Fluerasu, L. Wiegart, In-Operando Study of Shape Retention and Microstructure Development in a Hydrolyzing Sol-Gel Ink during 3D-Printing, ACS Appl Mater Interfaces 12 (2020) 51044–51056. https://doi.org/10.1021/acsami.0c14743.
- [59] A. De Marzi, G. Giometti, J. Erler, P. Colombo, G. Franchin, Hybrid additive manufacturing for the fabrication of freeform transparent silica glass components, Addit Manuf 54 (2022) 102727. https://doi.org/10.1016/j.addma.2022.102727.
- [60] J. Darsell, S. Bose, H.L. Hosick, A. Bandyopadhyay, From CT scan to ceramic bone graft, Journal of the American Ceramic Society 86 (2003) 1076–1080. https://doi.org/10.1111/J.1151-2916.2003.TB03427.X.
- [61] E. Shukrun Farrell, Y. Schilt, M.Y. Moshkovitz, Y. Levi-Kalisman, U. Raviv, S. Magdassi, 3D Printing of Ordered Mesoporous Silica Complex Structures, Nano Lett 20 (2020) 6598–6605. https://doi.org/10.1021/acs.nanolett.0c02364.
- [62] M. Griffith, J. Halloran, Ultraviolet curable ceramic suspensions for stereolithography of ceramics, (1994).
- [63] U. Klammert, U. Gbureck, E. Vorndran, J. Rödiger, P. Meyer-Marcotty, A.C. Kübler, 3D powder printed calcium phosphate implants for reconstruction of cranial and maxillofacial defects, Journal of Cranio-Maxillofacial Surgery 38 (2010) 565–570. https://doi.org/10.1016/J.JCMS.2010.01.009.
- [64] X. Bai, G. Ding, K. Zhang, W. Wang, N. Zhou, D. Fang, R. He, Stereolithography additive manufacturing and sintering approaches of SiC ceramics, Open Ceramics 5 (2021) 100046. https://doi.org/10.1016/J.OCERAM.2020.100046.

- [65] G. Konstantinou, E. Kakkava, L. Hagelüken, P.V. Warriam Sasikumar, J. Wang, M.G. Makowska, G. Blugan, N. Nianias, F. Marone, H. Van Swygenhoven, J. Brugger, D. Psaltis, C. Moser, Additive micro-manufacturing of crack-free PDCs by two-photon polymerization of a single, low-shrinkage preceramic resin, Addit Manuf 35 (2020) 101343. https://doi.org/10.1016/j.addma.2020.101343.
- [66] W. J. Costakis, C. Wyckoff, A. Schlup, M. Wallace, T. Craigs, E. Malek, A. Hilmas, L. Rueschhoff, Material extrusion of highly-loaded silicon nitride aqueous inks for solid infilled structures, Addit Manuf 64 (2023) 103425. https://doi.org/10.1016/J.ADDMA.2023.103425.
- [67] A. Bandyopadhyay, I. Mitra, S. Bose, 3D Printing for Bone Regeneration, Curr Osteoporos Rep 18 (2020) 505–514. https://doi.org/10.1007/S11914-020-00606-2/METRICS.
- [68] S. Bose, S. Tarafder, Calcium phosphate ceramic systems in growth factor and drug delivery for bone tissue engineering: A review, Acta Biomater 8 (2012) 1401–1421. https://doi.org/10.1016/J.ACTBIO.2011.11.017.
- [69] A. Khalyfa, S. Vogt, J. Weisser, G. Grimm, A. Rechtenbach, W. Meyer, M. Schnabelrauch, Development of a new calcium phosphate powder-binder system for the 3D printing of patient specific implants, J Mater Sci Mater Med 18 (2007) 909–916. https://doi.org/10.1007/s10856-006-0073-2.
- [70] A. Zocca, C.M. Gomes, E. Bernardo, R. Müller, J. Günster, P. Colombo, LAS glass-ceramic scaffolds by three-dimensional printing, J Eur Ceram Soc 33 (2013) 1525–1533. https://doi.org/10.1016/j.jeurceramsoc.2012.12.012.
- [71] M. Mariani, R. Beltrami, P. Brusa, C. Galassi, R. Ardito, N. Lecis, 3D printing of fine alumina powders by binder jetting, J Eur Ceram Soc 41 (2021) 5307–5315. https://doi.org/10.1016/j.jeurceramsoc.2021.04.006.
- [72] X. Yin, N. Travitzky Ã, P. Greil, Near-Net-Shape Fabrication of Ti 3 AlC 2-Based Composites A redox re-action at 14001C resulted in the formation of dense Ti-Al-O-C composites mainly composed of Ti, (n.d.). https://doi.org/10.1111/j.1744-7402.2007.02123.x.
- [73] "Additive Manufacturing 2nd Edition" Edited by Amit Bandyopadhyay and Susmita Bose, CRC Press (2019).
- [74] J. Suwanprateeb, F. Thammarakcharoen, K. Wasoontararat, W. Suvannapruk, Influence of printing parameters on the transformation efficiency of 3D-printed plaster of paris to hydroxyapatite and its properties, (n.d.). https://doi.org/10.1108/13552541211272036.

- [75] D. C. Tancred, B.A.O. Mccormack, A.J. Carr, A synthetic bone implant macroscopically identical to cancellous bone, Biomaterials 19 (1998) 2303–2311.
- [76] J. Suwanprateeb, R. Sanngam, T. Panyathanmaporn, Influence of raw powder preparation routes on properties of hydroxyapatite fabricated by 3D printing technique, Materials Science & Engineering C 30 (2010) 610–617. https://doi.org/10.1016/j.msec.2010.02.014.
- [77] A. Arnesano, S. Kunjalukkal Padmanabhan, A. Notarangelo, F. Montagna, A. Licciulli, Fused deposition modeling shaping of glass infiltrated alumina for dental restoration, Ceram Int 46 (2020) 2206–2212. https://doi.org/10.1016/J.CERAMINT.2019.09.205.
- [78] S. Tarafder, V.K. Balla, N.M. Davies, A. Bandyopadhyay, S. Bose, Microwave-sintered 3D printed tricalcium phosphate scaffolds for bone tissue engineering, J Tissue Eng Regen Med 7 (2013) 631–641. https://doi.org/10.1002/TERM.555.
- [79] Y. Jo, N. Sarkar, S. Bose, In vitro biological evaluation of epigallocatechin gallate (EGCG) release from three-dimensional printed (3DP) calcium phosphate bone scaffolds, J Mater Chem B 11 (2023) 5503–5513. https://doi.org/10.1039/D2TB02210A.
- [80] K. Cox, The Influence of Print Layer Orientation on the Mechanical Properties of Sic and Cf/Sic Cmcs Formed Via Direct Ink Writing, Purdue University, 2021.
- [81] J. Cesarano, A review of robocasting technology, Materials Research Society Symposium Proceedings 542 (1999) 133–139. https://doi.org/10.1557/proc-542-133.
- [82] J. A. Lewis, J.E. Smay, J. Stuecker, J. Cesarano, Direct ink writing of three-dimensional ceramic structures, Journal of the American Ceramic Society 89 (2006) 3599–3609. https://doi.org/10.1111/j.1551-2916.2006.01382.x.
- [83] E. Peng, D. Zhang, J. Ding, Ceramic Robocasting: Recent Achievements, Potential, and Future Developments, Advanced Materials 30 (2018) 1–14. https://doi.org/10.1002/adma.201802404.
- [84] A. Shahzad, I. Lazoglu, Direct ink writing (DIW) of structural and functional ceramics: Recent achievements and future challenges, Compos B Eng 225 (2021) 109249. https://doi.org/10.1016/j.compositesb.2021.109249.
- [85] L. Rueschhoff, Correction to: Ceramic Additive for Aerospace, in: S.M. DelVecchio (Ed.), Women in 3D Printing, Spinger, Cham, 2021. https://doi.org/10.1007/978-3-030-70736-1_13.
- [86] Z. Lu, Y. Xia, K. Miao, S. Li, L. Zhu, H. Nan, J. Cao, D. Li, Microstructure control of highly oriented short carbon fibres in SiC matrix composites fabricated by direct ink writing, Ceram Int 45 (2019) 17262–17267. https://doi.org/10.1016/j.ceramint.2019.05.283.

- [87] S. Rangarajan, G. Qi, N. Venkataraman, A. Safari, S.C. Danforth, Powder Processing, Rheology, and Mechanical Properties of Feedstock for Fused Deposition of Si3N4 Ceramics, Journal of the American Ceramic Society 83 (2000) 1663–1669. https://doi.org/10.1111/J.1151-2916.2000.TB01446.X.
- [88] E. K. Akdogan, M. Allahverdi, A. Safari, Piezoelectric composites for sensor and actuator applications, IEEE Trans Ultrason Ferroelectr Freq Control 52 (2005) 746–775. https://doi.org/10.1109/TUFFC.2005.1503962.
- [89] A. Safari, E.K. Akdogan, Rapid Prototyping of Novel Piezoelectric Composites, Ferroelectrics 331 (2006) 153–179. https://doi.org/10.1080/00150190600737727.
- [90] G. M. Lous, I.A. Cornejo, T.F. McNulty, A. Safari, S.C. Danforth, Fabrication of Piezoelectric Ceramic/Polymer Composite Transducers Using Fused Deposition of Ceramics, Journal of the American Ceramic Society 83 (2000) 124–28. https://doi.org/10.1111/J.1151-2916.2000.TB01159.X.
- [91] F. Mohammadi, A.L. Kholkin, B. Jadidian, A. Safari, High-displacement spiral piezoelectric actuators, Appl Phys Lett 75 (1999) 2488–2490. https://doi.org/10.1063/1.125057.
- [92] F. Mohammadi, Mohammadi, Farhad, An investigation of the development of novel piezoelectric actuator designs by fused deposition of ceramics (FDC), PhDT (2001). https://ui.adsabs.harvard.edu/abs/2001PhDT......250M/abstract (accessed February 21, 2024).
- [93] P. Ngernchuklin, E.K. Akdoğan, A. Safari, B. Jadidian, Electromechanical displacement of piezoelectric-electrostrictive monolithic bilayer composites, J Appl Phys 105 (2009) 34102. https://doi.org/10.1063/1.3073990/383775.
- [94] A. Hall, M. Allahverdi, E.K. Akdogan, A. Safari, Piezoelectric/electrostrictive multimaterial PMN-PT monomorph actuators, J Eur Ceram Soc 25 (2005) 2991–2997. https://doi.org/10.1016/J.JEURCERAMSOC.2005.03.196.
- [95] L. Rueschhoff, W. Costakis, M. Michie, J. Youngblood, R. Trice, Additive Manufacturing of Dense Ceramic Parts via Direct Ink Writing of Aqueous Alumina Suspensions, Int J Appl Ceram Technol 13 (2016) 821–830. https://doi.org/10.1111/ijac.12557.
- [96] J. S. Pelz, N. Ku, W.T. Shoulders, M.A. Meyers, L.R. Vargas-Gonzalez, Multi-material additive manufacturing of functionally graded carbide ceramics via active, in-line mixing, Addit Manuf 37 (2021) 101647. https://doi.org/10.1016/J.ADDMA.2020.101647.
- [97] F. Klocke, A.E. Christian, D. Ae, C.A. Ae, A. Demmer, PRODUCTION PROCESS Investigations on laser sintering of ceramic slurries, (n.d.). https://doi.org/10.1007/s11740-007-0047-3.

- [98] J. Wilkes, Y.C. Hagedorn, W. Meiners, K. Wissenbach, Additive manufacturing of ZrO2-Al2O3 ceramic components by selective laser melting, Rapid Prototyp J 19 (2013) 51–57. https://doi.org/10.1108/13552541311292736/FULL/PDF.
- [99] P. Bertrand, F. Bayle, C. Combe, P. Goeuriot, I. Smurov, Ceramic components manufacturing by selective laser sintering, Appl Surf Sci 254 (2007) 989–992. https://doi.org/10.1016/j.apsusc.2007.08.085.
- [100] H. Yves-Christian, W. Jan, M. Wilhelm, W. Konrad, P. Reinhart, Net shaped high performance oxide ceramic parts by selective laser melting, Phys Procedia 5 (2010) 587–594. https://doi.org/10.1016/J.PHPRO.2010.08.086.
- [101] I. Gibson, D. Rosen, B. Stucker, Additive manufacturing technologies: 3D printing, rapid prototyping, and direct digital manufacturing, second edition, Additive Manufacturing Technologies: 3D Printing, Rapid Prototyping, and Direct Digital Manufacturing, Second Edition (2015) 1–498. https://doi.org/10.1007/978-1-4939-2113-3/COVER.
- [102] C. R. Deckard, Method and apparatus for producing parts by selective sintering, 4,863,538, 1989.
- [103] N. K. Tolochko, T. Laoui, Y. V Khlopkov, S.E. Mozzharov, V.I. Titov, M.B. Ignatiev, Absorptance of powder materials suitable for laser sintering, (n.d.). http://www.mcbup.com/research_registers/aa.asp (accessed October 5, 2023).
- [104] W. Y. Yeong, N. Sudarmadji, H.Y. Yu, C.K. Chua, K.F. Leong, S.S. Venkatraman, Y.C.F. Boey, L.P. Tan, Porous polycaprolactone scaffold for cardiac tissue engineering fabricated by selective laser sintering, Acta Biomater 6 (2010) 2028–2034. https://doi.org/10.1016/J.ACTBIO.2009.12.033.
- [105] F. Verga, M. Borlaf, L. Conti, K. Florio, M. Vetterli, T. Graule, M. Schmid, K. Wegener, Laser-based powder bed fusion of alumina toughened zirconia, (2019). https://doi.org/10.1016/j.addma.2019.100959.
- [106] W. Konrad, Net Shaped High Performance Oxide Ceramic Parts by Selective Laser Melting, (2010). https://doi.org/10.1016/j.phpro.2010.08.086.
- [107] V. K. Balla, S. Bodhak, P. Datta, B. Kundu, M. Das, A. Bandyopadhyay, S. Bose, Biointegration of three-dimensional—printed biomaterials and biomedical devices, in: Biointegration of Medical Implant Materials, Elsevier, 2020: pp. 433–482. https://doi.org/10.1016/B978-0-08-102680-9.00016-0.
- [108] M.Q. Shaikh, S.D. Nath, A.A. Akilan, S. Khanjar, V.K. Balla, G.T. Grant, S.V. Atre, Investigation of patient-specific maxillofacial implant prototype development by metal fused filament fabrication (Mf3) of ti-6al-4v, Dent J (Basel) 9 (2021). https://doi.org/10.3390/dj9100109.

- [109] J. E. Kanyo, S. Schafföner, R.S. Uwanyuze, K.S. Leary, An overview of ceramic molds for investment casting of nickel superalloys, J Eur Ceram Soc 40 (2020) 4955–4973. https://doi.org/10.1016/j.jeurceramsoc.2020.07.013.
- [110] A. A. Altun, T. Prochaska, T. Konegger, M. Schwentenwein, Dense, strong, and precise silicon nitride-based ceramic parts by lithography-based ceramic manufacturing, Applied Sciences (Switzerland) 10 (2020). https://doi.org/10.3390/app10030996.
- [111] M. C. Halbig, J.E. Grady, M. Singh, J. Ramsey, C. Patterson, T. Santelle, A Fully Non-Metallic Gas Turbine Engine Enabled by Addtive Manufacturing, NASA/TM 2015-218892 (2015). https://ntrs.nasa.gov/api/citations/20150023455/downloads/20150023455.pdf.
- [112] Z. C. Eckel, C. Zhou, J.H. Martin, A.J. Jacobsen, W.B. Carter, T.A. Schaedler, Additive manufacturing of polymer-derived ceramics, Science (1979) 351 (2016) 58–62. https://doi.org/10.1126/science.aad2688.
- [113] T. Chu, S. Park, K. Fu, 3D printing-enabled advanced electrode architecture design, Carbon Energy 3 (2021) 424–439. https://doi.org/10.1002/cey2.114.
- [114] J. H. L. Voncken, Recovery of Ce and La from Spent Automotive Catalytic Converters, in: Critical and Rare Earth Elements, CRC Press, 2019: pp. 267–273. https://doi.org/10.1201/9780429023545-12.
- [115] M. Pelanconi, S. Zavattoni, L. Cornolti, R. Puragliesi, E. Arrivabeni, L. Ferrari, S. Gianella, M. Barbato, A. Ortona, Application of ceramic lattice structures to design compact, high temperature heat exchangers: Material and architecture selection, Materials 14 (2021). https://doi.org/10.3390/ma14123225.
- [116] S. Smolentsev, N.B. Morley, M.A. Abdou, S. Malang, Dual-coolant lead-lithium (DCLL) blanket status and R&D needs, Fusion Engineering and Design 100 (2015) 44–54. https://doi.org/10.1016/j.fusengdes.2014.12.031.
- [117] K. Terrani, B. Jolly, M. Trammell, 3D printing of high-purity silicon carbide, Journal of the American Ceramic Society 103 (2020) 1575–1581. https://doi.org/10.1111/jace.16888.
- [118] M. Ziaee, N.B. Crane, Binder jetting: A review of process, materials, and methods, Addit Manuf 28 (2019) 781–801. https://doi.org/10.1016/J.ADDMA.2019.05.031.
- [119] K.M. Rahman, H. Miyanaji, C.B. Williams, Effects of binder droplet size and powder particle size on binder jetting part properties, (n.d.). https://doi.org/10.1108/RPJ-10-2022-0358.

- [120] M. P. Watters, M.L. Bernhardt, Modified curing protocol for improved strength of binder-jetted 3D parts, Rapid Prototyp J 23 (2017) 1195–1201. https://doi.org/10.1108/RPJ-09-2016-0146/FULL/HTML.
- [121] A. Levy, A. Miriyev, A. Elliott, S. Babu, N.F.-M.& Design, undefined 2017, Additive manufacturing of complex-shaped graded TiC/steel composites, Elsevier (n.d.). https://www.sciencedirect.com/science/article/pii/S026412751730031X (accessed January 27, 2024).
- [122] E. Garzón, J. Alves, R.N.-M. design and applications, undefined 2017, Post-process influence of infiltration on binder jetting technology, SpringerEO Garzón, JL Alves, RJ NetoMaterials Design and Applications, 2017•Springer (n.d.). https://link.springer.com/chapter/10.1007/978-3-319-50784-2_19 (accessed January 27, 2024).
- [123] S. Bose, Y. Jo, U. Majumdar, A. Bandyopadhyay, Binder Jet Additive Manufacturing of Biomaterials, in: R.J. Narayan (Ed.), Additive Manufacturing in Biomedical Applications, ASM International, 2022: pp. 77–91. https://doi.org/10.31399/asm.hb.v23a.a0006903.
- [124] A. Mostafaei, A.M. Elliott, J.E. Barnes, F. Li, W. Tan, C.L. Cramer, P. Nandwana, M. Chmielus, Binder jet 3D printing—Process parameters, materials, properties, modeling, and challenges, Prog Mater Sci 119 (2021) 100707. https://doi.org/10.1016/J.PMATSCI.2020.100707.
- [125] T. Do, P. Kwon, C.S. Shin, Process development toward full-density stainless steel parts with binder jetting printing, Int J Mach Tools Manuf 121 (2017) 50–60. https://doi.org/10.1016/j.ijmachtools.2017.04.006.
- [126] C. Sun, X. Tian, L. Wang, Y. Liu, C.M. Wirth, J. Günster, D. Li, Z. Jin, Effect of particle size gradation on the performance of glass-ceramic 3D printing process A R T I C L E I N F O, (2016). https://doi.org/10.1016/j.ceramint.2016.09.197.
- [127] J. Bredt, Binder stability and powder/binder interaction in three-dimensional printing., (1997). https://elibrary.ru/item.asp?id=5578190 (accessed January 27, 2024).
- [128] J. Liu, 585,930 M Rynerson US Patent 6, undefined 2003, Method for article fabrication using carbohydrate binder, Google Patents (n.d.). https://patents.google.com/patent/US6585930B2/en (accessed January 27, 2024).
- [129] N. A. Meisel, C.B. Williams, A. Druschitz, Lightweight Metal Cellular Structures via Indirect 3D Printing and Casting, (2012). https://doi.org/10.26153/TSW/15340.
- [130] X. Lv, F. Ye, L. Cheng, S. Fan, Y. Liu, Binder jetting of ceramics: Powders, binders, printing parameters, equipment, and post-treatment, Ceram Int 45 (2019) 12609–12624. https://doi.org/10.1016/J.CERAMINT.2019.04.012.

- [131] J. Bai, K. Creehan, 040,216 HA Kuhn US Patent 10, undefined 2018, Powder particle layerwise three-dimensional printing process, Google Patents (n.d.). https://patents.google.com/patent/US10040216B2/en (accessed January 27, 2024).
- [132] E. Sachs, C. Hadjiloucas, S. Allen, H. Yoo, Metal and ceramic containing parts produced from powder using binders derived from salt, 1998.
- [133] W. Zhang, R. Melcher, N. Travitzky, R. Kumar Bordia, P. Greil, Three-dimensional printing of complex-shaped alumina/glass composites, Wiley Online Library W Zhang, R Melcher, N Travitzky, RK Bordia, P GreilAdvanced Engineering Materials, 2009•Wiley Online Library 11 (2009) 1039–1043. https://doi.org/10.1002/adem.200900213.
- [134] M. Vaezi, C.K. Chua, Effects of layer thickness and binder saturation level parameters on 3D printing process, The International Journal of Advanced Manufacturing Technology 53 (2010) 275–284.
- [135] S. J. Li, S. Coa, Print Parameters Influence on Parts' Quality and Calibration with 3DP-Part I: Print Parameters Influence on Parts' Surface Topography, Advanced Materials Research 399–401 (2011) 1639–1645.
- [136] M. Castilho, M. Dias, U. Gbureck, J. Groll, P. Fernandes, I. Pires, B. Gouveia, J. Rodrigues, E. Vorndran, Fabrication of computationally designed scaffolds by low temperature 3D printing, Biofabrication 5 (2013) 35012–35024. https://doi.org/10.1088/1758-5082/5/3/035012.
- [137] M. Asadi-Eydivand, M. Solati-Hashjin, A. Farzad, N. Azuan, A. Osman, Effect of technical parameters on porous structure and strength of 3D printed calcium sulfate prototypes, (2015). https://doi.org/10.1016/j.rcim.2015.06.005.
- [138] A. Farzadi, M. Solati-Hashjin, M. Asadi-Eydivand, A. Osman, Effect of Layer Thickness and Printing Orientation on Mechanical Properties and Dimensional Accuracy of 3D Printed Porous Samples for Bone Tissue Engineering, PLoS One 9 (2014) 108252. https://doi.org/10.1371/journal.pone.0108252.
- [139] G. Arumaikkannu, N. Kumar, R. Saravanan, STUDY ON THE INFLUENCE OF RAPID PROTOTYPING PARAMETERS ON PRODUCT QUALITY IN 3D PRINTING, (2008).
- [140] A. A. Vu, D.A. Burke, A. Bandyopadhyay, S. Bose, Effects of surface area and topography on 3D printed tricalcium phosphate scaffolds for bone grafting applications, Addit Manuf 39 (2021) 101870. https://doi.org/10.1016/J.ADDMA.2021.101870.
- [141] A. Zocca, J. Lüchtenborg, T. Mühler, J. Wilbig, G. Mohr, T. Villatte, F. Léonard, G. Nolze, M. Sparenberg, J. Melcher, K. Hilgenberg, J. Günster, Enabling the 3D Printing of Metal Components in μ-Gravity, Adv Mater Technol 4 (2019) 1900506. https://doi.org/10.1002/ADMT.201900506.

- [142] S. Pal, N. Gubeljak, T. Bončina, R. Hudák, T. Toth, J. Zivcak, G. Lojen, N. Leben, I. Drstvenšek, The effects of locations on the build tray on the quality of specimens in powder bed additive manufacturing, International Journal of Advanced Manufacturing Technology 112 (2021) 1159–1170. https://doi.org/10.1007/S00170-020-06563-5/FIGURES/8.
- [143] M. Castilho, B. Gouveia, I. Pires, J. Rodrigues, M. Pereira, The role of shell/core saturation level on the accuracy and mechanical characteristics of porous calcium phosphate models produced by 3Dprinting, (n.d.). https://doi.org/10.1108/RPJ-02-2013-0015.
- [144] P. R. (Peter R. Baker, Three dimensional printing with fine metal powders, (1997). https://dspace.mit.edu/handle/1721.1/46287 (accessed September 19, 2023).
- [145] S. C. Cox, J.A. Thornby, G.J. Gibbons, M.A. Williams, K.K. Mallick, 3D printing of porous hydroxyapatite scaffolds intended for use in bone tissue engineering applications, (2014). https://doi.org/10.1016/j.msec.2014.11.024.
- [146] Process for removing loose powder particles from interior passages of a body, (1992).
- [147] A. Mostafaei, J. Toman, E.L. Stevens, E.T. Hughes, Y.L. Krimer, M. Chmielus, Microstructural evolution and mechanical properties of differently heat-treated binder jet printed samples from gas-and water-atomized alloy 625 powders, (2016). https://doi.org/10.1016/j.actamat.2016.11.021.
- [148] P. Nandwana, A.M. Elliott, D. Siddel, A. Merriman, W.H. Peter, S.S. Babu, Powder bed binder jet 3D printing of Inconel 718: Densification, microstructural evolution and challengesq, (n.d.). https://doi.org/10.1016/j.cossms.2016.12.002.
- [149] R. R. Mishra, A.K. Sharma, Microwave–material interaction phenomena: Heating mechanisms, challenges and opportunities in material processing, Compos Part A Appl Sci Manuf 81 (2016) 78–97. https://doi.org/10.1016/J.COMPOSITESA.2015.10.035.
- [150] P. Yadoji, R. Peelamedu, D. Agrawal, R. Roy, Microwave sintering of Ni–Zn ferrites: comparison with conventional sintering, Materials Science and Engineering: B 98 (2003) 269–278. https://doi.org/10.1016/S0921-5107(03)00063-1.
- [151] T. Nakamoto, K. Yamaguchi, Consideration on the producing of high aspect ratio micro parts using UV sensitive photopolymer, Proceedings of the International Symposium on Micro Machine and Human Science (1996) 53–58. https://doi.org/10.1109/MHS.1996.563401.
- [152] A. Bertsch, S. Zissi, J.Y. Jézéquel, S. Corbel, J.C. André, Microstereophotolithography using a liquid crystal display as dynamic mask-generator, Microsystem Technologies 3 (1997) 42–47. https://doi.org/10.1007/S005420050053/METRICS.

- [153] V. Truxova, J. Safka, M. Seidl, I. Kovalenko, L. Volesky, M. Ackermann, Ceramic 3d printing: Comparison of SLA and DLP technologies, MM Science Journal 2020 (2020) 3905–3911. https://doi.org/10.17973/MMSJ.2020_06_2020006.
- [154] O. Santoliquido, P. Colombo, A. Ortona, Additive Manufacturing of ceramic components by Digital Light Processing: A comparison between the "bottom-up" and the "top-down" approaches, J Eur Ceram Soc 39 (2019) 2140–2148. https://doi.org/10.1016/J.JEURCERAMSOC.2019.01.044.
- [155] H. Chen, B. Chen, J. Li, H. Yan, Y. Zeng, J. Chen, Optimization of Vat-Polymerization binder formulation for 3D printing ceramic slurry using D-optimal mixture experimental design, Compos B Eng 260 (2023) 110777. https://doi.org/10.1016/J.COMPOSITESB.2023.110777.
- [156] T. Chen, D. Wang, Q. Cao, H. Xiong, X. Chen, Y. Fan, Optimizing photocuring properties of ceramic slurry for 3D printing of ceramic membranes, Ceram Int 50 (2024) 1732–1741. https://doi.org/10.1016/J.CERAMINT.2023.10.272.
- [157] H. Li, Y. Liu, Y. Liu, K. Hu, Z. Lu, J. Liang, Investigating the relation between debinding atmosphere and mechanical properties of stereolithography-based three-dimensional printed Al2O3 ceramic, Https://Doi.Org/10.1177/0954405420937855 234 (2020) 1686–1694. https://doi.org/10.1177/0954405420937855.
- [158] A. Bove, F. Calignano, M. Galati, L. Iuliano, Photopolymerization of Ceramic Resins by Stereolithography Process: A Review, Applied Sciences 2022, Vol. 12, Page 3591 12 (2022) 3591. https://doi.org/10.3390/APP12073591.
- [159] V.M. Vaz, L. Kumar, 3D Printing as a Promising Tool in Personalized Medicine, AAPS PharmSciTech 22 (2021) 1–20. https://doi.org/10.1208/S12249-020-01905-8/TABLES/3.
- [160] T. Billiet, M. Vandenhaute, J. Schelfhout, S. Van Vlierberghe, P. Dubruel, A review of trends and limitations in hydrogel-rapid prototyping for tissue engineering, Biomaterials 33 (2012) 6020–6041. https://doi.org/10.1016/J.BIOMATERIALS.2012.04.050.
- [161] C.L. Liu, Q. Du, C. Zhang, J.M. Wu, G. Zhang, Y.S. Shi, Fabrication and properties of BaTiO3 ceramics via digital light processing for piezoelectric energy harvesters, Addit Manuf 56 (2022) 102940. https://doi.org/10.1016/J.ADDMA.2022.102940.
- [162] P. Colombo, G. Mera, R. Riedel, G.D. Sorarù, Polymer-derived ceramics: 40 Years of research and innovation in advanced ceramics, Journal of the American Ceramic Society 93 (2010) 1805–1837. https://doi.org/10.1111/j.1551-2916.2010.03876.x.
- [163] J. Livage, Sol-gel processes, Curr Opin Solid State Mater Sci 2 (1997) 132–138. https://doi.org/10.1016/s1359-0286(97)80057-5.

- [164] E. Zanchetta, M. Cattaldo, G. Franchin, M. Schwentenwein, J. Homa, G. Brusatin, P. Colombo, Stereolithography of SiOC Ceramic Microcomponents, Advanced Materials 28 (2016) 370–376. https://doi.org/10.1002/adma.201503470.
- [165] K. Huang, H. Elsayed, G. Franchin, P. Colombo, 3D printing of polymer-derived SiOC with hierarchical and tunable porosity, Addit Manuf 36 (2020) 101549. https://doi.org/10.1016/j.addma.2020.101549.
- [166] J. F. Destino, N.A. Dudukovic, M.A. Johnson, D.T. Nguyen, T.D. Yee, G.C. Egan, A.M. Sawvel, W.A. Steele, T.F. Baumann, E.B. Duoss, T. Suratwala, R. Dylla-Spears, 3D Printed Optical Quality Silica and Silica—Titania Glasses from Sol—Gel Feedstocks, Adv Mater Technol 3 (2018) 1–10. https://doi.org/10.1002/admt.201700323.
- [167] K. Sasan, A. Lange, T.D. Yee, N. Dudukovic, D.T. Nguyen, M.A. Johnson, O.D. Herrera, J.H. Yoo, A.M. Sawvel, M.E. Ellis, C.M. Mah, R. Ryerson, L.L. Wong, T. Suratwala, J.F. Destino, R. Dylla-Spears, Additive Manufacturing of Optical Quality Germania-Silica Glasses, ACS Appl Mater Interfaces 12 (2020) 6736–6741. https://doi.org/10.1021/acsami.9b21136.
- [168] N.R. Brodnik, J. Schmidt, P. Colombo, K.T. Faber, Analysis of Multi-scale Mechanical Properties of Ceramic Trusses Prepared from Preceramic Polymers (Revision Prepared for Additive Manufacturing), Addit Manuf 31 (2020) 100957. https://doi.org/10.1016/j.addma.2019.100957.
- [169] L. Brigo, J.E.M. Schmidt, A. Gandin, N. Michieli, P. Colombo, G. Brusatin, 3D Nanofabrication of SiOC Ceramic Structures, Advanced Science 5 (2018). https://doi.org/10.1002/advs.201800937.
- [170] J. Schmidt, L. Brigo, A. Gandin, M. Schwentenwein, P. Colombo, G. Brusatin, Multiscale ceramic components from preceramic polymers by hybridization of vat polymerization-based technologies, Addit Manuf 30 (2019) 100913. https://doi.org/10.1016/j.addma.2019.100913.
- [171] J. Bauer, C. Crook, A. Guell Izard, Z.C. Eckel, N. Ruvalcaba, T.A. Schaedler, L. Valdevit, Additive Manufacturing of Ductile, Ultrastrong Polymer-Derived Nanoceramics, Matter 1 (2019) 1547–1556. https://doi.org/10.1016/j.matt.2019.09.009.
- [172] M. Kollep, G. Konstantinou, J. Madrid-Wolff, A. Boniface, L. Hagelüken, P.V.W. Sasikumar, G. Blugan, P. Delrot, D. Loterie, J. Brugger, C. Moser, Tomographic Volumetric Additive Manufacturing of Silicon Oxycarbide Ceramics, Adv Eng Mater 24 (2022). https://doi.org/10.1002/adem.202101345.
- [173] J. A. Lewis, Colloidal Processing of Ceramics, Journal of the American Ceramic Society 83 (2004) 2341–2359. https://doi.org/10.1111/j.1151-2916.2000.tb01560.x.

- [174] W. J. Costakis, L.M. Rueschhoff, A.I. Diaz-Cano, J.P. Youngblood, R.W. Trice, Additive manufacturing of boron carbide via continuous filament direct ink writing of aqueous ceramic suspensions, J Eur Ceram Soc 36 (2016) 3249–3256. https://doi.org/10.1016/j.jeurceramsoc.2016.06.002.
- [175] Y. yun Li, L. tu Li, B. Li, Direct write printing of three-dimensional ZrO2 biological scaffolds, Mater Des 72 (2015) 16–20. https://doi.org/10.1016/j.matdes.2015.02.018.
- [176] B. G. Compton, J.A. Lewis, 3D-printing of lightweight cellular composites, Advanced Materials 26 (2014) 5930–5935. https://doi.org/10.1002/adma.201401804.
- [177] K. R. Cox, THE INFLUENCE OF PRINT LAYER ORIENTATION ON THE MECHANICAL PROPERTIES OF SIC AND CF/SIC CMCS FORMED VIA DIRECT INK WRITING, (2021). https://doi.org/10.25394/PGS.17144612.V1.
- [178] J. Steibel, Ceramic matrix composites taking flight at GE Aviation, American Ceramic Society Bulletin 98 (2019) 30–33.
- [179] F. Christin, Design, Fabrication, and Application of Thermostructural Composites (TSC) like C/C, C/SiC, and SiC/SiC Composites, Adv Eng Mater 4 (2002) 903–912. https://doi.org/10.1002/adem.200290001.
- [180] K. K. Chawla, Ceramic Matrix Composites, Composite Materials (1987) 134–149. https://doi.org/10.1007/978-1-4757-3912-1 7.
- [181] B. P. Croom, A. Abbott, J.W. Kemp, L. Rueschhoff, L. Smieska, A. Woll, S. Stoupin, H. Koerner, Mechanics of nozzle clogging during direct ink writing of fiber-reinforced composites, Addit Manuf 37 (2021) 101701. https://doi.org/10.1016/j.addma.2020.101701.
- [182] G. Franchin, L. Wahl, P. Colombo, Direct ink writing of ceramic matrix composite structures, Journal of the American Ceramic Society 100 (2017) 4397–4401. https://doi.org/10.1111/jace.15045.
- [183] S. C. Danforth, M. Agarwala, A. Bandyopadhyay, N. Langrana, V.R. Jamalabad, A. Safari, R. Van Weeren, Solid freeform fabrication methods, U.S. Patent No. 5,738,817, 1998.
- [184] A. Safari, M. Allahverdi, E.K. Akdogan, Solid freeform fabrication of piezoelectric sensors and actuators, Frontiers of Ferroelectricity: A Special Issue of the Journal of Materials Science (2007) 177–198. https://doi.org/10.1007/978-0-387-38039-1_17/COVER.
- [185] S. H. Huang, P. Liu, A. Mokasdar, L. Hou, Additive manufacturing and its societal impact: A literature review, International Journal of Advanced Manufacturing Technology 67 (2013) 1191–1203. https://doi.org/10.1007/S00170-012-4558-5/METRICS.

- [186] T. F. McNulty, F. Mohammadi, A. Bandyopadhyay, D.J. Shanefield, S.C. Danforth, A. Safari, Development of a binder formulation for fused deposition of ceramics, Rapid Prototyp J 4 (1998) 144–150. https://doi.org/10.1108/13552549810239012/FULL/PDF.
- [187] A. Bandyopadhyay, R.K. Panda, V.F. Janas, M.K. Agarwala, S.C. Danforth, A. Safari, Processing of Piezocomposites by Fused Deposition Technique, Journal of the American Ceramic Society 80 (1997) 1366–1372. https://doi.org/10.1111/J.1151-2916.1997.TB02993.X.
- [188] D. Qiu, N.A. Langrana, S.C. Danforth, A. Safari, M. Jafari, Intelligent toolpath for extrusion-based LM process, Rapid Prototyp J 7 (2001) 18–23. https://doi.org/10.1108/13552540110365126/FULL/PDF.
- [189] W. Han, M.A. Jafari, S.C. Danforth, A. Safari, Tool Path-Based Deposition Planning in Fused Deposition Processes, J Manuf Sci Eng 124 (2002) 462–472. https://doi.org/10.1115/1.1455026.
- [190] A. Safari, E.K. Akdoğan, Piezoelectric and acoustic materials for transducer applications, Piezoelectric and Acoustic Materials for Transducer Applications (2008) 1–481. https://doi.org/10.1007/978-0-387-76540-2/COVER.
- [191] A. Safari, V. Janas, A.B.-Aic. journal, undefined 1997, Development of fine-scale piezoelectric composites for transducers, Wiley Online Library A Safari, VF Janas, A Bandyopadhyay AIChE Journal, 1997•Wiley Online Library 43 (1997) 2849–2856. https://doi.org/10.1002/aic.690431334.
- [192] S. Turcu, B. Jadidian, S.C. Danforth, A. Safari, Piezoelectric properties of novel oriented ceramic-polymer composites with 2-2 and 3-3 connectivity, J Electroceram 9 (2002) 165–171. https://doi.org/10.1023/A:1023209107995/METRICS.
- [193] J. Sun, P. Ngernchuklin, M. Vittadello, E.K. Akdoğan, A. Safari, Development of 2-2 piezoelectric ceramic/polymer composites by direct-write technique, J Electroceram 24 (2010) 219–225. https://doi.org/10.1007/S10832-009-9561-3.
- [194] 5 Ways GE Is Changing The World With 3D Printing | GE News, (n.d.). https://www.ge.com/news/reports/5-ways-ge-changing-world-3d-printing (accessed January 27, 2024).
- [195] B. A. Turtle, J.E. Smay, J. Cesarano, J.A. Voigt, T.W. Scofield, W.R. Olson, J.A. Lewis, Robocast Pb(Zr0.95Ti0.05)O3 Ceramic Monoliths and Composites, Journal of the American Ceramic Society 84 (2001) 872–874. https://doi.org/10.1111/J.1151-2916.2001.TB00756.X.

- [196] J. E. Smay, J. Cesarano, B.A. Tuttle, J.A. Lewis, Piezoelectric properties of 3-X periodic Pb(ZrxTi1-x)O3-polymer composites, J Appl Phys 92 (2002) 6119–6127. https://doi.org/10.1063/1.1513202.
- [197] Y. Yang, X. Song, X. Li, Z. Chen, C. Zhou, Q. Zhou, Y. Chen, Y. Yang, X. Li, Y. Chen, X. Song, Z. Chen, Q. Zhou, C. Zhou, Recent Progress in Biomimetic Additive Manufacturing Technology: From Materials to Functional Structures, Advanced Materials 30 (2018) 1706539. https://doi.org/10.1002/ADMA.201706539.
- [198] Z. Chen, X. Song, L. Lei, X. Chen, C. Fei, C.T. Chiu, X. Qian, T. Ma, Y. Yang, K. Shung, Y. Chen, Q. Zhou, 3D printing of piezoelectric element for energy focusing and ultrasonic sensing, Nano Energy 27 (2016) 78–86. https://doi.org/10.1016/J.NANOEN.2016.06.048.
- [199] E. Sharifi, A. Chaudhuri, B.V. Waehrens, L.G. Staal, S.D. Farahani, Assessing the Suitability of Freeform Injection Molding for Low Volume Injection Molded Parts: A Design Science Approach, Sustainability 2021, Vol. 13, Page 1313 13 (2021) 1313. https://doi.org/10.3390/SU13031313.
- [200] C. Gadea, T. Spelta, S.B. Simonsen, V. Esposito, J.R. Bowen, A.B. Haugen, Hybrid inks for 3D printing of tall BaTiO3-based ceramics, Open Ceramics 6 (2021) 100110. https://doi.org/10.1016/J.OCERAM.2021.100110.
- [201] A. Ikei, J. Wissman, K. Sampath, G. Yesner, S.N. Qadri, Tunable In Situ 3D-Printed PVDF-TrFE Piezoelectric Arrays, Sensors 2021, Vol. 21, Page 5032 21 (2021) 5032. https://doi.org/10.3390/S21155032.
- [202] G. L. Goh, H. Zhang, T.H. Chong, W.Y. Yeong, 3D Printing of Multilayered and Multimaterial Electronics: A Review, Adv Electron Mater 7 (2021) 2100445. https://doi.org/10.1002/AELM.202100445.
- [203] I. Fraile, M. Gabilondo, N. Burgos, M. Azcona, F. Castro, Laser sintered ceramic coatings of PZT nanoparticles deposited by Inkjet Printing on metallic and ceramic substrates, Ceram Int 44 (2018) 15603–15610. https://doi.org/10.1016/J.CERAMINT.2018.05.225.
- [204] N. McKibben, B. Ryel, J. Manzi, F. Muramutsa, J. Daw, H. Subbaraman, D. Estrada, Z. Deng, Aerosol jet printing of piezoelectric surface acoustic wave thermometer, Microsyst Nanoeng 9 (2023). https://doi.org/10.1038/S41378-023-00492-5.
- [205] Y. Waku, N. Nakagawa, T. Wakamoto, H. Ohtsubo, K. Shimizu, Y. Kohtoku, A ductile ceramic eutectic composite with high strength at 1,873 K, Nature 389 (1997) 49–52. https://doi.org/10.1038/37937.
- [206] A. Sayir, S.C. Farmer, Effect of the microstructure on mechanical properties of directionally solidified Al2O3/ZrO2(Y2O3) eutectic, Acta Mater 48 (2000) 4691–4697. https://doi.org/10.1016/S1359-6454(00)00259-7.

- [207] N. Nakagawa, H. Ohtsubo, A. Mitani, K. Shimizu, Y. Waku, High temperature strength and thermal stability for melt growth composite, J Eur Ceram Soc 25 (2005) 1251–1257. https://doi.org/10.1016/j.jeurceramsoc.2005.01.030.
- [208] J. LLorca, V.M. Orera, Directionally solidified eutectic ceramic oxides, Prog Mater Sci 51 (2006) 711–809. https://doi.org/10.1016/j.pmatsci.2005.10.002.
- [209] S. Pfeiffer, K. Florio, D. Puccio, M. Grasso, B.M. Colosimo, C.G. Aneziris, K. Wegener, T. Graule, Direct laser additive manufacturing of high performance oxide ceramics: A state-of-the-art review, J Eur Ceram Soc 41 (2021) 6087–6114. https://doi.org/10.1016/j.jeurceramsoc.2021.05.035.
- [210] Y. Li, Y. Hu, W. Cong, L. Zhi, Z. Guo, Additive manufacturing of alumina using laser engineered net shaping: Effects of deposition variables, Ceram Int 43 (2017) 7768–7775. https://doi.org/10.1016/j.ceramint.2017.03.085.
- [211] F. Niu, D. Wu, S. Zhou, G. Ma, Power prediction for laser engineered net shaping of Al2O3 ceramic parts, J Eur Ceram Soc 34 (2014) 3811–3817. https://doi.org/10.1016/j.jeurceramsoc.2014.06.023.
- [212] F. Niu, D. Wu, F. Lu, G. Liu, G. Ma, Z. Jia, Microstructure and macro properties of Al2O3 ceramics prepared by laser engineered net shaping, Ceram Int 44 (2018) 14303–14310. https://doi.org/10.1016/j.ceramint.2018.05.036.
- [213] G. K. Mishra, C.P. Paul, A.K. Rai, A.K. Agrawal, S.K. Rai, K.S. Bindra, Experimental investigation on Laser Directed Energy Deposition based additive manufacturing of Al2O3 bulk structures, Ceram Int 47 (2021) 5708–5720. https://doi.org/10.1016/j.ceramint.2020.10.157.
- [214] Z. Fan, Y. Zhao, M. Lu, H. Huang, Yttria stabilized zirconia (YSZ) thin wall structures fabricated using laser engineered net shaping (LENS), The International Journal of Advanced Manufacturing Technology 105 (2019) 4491–4498. https://doi.org/10.1007/s00170-019-03322-z.
- [215] Z. Liu, K. Song, B. Gao, T. Tian, H. Yang, X. Lin, W. Huang, Microstructure and Mechanical Properties of Al2O3/ZrO2 Directionally Solidified Eutectic Ceramic Prepared by Laser 3D Printing, J Mater Sci Technol 32 (2016) 320–325. https://doi.org/10.1016/j.jmst.2015.11.017.
- [216] Y. Hu, F. Ning, W. Cong, Y. Li, X. Wang, H. Wang, Ultrasonic vibration-assisted laser engineering net shaping of ZrO2-Al2O3 bulk parts: Effects on crack suppression, microstructure, and mechanical properties, Ceram Int 44 (2018) 2752–2760. https://doi.org/10.1016/j.ceramint.2017.11.013.

- [217] Y. Hu, H. Wang, W. Cong, B. Zhao, Directed Energy Deposition of Zirconia-Toughened Alumina Ceramic: Novel Microstructure Formation and Mechanical Performance, Journal of Manufacturing Science and Engineering, Transactions of the ASME 142 (2020) 1–10. https://doi.org/10.1115/1.4045626.
- [218] J. M. Pappas, A.R. Thakur, X. Dong, Effects of zirconia doping on additively manufactured alumina ceramics by laser direct deposition, Mater Des 192 (2020) 108711. https://doi.org/10.1016/j.matdes.2020.108711.
- [219] A. R. Thakur, J.M. Pappas, X. Dong, Fabrication and Characterization of High-Purity Alumina Ceramics Doped with Zirconia via Laser Direct Deposition, JOM 72 (2020) 1299–1306. https://doi.org/10.1007/s11837-019-03969-9.
- [220] S. Yan, Y. Huang, D. Zhao, F. Niu, G. Ma, D. Wu, 3D printing of nano-scale Al2O3-ZrO2 eutectic ceramic: Principle analysis and process optimization of pores, Addit Manuf 28 (2019) 120–126. https://doi.org/10.1016/j.addma.2019.04.024.
- [221] X. Yu, D. Wu, W. Bi, X. Feng, Z. Zhao, Y. Hao, G. Ma, C. Zhou, F. Niu, Direct additive manufacturing of Al2O3–TiCp functionally graded ceramics by laser-directed energy deposition, Journal of the American Ceramic Society 107 (2024) 3522–3533. https://doi.org/10.1111/JACE.19653.
- [222] D. Wu, X. Yu, Z. Zhao, G. Ma, C. Zhou, B. Zhang, G. Ren, J. Han, H. Wang, F. Niu, Direct additive manufacturing of TiCp reinforced Al2O3-ZrO2 eutectic functionally graded ceramics by laser directed energy deposition, J Eur Ceram Soc 43 (2023) 2718–2723. https://doi.org/10.1016/J.JEURCERAMSOC.2022.12.068.
- [223] D. Wu, J. Shi, F. Niu, G. Ma, C. Zhou, B. Zhang, Direct additive manufacturing of melt growth Al2O3-ZrO2 functionally graded ceramics by laser directed energy deposition, J Eur Ceram Soc 42 (2022) 2957–2973. https://doi.org/10.1016/j.jeurceramsoc.2022.01.034.
- [224] F. Niu, D. Wu, Y. Huang, S. Yan, G. Ma, C. Li, J. Ding, Direct additive manufacturing of large-sized crack-free alumina/aluminum titanate composite ceramics by directed laser deposition, Rapid Prototyp J 25 (2019) 1370–1378. https://doi.org/10.1108/RPJ-08-2018-0215.
- [225] D. Wu, Y. Huang, F. Niu, G. Ma, S. Yan, C. Li, J. Ding, Effects of TiO2 doping on microstructure and properties of directed laser deposition alumina/aluminum titanate composites, Virtual Phys Prototyp 14 (2019) 371–381. https://doi.org/10.1080/17452759.2019.1622987.
- [226] Y. Huang, D. Wu, D. Zhao, F. Niu, H. Zhang, S. Yan, G. Ma, Process optimization of melt growth alumina/aluminum titanate composites directed energy deposition: Effects of scanning speed, Addit Manuf 35 (2020) 101210. https://doi.org/10.1016/j.addma.2020.101210.

- [227] Y. Huang, D. Wu, D. Zhao, F. Niu, G. Ma, Investigation of melt-growth alumina/aluminum titanate composite ceramics prepared by directed energy deposition, International Journal of Extreme Manufacturing 3 (2021). https://doi.org/10.1088/2631-7990/abf71a.
- [228] D. Zhao, D. Wu, J. Shi, F. Niu, G. Ma, Microstructure and mechanical properties of melt-grown alumina-mullite/glass composites fabricated by directed laser deposition, Journal of Advanced Ceramics 11 (2022) 75–93. https://doi.org/10.1007/s40145-021-0518-6.
- [229] D. Wu, D. Zhao, F. Niu, Y. Huang, J. Zhu, G. Ma, In situ synthesis of melt-grown mullite ceramics using directed laser deposition, J Mater Sci 55 (2020) 12761–12775. https://doi.org/10.1007/s10853-020-04938-3.
- [230] H. J. Su, J. Zhang, L. Liu, J. Eckert, H.Z. Fu, Rapid growth and formation mechanism of ultrafine structural oxide eutectic ceramics by laser direct forming, Appl Phys Lett 99 (2011) 1–4. https://doi.org/10.1063/1.3664108.
- [231] D. Wu, H. Liu, F. Lu, G. Ma, S. Yan, F. Niu, D. Guo, Al2O3-YAG eutectic ceramic prepared by laser additive manufacturing with water-cooled substrate, Ceram Int 45 (2019) 4119–4122. https://doi.org/10.1016/j.ceramint.2018.11.032.
- [232] J. M. Pappas, E.C. Kinzel, X. Dong, Laser direct deposited transparent magnesium aluminate spinel ceramics, Manuf Lett 24 (2020) 92–95. https://doi.org/10.1016/j.mfglet.2020.04.003.
- [233] J. M. Pappas, X. Dong, Porosity characterization of additively manufactured transparent MgAl2O4 spinel by laser direct deposition, Ceram Int 46 (2020) 6745–6755. https://doi.org/10.1016/j.ceramint.2019.11.164.
- [234] H. Liu, H. Su, Z. Shen, D. Zhao, Y. Liu, Y. Guo, H. Guo, M. Guo, K. Xie, J. Zhang, L. Liu, H. Fu, One-step additive manufacturing and microstructure evolution of melt-grown Al2O3/GdAlO3/ZrO2 eutectic ceramics by laser directed energy deposition, J Eur Ceram Soc 41 (2021) 3547–3558. https://doi.org/10.1016/j.jeurceramsoc.2021.01.047.
- [235] H. Liu, H. Su, Z. Shen, D. Zhao, Y. Liu, Y. Guo, J. Zhang, L. Liu, H. Fu, Insights into high thermal stability of laser additively manufactured Al2O3/GdAlO3/ZrO2 eutectic ceramics under high temperatures, Addit Manuf 48 (2021) 102425. https://doi.org/10.1016/j.addma.2021.102425.
- [236] Z. Fan, Y. Zhao, Q. Tan, N. Mo, M.X. Zhang, M. Lu, H. Huang, Nanostructured Al2O3 YAG-ZrO 2 ternary eutectic components prepared by laser engineered net shaping, Acta Mater 170 (2019) 24–37. https://doi.org/10.1016/j.actamat.2019.03.020.
- [237] J. LLorca, V.M. Orera, Directionally solidified eutectic ceramic oxides, Prog Mater Sci 51 (2006) 711–809. https://doi.org/10.1016/j.pmatsci.2005.10.002.

- [238] S. Pfeiffer, K. Florio, D. Puccio, M. Grasso, B.M. Colosimo, C.G. Aneziris, K. Wegener, T. Graule, Direct laser additive manufacturing of high performance oxide ceramics: A state-of-the-art review, J Eur Ceram Soc 41 (2021) 6087–6114. https://doi.org/10.1016/j.jeurceramsoc.2021.05.035.
- [239] Q. Liu, Y. Danlos, B. Song, B. Zhang, S. Yin, H. Liao, Effect of high-temperature preheating on the selective laser melting of yttria-stabilized zirconia ceramic, J Mater Process Technol 222 (2015) 61–74. https://doi.org/10.1016/j.jmatprotec.2015.02.036.
- [240] S. Yan, D. Wu, F. Niu, Y. Huang, N. Liu, G. Ma, Effect of ultrasonic power on forming quality of nano-sized Al2O3-ZrO2 eutectic ceramic via laser engineered net shaping (LENS), Ceram Int 44 (2018) 1120–1126. https://doi.org/10.1016/j.ceramint.2017.10.067.
- [241] D. Grossin, A. Montón, P. Navarrete-Segado, E. Özmen, G. Urruth, F. Maury, D. Maury, C. Frances, M. Tourbin, P. Lenormand, G. Bertrand, A review of additive manufacturing of ceramics by powder bed selective laser processing (sintering / melting): Calcium phosphate, silicon carbide, zirconia, alumina, and their composites, Open Ceramics 5 (2021) 100073. https://doi.org/10.1016/J.OCERAM.2021.100073.
- [242] K. Shahzad, J. Deckers, J.P. Kruth, J. Vleugels, Additive manufacturing of alumina parts by indirect selective laser sintering and post processing, J Mater Process Technol 213 (2013) 1484–1494. https://doi.org/10.1016/J.JMATPROTEC.2013.03.014.
- [243] W. Wang, Y.X. Liu, J.Y.H. Fuh, P.J. Wang, Alumina-Zirconia-Silica Ceramics Synthesis by Selective Laser Sintering/Melting, Applied Mechanics and Materials 121–126 (2011) 2487–2491.
- [244] A. N. Chen, J.M. Wu, K. Liu, J.Y. Chen, H. Xiao, P. Chen, C.H. Li, Y.S. Shi, High-performance ceramic parts with complex shape prepared by selective laser sintering: a review, Advances in Applied Ceramics 117 (2018) 100–117. https://doi.org/10.1080/17436753.2017.1379586.
- [245] H.-C. Yen, A new slurry-based shaping process for fabricating ceramic green part by selective laser scanning the gelled layer, J Eur Ceram Soc 32 (2012) 3123–3128. https://doi.org/10.1016/j.jeurceramsoc.2012.04.014.
- [246] F. Klocke, A.E. Christian, D. Ae, C.A. Ae, A. Demmer, PRODUCTION PROCESS Investigations on laser sintering of ceramic slurries, (n.d.). https://doi.org/10.1007/s11740-007-0047-3.
- [247] D. Drummer, S. Greiner, M. Zhao, K. Wudy, A novel approach for understanding laser sintering of polymers, (2019). https://doi.org/10.1016/j.addma.2019.03.012.

- [248] D. Drummer, D. Rietzel, F. Kühnlein, Development of a characterization approach for the sintering behavior of new thermoplastics for selective laser sintering, (2010). https://doi.org/10.1016/j.phpro.2010.08.081.
- [249] B. Ma, L. Lin, X. Huang, Q. Hu, M. Fang, Bone tissue engineering using B-tricalcium phosphate scaffolds fabricated via selective laser sintering, IFIP International Federation for Information Processing 207 (2006) 710–716. https://doi.org/10.1007/0-387-34403-9 99/COVER.
- [250] J. Christian Nelson, N.K. Vail, J.W. Barlow, J.J. Beaman, D.L. Bourell, H.L. Marcus, Selective Laser Sintering of Polymer-Coated Silicon Carbide Powders, Ind Eng Chem Res 34 (1995) 1641–1651. https://doi.org/10.1021/IE00044A017.
- [251] L. Cardon, J. Deckers, A. Verberckmoes, K. Ragaert, L. Delva, K. Shahzad, J. Vleugels, J.P. Kruth, Polystyrene-coated alumina powder via dispersion polymerization for indirect selective laser sintering applications, J Appl Polym Sci 128 (2013) 2121–2128. https://doi.org/10.1002/APP.38388.
- [252] D. T. Pham, R.S. Gault, A comparison of rapid prototyping technologies, Int J Mach Tools Manuf 38 (1998) 1257–1287.
- [253] N. K. Tolochko, T. Laoui, Y. V Khlopkov, S.E. Mozzharov, V.I. Titov, M.B. Ignatiev, Absorptance of powder materials suitable for laser sintering, (n.d.). http://www.mcbup.com/research_registers/aa.asp (accessed October 5, 2023).
- [254] L. E. Murr, E. Martinez, J. Hernandez, S. Collins, K.N. Amato, S.M. Gaytan, P.W. Shindo, Microstructures and Properties of 17-4 PH Stainless Steel Fabricated by Selective Laser Melting, Journal of Materials Research and Technology 1 (2012) 167–177. https://doi.org/10.1016/S2238-7854(12)70029-7.
- [255] A. Rosenberger, N. Ku, L. Vargas-Gonzalez, M. Alazzawi, R. Haber, Rheology and processing of UV-curable textured alumina inks for additive manufacturing, Int J Appl Ceram Technol 18 (2021) 1457–1465. https://doi.org/10.1111/IJAC.13784.
- [256] J. W. Kemp, A.A. Diaz, E.C. Malek, B.P. Croom, Z.D. Apostolov, S.R. Kalidindi, B.G. Compton, L.M. Rueschhoff, Direct ink writing of ZrB2-SiC chopped fiber ceramic composites, Addit Manuf 44 (2021) 102049. https://doi.org/10.1016/J.ADDMA.2021.102049.
- [257] R. L. Walton, M.J. Brova, B.H. Watson, E.R. Kupp, M.A. Fanton, R.J. Meyer, G.L. Messing, Direct writing of textured ceramics using anisotropic nozzles, J Eur Ceram Soc 41 (2021) 1945–1953. https://doi.org/10.1016/J.JEURCERAMSOC.2020.10.021.
- [258] Slic3r Open source 3D printing toolbox, (n.d.). https://slic3r.org/ (accessed October 19, 2023).

- [259] M. Rubat Du Merac, H.J. Kleebe, M.M. Müller, I.E. Reimanis, Fifty Years of Research and Development Coming to Fruition; Unraveling the Complex Interactions during Processing of Transparent Magnesium Aluminate (MgAl2O4) Spinel, Journal of the American Ceramic Society 96 (2013) 3341–3365. https://doi.org/10.1111/JACE.12637.
- [260] J. Li, Y. Pan, Y. Zeng, W. Liu, B. Jiang, J. Guo, The history, development, and future prospects for laser ceramics: A review, Int J Refract Metals Hard Mater 39 (2013) 44–52. https://doi.org/10.1016/J.IJRMHM.2012.10.010.
- [261] Z. Xiao, S. Yu, Y. Li, S. Ruan, L.B. Kong, Q. Huang, Z. Huang, K. Zhou, H. Su, Z. Yao, W. Que, Y. Liu, T. Zhang, J. Wang, P. Liu, D. Shen, M. Allix, J. Zhang, D. Tang, Materials development and potential applications of transparent ceramics: A review, Materials Science and Engineering: R: Reports 139 (2020) 100518. https://doi.org/10.1016/J.MSER.2019.100518.
- [262] N. J. Cherepy, Z.M. Seeley, S.A. Payne, E.L. Swanberg, P.R. Beck, D.J. Schneberk, G. Stone, B.M. Wihl, S.E. Fisher, S.L. Hunter, P.A. Thelin, T. Stefanik, J. Kindem, Transparent Ceramic Scintillators for Gamma Spectroscopy and Imaging, 2017 IEEE Nuclear Science Symposium and Medical Imaging Conference, NSS/MIC 2017 Conference Proceedings (2018). https://doi.org/10.1109/NSSMIC.2017.8533003.
- [263] F. Tian, A. Ikesue, J. Li, Progress and perspectives on composite laser ceramics: A review, J Eur Ceram Soc 42 (2022) 1833–1851. https://doi.org/10.1016/J.JEURCERAMSOC.2021.12.061.
- [264] H. E. Meissner, R.J. Beach, C. Bibeau, S.B. Sutton, S. Mitchell, I. Bass, C. Valley, E. Honea, Laser rods with undoped, flanged end-caps for end-pumped laser applications, (1998).
- [265] A. Ikesue, Y.L. Aung, T. Kamimura, S. Honda, Y. Iwamoto, Composite Laser Ceramics by Advanced Bonding Technology, Materials 11 (2018). https://doi.org/10.3390/MA11020271.
- [266] I.K. Jones, Z.M. Seeley, N.J. Cherepy, E.B. Duoss, S.A. Payne, Direct ink write fabrication of transparent ceramic gain media, Opt Mater (Amst) 75 (2018) 19–25. https://doi.org/10.1016/J.OPTMAT.2017.10.005.
- [267] Z. Seeley, T. Yee, N. Cherepy, A. Drobshoff, O. Herrera, R. Ryerson, S.A. Payne, 3D printed transparent ceramic YAG laser rods: Matching the core-clad refractive index, Opt Mater (Amst) 107 (2020) 110121. https://doi.org/10.1016/J.OPTMAT.2020.110121.
- [268] T. J. Rudzik, Z.M. Seeley, F.J. Ryerson, N.J. Cherepy, S.A. Payne, (INVITED)Counter-ion effect on the diffusion behavior of Yb, Lu, and Nd ions in YAG transparent ceramics, Optical Materials: X 13 (2022) 100132. https://doi.org/10.1016/J.OMX.2021.100132.

- [269] Z. M. Seeley, I.R. Phillips, T.J. Rudzik, N.J. Cherepy, A.D. Drobshoff, S.A. Payne, Material jet printing of transparent ceramic Yb:YAG planar waveguides, Opt Lett 46 (2021) 2433. https://doi.org/10.1364/OL.420504.
- [270] A. Bandyopadhyay, S. Ciliveri, S. Bose, Metal Additive Manufacturing for Load-Bearing Implants, Journal of the Indian Institute of Science 2022 102:1 102 (2022) 561–584. https://doi.org/10.1007/S41745-021-00281-X.
- [271] A. Bandyopadhyay, K.D. Traxel, S. Bose, Nature-inspired materials and structures using 3D Printing, Materials Science and Engineering: R: Reports 145 (2021) 100609. https://doi.org/10.1016/J.MSER.2021.100609.
- [272] F. Chen, Y.R. Wu, J.M. Wu, H. Zhu, S. Chen, S. Bin Hua, Z.X. He, C.Y. Liu, J. Xiao, Y.S. Shi, Preparation and characterization of ZrO2-Al2O3 bioceramics by stereolithography technology for dental restorations, Addit Manuf 44 (2021) 102055. https://doi.org/10.1016/J.ADDMA.2021.102055.
- [273] M. Rahmati, M. Mozafari, Biocompatibility of alumina-based biomaterials—A review, J Cell Physiol 234 (2019) 3321–3335. https://doi.org/10.1002/jcp.27292.
- [274] L. Treccani, T.Y. Klein, F. Meder, K. Pardun, K. Rezwan, Functionalized ceramics for biomedical, biotechnological and environmental applications, (2013). https://doi.org/10.1016/j.actbio.2013.03.036.
- [275] L. Sedel, Evolution of alumina-on-alumina implants: a review, Clin Orthop Relat Res 379 (2000) 48–54. https://doi.org/10.1097/00003086-200010000-00008.
- [276] C. R. Howlett, H. Zreioat, R. O'Dell, J. Noorman, P. Evans, B.A. Dalton, C. McFarland, J.G. Steele, The effect of magnesium ion implantation into alumina upon the adhesion of human bone derived cells, J Mater Sci Mater Med 5 (1994) 715–722. https://doi.org/10.1007/BF00120363/METRICS.
- [277] M. B. Pabbruwe, O.C. Standard, C.C. Sorrell, R. Howlett, Bone formation within alumina tubes: effect of calcium, manganese, and chromium dopants, Biomaterials 25 (2004) 4901–4910. https://doi.org/10.1016/j.biomaterials.2004.01.005.
- [278] Q. Zhao, G.J. Zhai, D.H.L. Ng, X.Z. Zhang, Z.Q. Chen, Surface modification of Al2O3 bioceramic by NH2+ ion implantation, Biomaterials 20 (1999) 595–599. https://doi.org/10.1016/S0142-9612(98)00218-X.
- [279] Q. L. Feng, T.N. Kim, J. Wu, E.S. Park, J.O. Kim, D.Y. Lim, F.Z. Cui, Antibacterial effects of Ag-HAp thin films on alumina substrates, Thin Solid Films 335 (1998) 214–219. https://doi.org/10.1016/S0040-6090(98)00956-0.

- [280] T. N. Kim, Q.L. Feng, Z.S. Luo, F.Z. Cui, J.O. Kim, Highly adhesive hydroxyapatite coatings on alumina substrates prepared by ion-beam assisted deposition, Surf Coat Technol 99 (1998) 20–23. https://doi.org/10.1016/S0257-8972(97)00121-7.
- [281] F. A. Al-Sanabani, A.A. Madfa, N.H. Al-Qudaimi, N.H. Al-Qudaimi Alumina,) Ceramic for Dental Applications: A Review Article, American Journal of Materials Research American Journal of Materials Research 1 (2014) 26–34. http://www.aascit.org/journal/ajmr (accessed October 10, 2023).
- [282] M. Dehurtevent, L. Robberecht, A. Thuault, E. Deveaux, A. Leriche, F. Petit, C. Denis, J.C. Hornez, P. Béhin, Effect of build orientation on the manufacturing process and the properties of stereolithographic dental ceramics for crown frameworks, J Prosthet Dent 125 (2021) 453–461. https://doi.org/10.1016/J.PROSDENT.2020.01.024.
- [283] S. Bose, S. Suguira, A. Bandyopadhyay, Processing of controlled porosity ceramic structures via fused deposition, Scr Mater 41 (1999) 1009–1014. https://doi.org/10.1016/S1359-6462(99)00250-X.
- [284] S. Bose, J. Darsell, H.L. Hosick, L. Yang, D.K. Sarkar, A. Bandyopadhyay, Processing and characterization of porous alumina scaffolds, J Mater Sci Mater Med 13 (2002) 23–28. https://doi.org/10.1023/A:1013622216071/METRICS.
- [285] P. A. Dcarnley, A review of metallic, ceramic and surface-treated metals used for bearing surfaces in human joint replacements, Proc Inst Mech Eng H 213 (1999) 107–135. https://doi.org/10.1243/0954411991534843.
- [286] Biomechanics and Biomaterials in Orthopedics, Biomechanics and Biomaterials in Orthopedics (2004). https://doi.org/10.1007/978-1-4471-3774-0.
- [287] G. Willmann, Ceramic femoral head retrieval data, Clin Orthop Relat Res 379 (2000) 22–28. https://doi.org/10.1097/00003086-200010000-00004.
- [288] M. Hisbergues, S. Vendeville, P. Vendeville, Review zirconia: Established facts and perspectives for a biomaterial in dental implantology, J Biomed Mater Res B Appl Biomater 88 (2009) 519–529. https://doi.org/10.1002/jbm.b.31147.
- [289] M. Navarro, A. Michiardi, O. Castaño, J.A. Planell, Biomaterials in orthopaedics, J R Soc Interface 5 (2008) 1137–1158. https://doi.org/10.1098/RSIF.2008.0151.
- [290] C. Piconi, G. Maccauro, F. Muratori, E.B. Del Prever, Alumina and Zirconia Ceramics in Joint Replacements, Https://Doi.Org/10.1177/228080000300100103 (2003). https://doi.org/10.1177/228080000300100103.
- [291] C. Piconi, G. Maccauro, Zirconia as a ceramic biomaterial, Biomaterials 20 (1999) 1–25. https://doi.org/10.1016/S0142-9612(98)00010-6.

- [292] M. H. Ghaemi, S. Reichert, A. Krupa, M. Sawczak, A. Zykova, K. Lobach, S. Sayenko, Y. Svitlychnyi, Zirconia ceramics with additions of Alumina for advanced tribological and biomedical applications, (2017). https://doi.org/10.1016/j.ceramint.2017.04.150.
- [293] Y. Josset, Z. Oum'hamed, A. Zarrinpour, M. Lorenzato, J.J. Adnet, D. Laurent-Maquin, In vitro reactions of human osteoblasts in culture with zirconia and alumina ceramics, (1999). https://doi.org/10.1002/(SICI)1097-4636(19991215)47:4.
- [294] H. Shin, H. Ko, M. Kim, Cytotoxicity and biocompatibility of Zirconia (Y-TZP) posts with various dental cements, Restor Dent Endod 41 (2016) 167–175. https://doi.org/10.5395/RDE.2016.41.3.167.
- [295] F. Doreau, C. Chaput, T.C.-A. Engineering, undefined 2000, Stereolithography for manufacturing ceramic parts, Wiley Online LibraryF Doreau, C Chaput, T ChartierAdvanced Engineering Materials, 2000•Wiley Online Library (n.d.). https://doi.org/10.1002/1527-2648(200008)2:8<493::AID-ADEM493>3.0.CO;2-C.
- [296] C. M. Cristache, M. Burlibaşa, G. Cristache, S. Drafta, I.A. Popovici, A.A. Iliescu, S. Zisi, L. Burlibaşa, ZIRCONIA AND ITS BIOMEDICAL APPLICATIONS, (2011).
- [297] Y. Lu, Z. Mei, J. Zhang, S. Gao, X. Yang, B. Dong, L. Yue, H. Yu, Flexural strength and Weibull analysis of Y-TZP fabricated by stereolithographic additive manufacturing and subtractive manufacturing, J Eur Ceram Soc 40 (2020) 826–834. https://doi.org/10.1016/J.JEURCERAMSOC.2019.10.058.
- [298] Z. Mei, Y. Lu, Y. Lou, P. Yu, M. Sun, X. Tan, J. Zhang, L. Yue, H. Yu, Determination of Hardness and Fracture Toughness of Y-TZP Manufactured by Digital Light Processing through the Indentation Technique, Biomed Res Int 2021 (2021). https://doi.org/10.1155/2021/6612840.
- [299] H. Nakai, M. Inokoshi, K. Nozaki, K. Komatsu, S. Kamijo, H. Liu, M. Shimizubata, S. Minakuchi, B. Van Meerbeek, J. Vleugels, F. Zhang, Additively Manufactured Zirconia for Dental Applications, Materials 14 (2021). https://doi.org/10.3390/MA14133694.
- [300] A. Ioannidis, D. Bomze, C.H.F. Hämmerle, J. Hüsler, O. Birrer, S. Mühlemann, Loadbearing capacity of CAD/CAM 3D-printed zirconia, CAD/CAM milled zirconia, and heatpressed lithium disilicate ultra-thin occlusal veneers on molars, Dental Materials 36 (2020) e109–e116. https://doi.org/10.1016/J.DENTAL.2020.01.016.
- [301] H. W. Kim, H.E. Kim, V. Salih, J.C. Knowles, Dissolution control and cellular responses of calcium phosphate coatings on zirconia porous scaffold, J Biomed Mater Res A 68A (2004) 522–530. https://doi.org/10.1002/JBM.A.20094.
- [302] M. G. Faga, A. Vallée, A. Bellosi, M. Mazzocchi, N.N. Thinh, G. Martra, S. Coluccia, Chemical treatment on alumina–zirconia composites inducing apatite formation with

- maintained mechanical properties, J Eur Ceram Soc 32 (2012) 2113–2120. https://doi.org/10.1016/J.JEURCERAMSOC.2011.12.020.
- [303] M. Ferraris, E. Verné, P. Appendino, C. Moisescu, A. Krajewski, A. Ravaglioli, A. Piancastelli, Coatings on zirconia for medical applications, Biomaterials 21 (2000) 765–773. https://doi.org/10.1016/S0142-9612(99)00209-4.
- [304] Y. Yokogawa, M. Toriyama, Y. Kawamoto, T. Suzuki, S. Kawamura, Apatite Coating on Yttria Doped Partially Stabilized Zirconia Plate in the Presence of Water Vapor, Journal of the Ceramic Society of Japan 100 (1992) 602–604. https://doi.org/10.2109/JCERSJ.100.602.
- [305] C. Piconi, S.G. Condo, T. Kosmač, Alumina- and Zirconia-based Ceramics for Load-bearing Applications, Advanced Ceramics for Dentistry (2014) 219–253. https://doi.org/10.1016/B978-0-12-394619-5.00011-0.
- [306] Y. Zhu, K. Liu, J. Deng, J. Ye, F. Ai, H. Ouyang, T. Wu, J. Jia, X. Cheng, X. Wang, 3D printed zirconia ceramic hip joint with precise structure and broad-spectrum antibacterial properties, Int J Nanomedicine 14 (2019) 5977–5987. https://doi.org/10.2147/IJN.S202457.
- [307] S. K. Nandi, G. Fielding, D. Banerjee, A. Bandyopadhyay, S. Bose, 3D-printed β-TCP bone tissue engineering scaffolds: Effects of chemistry on in vivo biological properties in a rabbit tibia model, J Mater Res 33 (2018) 1939–1947. https://doi.org/10.1557/JMR.2018.233.
- [308] J. D. Avila, Z. Alrawahi, S. Bose, A. Bandyopadhyay, Additively Manufactured Ti6Al4V-Si-Hydroxyapatite composites for articulating surfaces of load-bearing implants, Addit Manuf 34 (2020) 101241. https://doi.org/10.1016/J.ADDMA.2020.101241.
- [309] B. León, J. Jansen, Thin Calcium Phosphate Coatings for Medical Implants, Springer, 2009.
- [310] S. Samavedi, A.R. Whittington, A.S. Goldstein, Calcium phosphate ceramics in bone tissue engineering: A review of properties and their influence on cell behavior, Acta Biomater 9 (2013) 8037–8045. https://doi.org/10.1016/j.actbio.2013.06.014.
- [311] S. Bose, N. Sarkar, Natural Medicinal Compounds in Bone Tissue Engineering, Trends Biotechnol 38 (2020) 404–417. https://doi.org/10.1016/J.TIBTECH.2019.11.005.
- [312] S. Bose, N. Sarkar, D. Banerjee, Effects of PCL, PEG and PLGA polymers on curcumin release from calcium phosphate matrix for in vitro and in vivo bone regeneration, Mater Today Chem 8 (2018) 110–120. https://doi.org/10.1016/J.MTCHEM.2018.03.005.

- [313] A.J. Ambard, L. Mueninghoff, Calcium Phosphate Cement: Review of Mechanical and Biological Properties, Journal of Prosthodontics 15 (2006) 321–328. https://doi.org/10.1111/J.1532-849X.2006.00129.X.
- [314] R. Soundararajan, G. Kuhn, R. Atisivan, S. Bose, A. Bandyopadhyay, Processing of Mullite–Aluminum Composites, Journal of the American Ceramic Society 84 (2001) 509–513. https://doi.org/10.1111/J.1151-2916.2001.TB00691.X.
- [315] T. Gualtieri, A. Bandyopadhyay, Additive manufacturing of compositionally gradient metal-ceramic structures: Stainless steel to vanadium carbide, Mater Des 139 (2018) 419–428. https://doi.org/10.1016/J.MATDES.2017.11.007.
- [316] Y. Zhang, A. Bandyopadhyay, Direct fabrication of compositionally graded Ti-Al2O3 multi-material structures using Laser Engineered Net Shaping, Addit Manuf 21 (2018) 104–111. https://doi.org/10.1016/J.ADDMA.2018.03.001.
- [317] K. D. Traxel, A. Bandyopadhyay, Naturally architected microstructures in structural materials via additive manufacturing, Addit Manuf 34 (2020) 101243. https://doi.org/10.1016/J.ADDMA.2020.101243.